Interactions between Receptor Kinases and PXY SUMOylation define Radial Pattern in Arabidopsis

QING HE

Durham University

Interactions between Receptor Kinases and PXY SUMOylation define Radial Pattern in *Arabidopsis*

Main supervisor: Peter Etchells
Co-supervisor: Ehmke Pohl

Qing He
May 2024

Abstract

In plant development, a receptor kinase may be active in disparate cell types, with each requiring different signalling outputs. The ERECTA (ER) receptor kinase and its homologs ERL1 and ERL2 exemplify this pleiotropy. In Arabidopsis, they influence stomatal patterning, shoot meristem function, ovule morphogenesis, xylem fiber differentiation, and cell division in the vascular cambium. Such diverse expression and functionality raise the question of how ER signalling can specify such distinct cell behaviours. One explanation is that cell-type specific interactions with co-receptors, ligands, or other proteins modulate signalling. However, little is known about ER interactors in the vascular cambium, a bifacial stem cell niche that generates phloem and xylem. Combinatorial mutations between ER, ERL1 and ERL2 and receptor kinases of a second family, PXY, PXL1, and PXL2, show severe cambial defects. Here I discovered that PXY and PXL proteins form heterodimers with ER and ERL2. PXY signalling can be manipulated by altering levels of its cognate ligand, TDIF. In genetic analysis, plant lines in which TDIF levels were altered had dramatic phenotypes that required the presence of ER or ERL2. These results demonstrate that PXY signalling mediated cambium regulation depends on ER signalling and explains ER function in the cambium. Because the cambium produces xylem, which constitutes the wood in vascular plants, our findings position PXY-ER heterodimers at the centre of the accumulation of this versatile biomaterial and carbon sink.

The cambium and procambium are responsible for producing the majority of biomass in vascular plants. These meristems form a bifacial stem cell population, from which xylem and phloem are specified on opposing sides through positional signals. The PHLOEM INTERCALATED WITH XYLEM (PXY) receptor kinase plays a key role in promoting vascular cell division and organization. SUMO is a common post-translational protein decoration that affects many different biological processes such as plant immunity, and resistance to biotic and abiotic stresses. Here, PXY was found to be SUMOylated and SUMOylation sites were predicted. Mutation of PXY SUMO sites resulted in vascular defects including disorganized tissues, increased cell division and potential xylem differentiation defects. These data collectively indicate PXY

SUMO is likely to be a negative regulator of PXY signaling and play crucial roles in vascular development.

Gaining a comprehensive understanding of how PXY works at the plasma membrane may guide us in manipulating the system to increase or decrease signal transduction. A structural understanding of how PXY functions is therefore essential. The structure of the extracellular domain of PXY has been solved, but to fully understand its function, the structure of the cytoplasmic kinase domain would likely be informative. This could assist in understanding aspects of protein turnover and interactions with co-receptors.

Acknowledgement

I am deeply grateful to my supervisor, Peter Etchells, who not only shared his knowledge and practical expertise in plant sciences but also showed kindness and unwavering support. Without his guidance and assistance in various aspects, I wouldn't have made it to this point.

I would also like to extend my gratitude to Dr. Raymond for sharing FRET technologies and providing advice on FRET calculation, Dr. Wenbin for conducting the bioinformatic steps of the RNA-seq analysis, aligning the raw reads to the Arabidopsis genome, and generating figures for me. Additionally, my appreciation goes to Dr. Miguel, Johan, and Patrick for their guidance on Co-IP and western blot techniques. I am thankful to all the members of lab1004/1003 for their assistance. Special thanks to Wafa, who has been an exceptional lab mate, always bringing warmth and joy into the lab environment. Julien, thank you for your excellent company and valuable work advice.

My heartfelt thanks go out to my family and friends. I cannot imagine navigating through life without your love and support. Thank you for being there for me, loving me, and understanding me through both the happy and difficult times.

Contents

Abbreviations

ABA	Abscisic acid	**LRR**	Leucine-rich repeat
AIL	AINTEGUMENTA-LIKE	**MAPK**	Mitogen-activated protein kinase
ANT	AINTEGUMENTA	**MES**	2-(N-Morpholino) ethanesulfonic acid
AS1	ASYMMETRIC LEAVES1	**MMS21**	Methyl methanesulfonate
AS2	ASYMMETRIC LEAVES2	**mRNA**	Messenger RNA
ATHB	*ARABIDOPSIS THALIANA* HOMEOBOX	**MS**	Murashige and Skoog
BEK	Bacteria-expressed kinase	**MYB**	Myeloblastosis viral oncogene homolog
BIK	BCL2 Interacting Killer	**NAC**	NAM (no apical meristem, Petunia), ATAF1–2 (*Arabidopsis* thaliana activating factor), and CUC2 (cup-shaped cotyledon, *Arabidopsis*)
BIN	BRASSINOSTEROID INSENSITIVE	**NST**	NAC secondary wall thickening promoting factor
BR	Brassinosteroids	**OTS**	OOVERLY TOLERANT TO SALT
BRI	Brassinosteroids insensitive	**PCA**	Principal Component Analysis
BSA	Bovine Serum Albumin	**PCR**	Polymerase chain reaction
CA	Cluster Analysis	**PFS**	Pretty few seeds
CAGE	Cancer antigen	**PLINC**	Plant zinc finger
cDNA	Complementary DNA	**PLL**	POLTERGEIST LIKEoltergeist like

CFP	Cyan Fluorescent Protein	**PLT**	PLETHORAlethora
CLE	Clavata3-like/ ESR	**POL**	POLTERGEISTPoltergeist
CLV	CLAVATA	**PRE**	PACLOBUTRAZOL OF RESISTANCEaclobutrazol resistance
Co-IP	Co immunoprecipitation	**PRR**	Pattern Recognition Receptor
Col-0	Columbia-0	**PTM**	Post-translational protein modification
CORD	Cone Rod Dystrophy	**PXf**	PXY family
DNA	Deoxyribonucleic acid	**PXL**	PXY-like
DTT	DL-Dithiothreitol	**PEG**	Polyethylene Glycol
DMSO	Dimethyl sulfoxide		
E1	Ubl activating enzyme	**PXY**	PHLOEM INTERCALATED WITH XYLEM
E2	Ubl conjugating enzyme	**qPCR**	Quantitative PCR
E3	Ubl protein ligase	**RAM**	Root apical meristem
ECIA	Extracellular Interactome Assay	**RK**	Receptor kinase
EDTA	Ethylenediaminetetraacetic acid	**RLK**	Receptor-like kinase
EPFL	EPF-LIKE	**RNA**	Ribonucleic acid
ER	ERECTA	**SA**	Salicylic acid
ERf	ER family	**SAE**	SUMO1 ACTIVATING ENZYME
ERF	ETHYLENE-RESPONSIVE TRANSCRIPTION FACTOR	**SAM**	Shoot apical meristem
ERL	ERECTA-LIKE	**SIZ1**	SAP AND MIZ1 DOMAIN-CONTAINING LIGASE1

ESD4	EARLY IN SHORT DAYS4	**SDS**	Sodium dodecyl sulfate
FLA	FASCICLIN-LIKE ARABINOGALACTAN	**SERK**	SOMATIC EMBRYOGENESIS RECEPTOR KINASE
FLS	FLAGELLIN-SENSITIVE	**SPCH**	SPEECHLESS
FRA	FOS-RELATED ANTIGEN	**SUMO**	Small Ubiquitin Modifier
FRET	Förster resonance energy transfer	**TAE**	Tris base, acetic acid and EDTA
GA	Gibberellic acid	**TDIF**	TRACHEARY ELEMENT DIFFERENTIATION FACTOR
GID1	GIBBERELIN INSENSITIVE DWARF	**TMO**	TARGET OF MONOPTEROS
GM	glucose-mannitol	**VRLK**	Vaccinia-related like kinase
GO	Gene Ontology	**WBA**	Washing Buffer A
GSK	GLYCOGEN SYNTHASE KINASE	**WBB**	Washing Buffer B
IRX	IRREGULAR XYLEM	**WOX**	WUSCHEL-RELATED HOMEOBOX
JA	Jasmine acid	**WT**	Wild type
KNAT	KNOTTED-LIKE FROM *ARABIDOPSIS THALIANA*	**YFP**	Yellow Fluorescent Protein
LBD	Lateral organ boundaries domain	**XCP**	Extracellular protein
LBB	Lysis Binding Buffer		

List of Tables

List of Figures

Chapter 1. General Introduction

1.1 *Arabidopsis thaliana*: a model for plant development study

Arabidopsis thaliana, a modest member of the mustard family, has earned its stripes as the preferred model system for delving into the intricacies of plant biology. The study of its molecular genetics has yielded remarkable insights into the understanding of plant growth and development (Meinke et al., 1998).

Found across vast stretches of Europe, Asia, and North America, *Arabidopsis thaliana* stands as a botanical beacon for researchers. Among its various strains, the Columbia and Landsberg wild types have emerged as the top choices for the genetic and molecular studies of this plant. Its genome, containing a concise 157 million base pairs distributed across five chromosomes and harbouring an estimated 27,000 genes, is among the most compact within the plant kingdom. The small size of its genome makes *Arabidopsis* a unique utility in the genetic mapping and sequencing, serving as an indispensable tool for researchers in their pursuits. The most current iteration of the *Arabidopsis* thaliana genome can be readily accessed via The Arabidopsis Information Resource (TAIR; www.Arabidopsis.org), providing a compass for genetic exploration.

Besides, the entire life cycle of *Arabidopsis*, encompassing seed germination, formation of a rosette plant, bolting of the main stem, flowering, and maturation of the first seeds, culminates in a mere six weeks. This rapid progression, coupled with the plant's capacity for self-pollination and prolific seed production, underscores its capacity to fuel research endeavors. Technique for introducing genetic modifications into *Arabidopsis* has matured over time with the widely used floral dipping method (Clough and Bent, 1998), offering a direct avenue for transformation without the intricacies of tissue culture or plant regeneration. These attributes collectively render *Arabidopsis* an ideal specimen for scientific exploration, which is straightforward and avoid tissue culture or plant regeneration (Meinke et al., 1998).

Invaluable to the field of plant biology, the Arabidopsis gene knockout collections, realized through insertional mutagenesis, stand as a goldmine of information. Over

300,000 independent *Agrobacterium* transferred DNA (T-DNA) insertion events in the genome of the reference plant *Arabidopsis thaliana* have been created. The precise locations were determined for more than 88,000 T-DNA insertions, which resulted in the identification of mutations in more than 21,700 of the ~29,454 predicted *Arabidopsis* genes. This expansive collection of insertional mutants, each closely linked to a gene of interest, is conveniently catalogued and accessible through TAIR (Alonso et al., 2003). Therefore, all the features of Arabidopsis including small in stature and genome size, genetically tractable, short generation time, make it ideal for developmental research and study.

Specifically, because of the advances of Arabidopsis in plant genetics, tissue processing and microscopy, Arabidopsis has accelerated vascular development research in recent decades (Fischer et al., 2019; Lehmann and Hardtke, 2016; Nieminen et al., 2015; Wang, 2020). Despite the lack of persistent woody stem, Arabidopsis exhibits secondary growth of roots, hypocotyls and inflorescence stems. Moreover, there are striking similarities between the concentric pattern of xylem-cambium-phloem in the hypocotyls of Arabidopsis, stems of angiosperm trees, and storage roots of numerous crop species (Campilho et al., 2020; Chaffey et al., 2002; Hoang et al., 2020). Such characteristics highlights the potential benefits to be gained from using Arabidopsis as model to study secondary development.

1.2 Primary Growth and Secondary Growth

Animals demonstrate determinate growth, reaching a specific body size and shape before ceasing their growth. In contrast, plants exhibit indeterminate growth, continuously adding new organs like leaves, stems, and roots as long as they have access to essential resources. This perpetual growth in plants is made by specialized tissues known as meristems, which are tissues where cell division and growth occur continuously.

Meristems are essential for lifelong growth and development (Dinneny and Benfey, 2008; Hirakawa et al., 2010). They maintain populations of continuously dividing stem cells in tissues and therefore help plants to exhibit an extraordinary capacity for growth

and developmental plasticity. Two indeterminate meristems are established during embryogenesis. These are the root apical meristem (RAM), which gives rise to the root system, and the shoot apical meristem (SAM), from which all aerial tissues including leaves and flowers are derived. Meristems contribute to both primary growth and secondary growth. Primary growth is controlled by either SAM or RAM which results in plant elongation while secondary growth (widening) is controlled by the two lateral meristems, called the vascular cambium and the cork cambium.

Vascular cambium and cork cambium are two types of meristematic tissues in plants that play essential roles in growth and development. The vascular cambium is typically located between the xylem and phloem in the stems and roots of woody dicot plants. It forms a continuous cylinder. Vascular cambium is responsible for secondary growth (thickness) of the plant. It produces new vascular tissues, primarily xylem to the inside and phloem to the outside, adding to the plant's vascular system. Cork cambium, on the other hand, is involved in the production of cork cells for protective purposes in the outer bark of the plant. These two types of cambia serve different functions and are located in different regions of the plant (Figure 1.1).

Primary growth is primarily concerned with the lengthening and development of primary plant structures, while secondary growth is focused on the thickening of woody plants, resulting in the formation of secondary vascular tissues and protective layers. These two types of growth work together to help plants adapt to their environment and grow both vertically and horizontally as they mature.

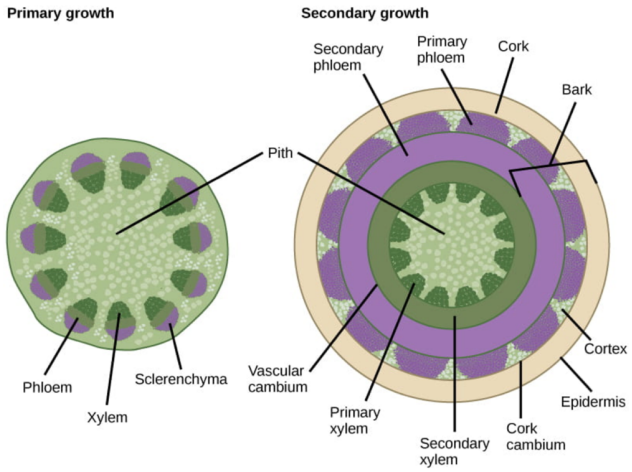

Figure 1.1 Primary growth and secondary growth in wood (Kerr, S.C. et al; 2023).

1.3 Structure and organisation of plant vascular tissue

Vascular cells like phloem and xylem, originate from meristems including RAM and SAM during postembryonic development (Lazar, 2003). Vascular tissue supports length-wise growth by providing both physical support and long-distance fluid and nutrient transport. There is a well-organized radial structure of vascular system: phloem, procambium or cambium and xylem (Figure 1.2). Xylem and phloem, the vascular conductive tissues, are derived from cell divisions in the procambium- and cambium on opposing sides (Larson, 1994).

The phloem is mainly responsible for movement of photosynthate from the leaves throughout the plant. It supports bidirectional transport of a variety of molecules, including sugars, proteins, amino acids, photosynthate and other metabolites from the leaves throughout the plant. Besides these, phloem functions in carrying long-distance RNA, phytohormone and electrical signals which make phloem important both in plant growth and biotic and abiotic stress resistance (Hilleary and Gilroy, 2018; Johns et al., 2021). The phloem is a complex tissue and is formed typically by different cell types: the sieve elements, companion cells, fibres and parenchyma cells. Sieve elements includes sieve cells and sieve tube elements and lack nucleus, ribosomes, and other

organelles. They are specialized for transportation and translocation of photosynthates. Companion cells are smaller, nucleated cells with dense cytoplasm and numerous mitochondria and connected to sieve tube elements via plasmodesmata. Companion cells therefore are able to provide metabolic support to sieve elements. Phloem parenchyma are involved in storage, lateral transport, and secretion but not specialized for long-distance transport. Fibres, which have thick and lignified cell walls and typically dead at a maturity, can provide structure support for phloem. An additional cell type, sclerenchyma, is sometimes present in primary and/or secondary phloem. It includes fibers (long and flexible) and sclereids (short and protective) and is specialized for providing mechanical support and protection with thick and lignified cell walls (Evert et al., 2006; Hafke et al., 2005; Taiz et al., 2023). The presence, quantities, and arrangements of these cell types in the xylem and phloem tissues commonly vary and may be taxonomic informative.

Arabidopsis xylem is mostly constituted of three cell types: vessels, parenchyma and fibres. Vessels, which undergo terminal differentiation are large, dead, tubular cells, with water-conducting function, characterised by pitted secondary cell walls. The vessel elements are joined end-to-end to transport water and dissolved minerals continuously from the root to shoot. Dead xylem fibres and living parenchyma cells are interspersed with these vessels, and the living parenchyma cells store starches, oils and tanniniferous compounds (Esau, 1977). In established vascular tissue, fibres which develop secondary walls are prevalent, but in young vascular tissue it is typically parenchyma that are formed, which do not have secondary cell walls (Etchells et al., 2016). Fibres provides majority of the plant's mechanical strength, as a consequence of the presence of cells with large woody secondary cell walls (Lazar, 2003).

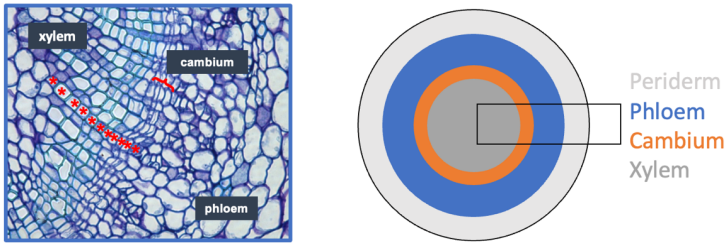

Figure 1.2 Organisation of vascular tissue in the *Arabidopsis* thaliana hypocotyl.

The tissue between xylem and phloem, either the procambium or cambium, is essential for dicot vascular plants. Procambium and cambium serve different roles in plant growth. Procambium is involved in the formation of primary vascular tissues during primary growth, while cambium, specifically the vascular cambium, is responsible for secondary growth and the production of secondary xylem and phloem, contributing to the thickening of woody stems and roots in certain plant species.

Vascular cambium of both roots and shoots contains two types of cells: long, spindle-shaped fusiform cells and in woody perennials, smaller, cuboidal ray parenchyma cells. These cambium/ procambium cells keep meristematic activity even when they are outside of the apical meristems. The procambium acts during primary growth, the cambium during lateral growth (secondary growth). Secondary growth in woody plant stems originates from post-embryonic meristematic cell divisions, described above as the vascular and cork cambia. The vascular cambium harbours a single, bifacial stem cell in each radial file which is unique among plant meristems, and these stem cells rapidly divides periclinally (parallel to the surface of the organ) to fuel the development of distinct specialised tissues on opposing sides (i.e. the xylem and phloem). As xylem constitutes the wood in plant tissue, these cell divisions underpin the provision of the majority of plant biomass (Shi et al., 2019; Smetana et al., 2019). Together, these dividing cells and their undifferentiated daughters (xylem and phloem progenitors) form a ‘cambial zone’, which is especially visible in transverse sections of mature hypocotyls (Figure 1.2).

The activity of cambia is undeniably crucial for the growth and survival of numerous plant species especially in dicots such as *Arabidopsis*, barley and woody species like oak trees. Furthermore, human beings have utilized the vascular tissues originating from these meristems as sustainable materials for centuries. Plants make a substantial contribution (approximately 80%) to the world's biomass, with stems and tree trunks alone accounting for 70% of this (Bar-On et al., 2018). Consequently, the secondary vascular tissues of trees play a significant role as a carbon sink and are poised to have a substantial impact on the ongoing efforts to mitigate global warming (Bastin et al., 2019). Secondary growth also plays a foundational role in the enlargement of root and tuber crops, which are essential sources of carbohydrates in human diets worldwide (Chandrasekara and Josheph Kumar, 2016). The improvement of both forestry and agricultural yields is increasingly vital, particularly considering the rapid growth of the human population and the concurrent threats to productivity due to anthropogenic climate change. Achieving this objective necessitates an enhanced and fundamental understanding of radial plant growth.

1.4 Overview of PXY signalling in vascular tissue

Several studies have described the presence of molecular and genetic components, including phytohormones, transcription factors and signalling mechanisms that coordinate the development of plant vascular tissues including vascular cell division (Etchells et al., 2013; Hirakawa et al., 2010) and xylem differentiation (Kondo et al., 2014). Besides, the maintenance of vascular cambium requires cell-to-cell communication and integration of multiple external signals (Busch et al., 2010; De Rybel et al., 2016; Trewavas, 2021).

Peptide perception by transmembrane receptor(-like) kinases (RK/RLK) is a key signaling mechanism underpinning vascular cambium activity. In the shoot apical meristem, it is well established that signaling via the receptor-like kinase (RLK) CLAVATA1 (CLV1) is essential for either cell proliferation or differentiation and the balance between them. CLV1 can not only control shoot and floral meristem size in Arabidopsis by encoding a putative receptor kinase but regulate organ formation at shoot and flower meristems by promoting the differentiation of stem cells on the

meristem flanks and the balance between differentiation and proliferation (Clark et al., 1997; DeYoung et al., 2006; Etchells and Turner, 2010; Fletcher et al., 1999; Schoof et al., 2000). The cognate ligand to CLV1 is CLAVATA3. In Arabidopsis, these gene constitute a large family (Jun et al., 2010), referred to as the CLAVATA3-LIKE/ESR-RELATED (CLE) proteins. Ectopic CLV3, CLE19 and CLE40 expression in roots results in disorganization in the normal pattern of highly orientated cell divisions (Fiers et al., 2005). POLTERGEIST (POL) and POLTERGEIST LIKE 1 (PLL1), phosphatases acting downstream of CLV1, influence the position of cell divisions in Arabidopsis embryos (Song et al., 2008; Song et al., 2006). These observations place these signaling factors at the centre of cell division and stem cell homeostasis in Arabidopsis.

TRACHEARY ELEMENT DIFFERENTIATION INHIBITORY FACTOR (TDIF) is a peptide ligand that is encoded by three genes: *CLAVATA3-LIKE/ESR- RELATED 41* (*CLE41*), *CLE42* and *CLE44*. TDIF promotes procambial cell proliferation while inhibiting these cells from differentiating into xylem vessel cells (Hirakawa et al., 2008). Moreover, TDIF is expressed from the phloem and perceived by a receptor-like kinase, PHLOEM INTERCALATED WITH XYLEM (PXY, also named as TDR), which is expressed in cambium. Interestingly, PXY and CLV1 (CLAVATA1) also belong to the same LRR-receptor-kinase family subgroup XI in *Arabidopsis* (Fisher and Turner, 2007). TDIF and PXY are a ligand-receptor pair (Hirakawa et al., 2008; Morita et al., 2016; Zhang et al., 2016a) that promote cell division in vascular meristems. Loss of TDIF-PXY resulted in a failure to correctly organize tissue layers in the vasculature. The vascular meristems participate in a highly ordered developmental process with a very prominent polarity, required for the spatial separation of xylem and phloem. In *pxy* mutants, both transverse and longitudinal organization of the vascular tissue are disrupted in stems. Staining sections with Aniline blue, which causes the sieve plates of the phloem to fluoresce yellow under UV light, demonstrated that the phloem appeared to be adjacent to, or interspersed with the xylem. Therefore, *PXY* is crucial to maintain the cell polarity required for the orientation of cell division and the organization of vascular tissues (Figure 1.3B-K) (Etchells and Turner, 2010; Fisher and Turner, 2007).

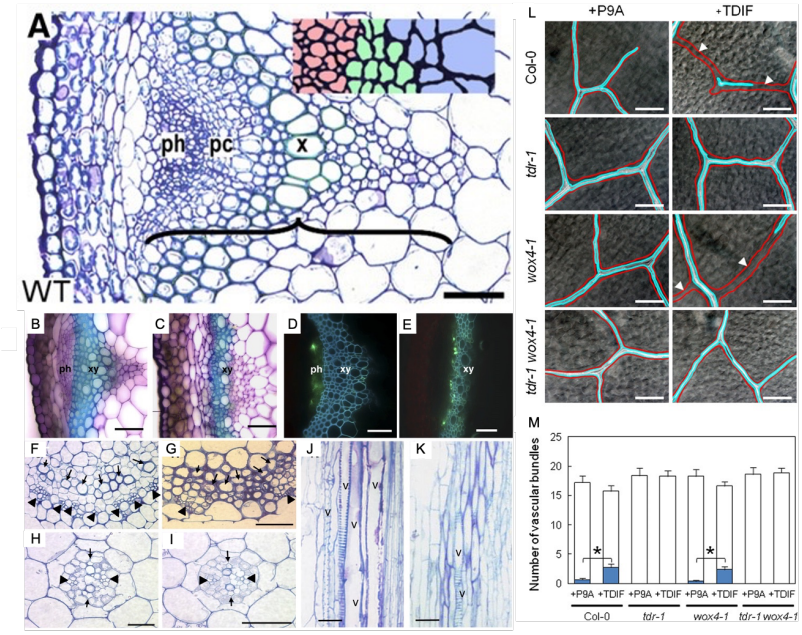

Figure 1.3. TDIF-PXY functions in vascular development.

A. Structure of vascular bundles from inflorescence stems in the wild type. ph, phloem; pc, procambium; x, xylem.

B–E. Hand-cut transverse sections from stem vascular bundles of wild-type (B and D) and *pxy* plants (C and E) stained with Toluidine blue (B and C) or Aniline blue (D and E). ph, phloem; xy, xylem.

F-G. Resin-embedded transverse sections of vascular bundles of petioles from wild-type (F) and *pxy* (G) plants. Xylem vessels (arrows) and phloem (arrowheads) are indicated. *pxy* is less organized.

H-I. Resin-embedded transverse sections of vascular bundles from the roots stele from wild-type (H) and *pxy* (I) plants. The xylem poles (arrow) and phloem poles (arrowhead) are marked. No significant difference.

J-K. Resin-embedded longitudinal sections of stem vascular bundles from wild-type (J) and *pxy* (K) plants. Vessels (V) are marked.

L-M. TDIF-sensitive xylem formation in *wox4* mutants. (L) Effects of 1 mM TDIF on 10-d-old leaf veins of different strains. TDIF caused fragmentation of xylem strands (indicated by white arrowheads) in *wox4-1* and in the wild type but did not in *pxy-1* or the *pxy-1 wox4-1* double mutant. Veins are outlined in red, and xylem strands are outlined in blue. (M) Quantification of

the effects of TDIF. The blue and white boxes indicate the frequencies of the xylem-absent and xylem-present veins, respectively. Bars = 100 mm in (L). Error bars indicate SE, n = 8; *Student's t test significance at $P < 0.01$ for different means of the frequency of xylem- absent veins in (M). Images adapted from (Fisher and Turner, 2007) and (Hirakawa et al., 2013).

In addition to influencing vascular organisation, vascular proliferation is also significantly promoted by TDIF-PXY through cambium-expressed *WUSCHEL-RELATED HOMEOBOX (WOX)* transcription factor genes*, WOX4* and *WOX14. WOX4* is expressed preferentially in the procambium and cambium, and its expression level was upregulated upon application of TDIF in a PXY-dependent manner. Such CLE-RLK-WOX signaling modules have been observed repeatedly in plants and proved to maintain the stability of SAM (Lee and Torii, 2012; Schoof et al., 2000) . *PXY* and *WOX4* work on the same genetic pathway to promote procambial cell proliferation (Figure 3L, M) (Hirakawa et al., 2010). Furthermore, *wox4* reduced vascular proliferation in the root, and cell numbers in stem vascular bundles were also reduced. This phenotype was enhanced by simultaneous knockout of *WOX14*, indicating that *WOX4* acts redundantly with *WOX14* in regulation of vascular cell division as downstream of *PXY* (Etchells et al., 2013). These gave us evidence that the TDIF-PXY-WOX4/14 module for cambial cell division regulation act parallel to the xylem differentiation regulation.

Finally, PXY suppresses xylem differentiation: glycogen synthase kinase 3 proteins (GSK3s) are crucial downstream components of the TDIF-PXY signaling pathway suppressing xylem differentiation in procambial cells (Figure 1.4A-H) (Ito et al., 2006; Kondo et al., 2014). It was revealed that PXY associates with the GSK3, BRASSINOSTERIOD INSENSITIVE 2 (BIN2) at the plasma membrane using yeast-2-hybrid and Förster resonance energy transfer (FRET) (Kondo et al., 2014). These cytoplasmic kinase proteins were confirmed to redundantly promote xylem and phloem differentiation in cell culture systems. For instance, GSK3s contribute to the procambium maintenance together with WOX4 by inhibiting xylem cell differentiation (Kondo et al., 2014; Saito et al., 2018). Therefore, TDIF-PXY signaling thus represents a mechanism through which differential growth in vascular tissue could be coordinated, regulating as it does, tissue organization, cell division and differentiation.

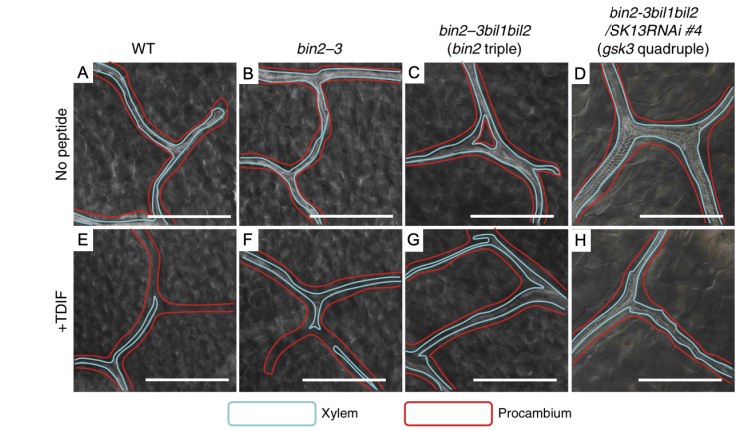

Figure 1.4. TDIF-PXY suppresses xylem differentiation.

A-H. Arabidopsis seeds for Ws (WT), *bin2-3*, *bin2* triple and *gsk3* quadruple mutants were germinated in liquid MS medium with or without 1000 nM TDIF. The vasculature of true leaves from 11-day-old seedlings is shown. Blue and red lines indicate the areas of xylem and procambial cells, respectively. Scale bar, 200 mm (Kondo et al., 2014).

Besides, while PXY clearly involves in regulating vascular development, this receptor kinase does not act alone. There are genetic interactions between phytohormones and PXY signaling. The expression of transcription factor WOX4 was shown to be induced at the site of auxin accumulation (Suer et al., 2011), suggesting that WOX4 may be one point of integration between PXY and auxin signaling. Ethylene signaling controls WOX4 to regulate cambial proliferation and inhibit xylem fibre development through suppression of NAC transcription factors simultaneously (Yang et al., 2020). ERF transcription factors, regulated by JA and ethylene, are connected to PXY signaling because one of the hallmarks of the *pxy* mutant transcriptome is increases in ERF expression (Etchells et al., 2012). In stem, WOX14 overexpression increase the gibberellic acid (GA) accumulation to induce lignification of secondary xylem (Denis et al., 2017). Overall, the interaction and co-ordination between PXY signaling and phytohormones is crucial for regulating the secondary growth. Moreover, there are other transcriptional targets of PXY signaling pathway except WOX4 and WOX14. BES1 (bri1-EMS-Suppressor 1), a transcription factor of BRI1 downstream, functions downstream of GSK3s from PXY-TDIF signaling pathway to regulate xylem

differentiation. BIN2-BES1 additionally regulate cambial activity and promote phloem differentiation (Anne et al., 2015; Hu et al., 2022; Kondo et al., 2014; Rodriguez-Villalon et al., 2014; Saito et al., 2018). Another PXY downstream transcription factor, TMO6, promote the expression of LBD4 along the phloem-procambium boundary. And LBD4 and TMO6 were identified to act downstream of WOX14 and a feed forward loop is formed between them to determine stem cell number (Smit et al., 2020). CAILs (CAMBIUM AINTEGUMENTA-LIKE) transcription factors were activated by TDIF-PXY to define cambium stem cell identity (Eswaran et al., 2023). Combining all the functions of TDIF-PXY signaling, the schematic figure was generated (Figure 1.5).

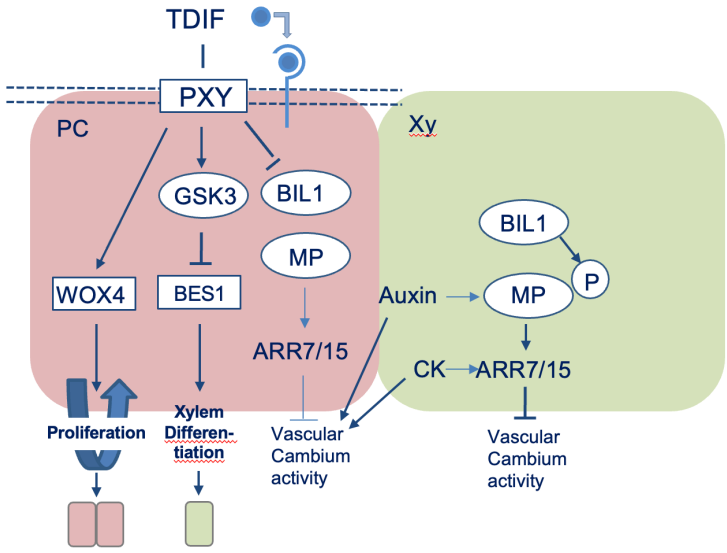

Figure 1.5. The PXY-CLE41 receptor ligand pair defines a multifunctional pathway that controls vascular development.

In the Arabidopsis genome, there are two paralogues of PXY, PXY-LIKE1 (PXL1) and PXY-LIKE2 (PXL2). It was reported that TDIF interacts with PXY, PXL1 and PXL2 in vitro and can bind to the binding pocket of PXL1 and PXL2 (Zhang et al., 2016a). Furthermore, *pxl1* and *pxl2* enhance the vascular organisation defects that are characteristic of *pxy* mutants (Etchells et al., 2013; Fisher and Turner, 2007; Wang et al., 2019b). PXY acts redundantly with PXL1 and PXL2 in cambium initiation as well.

pxy mutants demonstrate a delay to the onset of cambium formation, they nevertheless still make the transition to secondary growth, although the resulting cambium is somewhat disorganized (Figure 5C). So does the triple mutant, *pxy pxl1 pxl2*. Because both lines make the transition to secondary growth, further regulatory mechanism(s) must act with *PXY* in cambium specification (Wang et al., 2019b).

While TDIF-PXY signaling pathway plays multiple functions in vascular development, it is also affected by and interacted with other signaling pathways, hormones and protein decorations etc. There is another receptor-like kinase ER, which is involved in different developmental progresses in plants. Previous studies showed that PXf and ERf genetically interact to coordinate tissue integrity at the levels of both cell size and cell division and controls cambium stem cell initiation (Wang et al., 2019b). However, the mechanism(s) of the interaction is still unknown, and this interaction can be potentially post-translationally modified including SUMOylation. Here, we would like to answer the questions above in both chapter 3 and 4. We hypothesized the genetic interactions is underpinned by physical interaction, therefore, in chapter 3, the physical interaction between PXfs and ERfs will be checked and the function of ER in vasculature will be further explored. Furthermore, SUMO (Small ubiquitination modifier) is an important post-translational decoration which can target to proteins to modify their functions. However, the knowledge of PXY SUMOylation and whether it affected PXY functions and interactions with other signaling pathways are limited. In chapter 4, the functions of PXY SUMOylation will be prequisitively revealed, And all of the research will potentially help understanding truly vascular patterning.

Chapter 2. Materials and Methods

2.1. Plant Growth and Treatment

2.1.1 Plant Material

Arabidopsis thaliana (Columbia ecotype) wild type and *pxy-5* (SALK_002910), *er-124* , *erl2* mutants (Shpak et al., 2005) and *IRX3::CLE41*(Etchells and Turner, 2010), *pPXY::GUS*, *pPXL1::GUS*, *pPXL2::GUS*, *pER::GUS*, *pERL1::GUS*, *pERL2::GUS* (Wang et al., 2019b) transgenic seeds were obtained from lab stocks .

Accession numbers: PXY (At5g61480), PXL1 (At1g08590), PXL2 (At4g28650), ER (At2G26330), ERL1(At5g62230), ERL2 (At5g07180), CLE41 (At3g24770), ANT (At4g37750), AIL5/PLT5 (At5g57390), AIL6/PLT3 (At5g10510), AIL7/PLT7 (At5g65510) WOX4 (At1g46480), WOX14 (At1g20700), TMO6 (At5g60200), LBD4 (At1g31320), BES1 (At1g19350), BZR1 (At1g75080), KNAT7 (At1g62990), CORD1 (At3g14170)), IRX1 (At4g18780), MYB46 (At5g12870), IRX3 (At5g17420), NAC007 (At1g12260).

2.1.2 *Arabidopsis Thaliana* Tissue Culture

All Arabidopsis seedlings used, ecotype Col-0, were grown on ½ MS supplemented with 0.8% agar (Duchefa Biochemie), pH 5.6-5.8. All the media were autoclaved at 121℃ for 20 mins. Media was allowed to cool to 50°C before adding antibiotics if required.

2.1.3 *Arabidopsis thaliana* Sterilization for Tissue Culture

Arabidopsis thaliana seeds were surface-sterilized with absolute ethyl alcohol for 5 min and 75% ethanol for 15 min, followed by washing three or four times with sterilized distilled water under aseptic conditions. The sterilized Arabidopsis seeds were placed on 12 cm square plates containing half-strength Murashige and Skoog (MS) medium supplemented with 0.8% agar. Afterwards, the seeds were stratified for 48h in the dark at 4°C which helps synchronise germination. Finally, the plates were placed vertically in the growth cabinet to induce seed germination and growth.

2.1.4 Plant Growth Condition

Seedlings and isolated leaves were cultured on solidified media and incubated in the growth room or growth cabinets under 16 h light: 8 h dark at 22°C.

Nicothiana Benthamiana plants are first germinated in soil in a pot and grown at ~ 22°C, 12h: 12h day: night, 50%-60% humidity. Two-week-old seedlings are then transplanted into individual pots as necessary. Five-week-old plants were used for infiltration and further experiments.

2.1.5 *Arabidopsis thaliana* Transformation

Floral dipping was used for Arabidopsis transformation. 4-6-week-old plants in the inflorescence developmental stage were used for dipping. Agrobacterium cells were grown in the liquid LB medium with antibiotics for overnight and then aliquoted in several Falcon tubes and centrifuged (4200 rpm) for 15 mins. Agrobacterium were resuspended in 5% sucrose and 0.05% Silweet L-77. The Arabidopsis was simply transformed by dipping in the resuspended agrobacterium. Dipped plants were placed under a plastic dome or other humidity retaining covers for 12–24 h after inoculation (Clough and Bent, 1998).

2.1.6 *Arabidopsis thaliana* Crossing

er-124, and *erl2* were crossed with *IRX3::CLE41* as followings: Unopened flowers on the female plant were emasculated using forceps. Anthers carrying mature pollen from the male plant was then transferred manually to the female using forceps by gently brushing the anther against the stigma of the female plant (Weigel and Glazebrook, 2006).

2.1.7 Transgenic *Arabidopsis* Selection

Primary transformants (T_1 generation) were selected by spreading seeds on plates supplemented with different herbicides (according to the specific plant resistance on destination vector, normally hygromycin, kanamycin, sulfadiazine, BASTA etc.). After 7- 10 days, resistant seedlings were transferred onto fresh soil without selection for seed setting and collection.

Secondary transformants (T_2 generation) were steriled (method in 2.1.3) and spread individually on ½ MS plates with resistance. The plates were sealed with parafilm and placed at 4°C fridge for 48h for stratification and then moved to growth cabinets and grown for around 10 days. The seedlings were then screened for resistance at a ratio of 3:1 (resistant: susceptible) to select transgenic plants with a single transformation insert. Selected lines were then pricked out onto fresh soil with no selection for seeds setting and collection.

Tertiary transformants (T_3 generation) were sterilized and spread on ½ MS plates as described for T_2 transformants. Plants were then screened for complete resistance, indicating homozygous transgenic lines. Selected lines were then pricked out onto fresh soil with no selection for seed setting and collection.

2.1.8 Homozygote Selection of Crosses

Seeds from primary crosses (F_1 generation) were surface sterilised (method in 2.1.3) and spread individually on plates with no selection and then transferred onto soil with no selection for seed setting and collection of independent F_2 lines.

Secondary crosses (F_2 generation) were sterilised and spread on plates supplemented with herbicide to which each parent was resistant. Progeny of these plants (F_3) were then screened for complete resistance, indicating homozygous transgenic lines. If no fully resistant lines obtained, selection was done one by one, i.e. homozygous lines at one loci of interest was selected for, if resistance for the second was segregating. Double homozygous plants were then selected in the subsequent generation. At each stage, selected lines were pricked out onto fresh soil with no selection for seed setting and collection.

2.2 Microbiological Procedures

2.2.1 Chemically competent *E. coli*

Chemically Competent *E. coli* (DH5α and TOP10) were ordered from New England Biolab and Thermo Fisher respectively.

2.2.2 Electro competent *agrobacterium tumefaciens*

The *Agrobacterium* strain (GV3101) was streaked onto a freshly prepared LB agar plate with 50 µg/ml gentamycin and incubated at 28°C incubation room for 48 hours. A single colony from the plate was picked and inoculated into a 100 ml LB liquid medium in a 250 ml autoclaved flask using a sterile toothpick and incubated at 28 °C for 20 hours with vigorous shaking. 5 ml of the 20 hours grown culture was re-inoculated into a 1 litre flask containing 250 ml of LB medium and incubated at 28 °C until OD_{600} of cells is between 0.5-1.0 (1010 cells/ml). The cells were transferred aseptically to ice cold 50 ml Falcon tubes and cooled on ice for 30 minutes, followed by centrifugation at 4000 rpm for 15 minutes in a bench top refrigerated centrifuge at 4 °C. The resulting pellet was re-suspended in 50 ml of sterile cold ddH_2O. The above centrifugation and re-suspension steps were repeated three times. However, for the subsequent rounds, the cells were resuspended in 25 ml and 10 ml of sterile cold ddH_2O, and twice in 10% glycerol (all containing filter-sterilized cold solutions). Finally, the cells were re-suspended in 1-1.5 ml of filter-sterilized cold 10% glycerol, aliquoted into 50 µl portions, and stored at -80°C.

2.2.3 Transformation of chemically competent *E. coli* cells

100 and 200 ng of the plasmid was added into a vial containing One Shot Chemically Competent *E. coli* and thoroughly mixed. The mixture was then incubated on ice for 5 to 30 minutes. Following this, the cells underwent a 30-second heat-shock at 42°C without agitation, after which the tubes were promptly transferred to ice for 2 minutes. Subsequently, 600 µl of room-temperature S.O.C. Medium was added to the cells and they were incubated at 37°C for 1 hour for cell recovery. The transformed cells were then plated on a selective plate prewarmed to 37°C, with specific resistance corresponding to the vector used, and incubated overnight at 37°C. Following incubation, 5 to 10 colonies were selected and cultured in liquid LB with a concentration of 50 µg/ml kanamycin overnight. Positive colonies were analysed using PCR, and plasmid DNA was extracted using the NEB plasmid mini prep kit prior to sequencing.

2.2.4 Transformation of electro competent *agrobacterium* cells

200 to 1000 ng of the plasmid was introduced into 50 µl of electrocompetent GV3101 cells that had been defrosted ion ice, and thoroughly mixed. This mixture was then transferred to a prechilled 2 mm electroporation cuvette. Electroporation was conducted under the following conditions: capacitance: 25 µF, voltage: 2.4 KV, resistance: 200 Ω, and pulse length: 5 msec. Immediately after electroporation, 600 µl of LB was added to the cuvette. The bacterial suspension was subsequently transferred to a 1.5 ml Eppendorf tube and incubated for 2 hours at 28°C with gentle agitation. The cells were then spread onto an LB agar plate containing the appropriate antibiotic and incubated for 48 hours at 28°C. Small liquid cultures of the resulting colonies were prepared and checked using PCR. Glycerol stocks of the selected clones were created and stored at -80°C.

2.2.5 Plasmid Prep

Recombinant plasmids were purified from 6ml *E. coli* DH5α cultures incubated overnight at 37°C using Plasmid Miniprep Kit – NEW ENGLAND BIOLAB. The yield of plasmid was then quantified using a NanoDrop™ 1000 Spectrophotometer (Thermo Scientific).

2.3 Molecular Biology

2.3.1 PCR (Polymerase Chain Reaction)

VeriFi™ (PCRBIOSYSTEMS) DNA polymerase was used in cloning PCR amplifications to amplify *PXY*, *PXL1*, *PXL2*, *ER*, *ERL1*, *ERL2* coding sequences using settings and reactions system below:

Master Mix was prepared on ice based on the following table:

Reagent	**25 µl reaction**	**50 µl reaction**	**Final concentration**
2x VeriFi™ Mix	12.5 µl	25 µl	1x
Forward Primer (10 µM)	1.0 µl	2.0 µl	400 nM
Reverse Primer (10 µM)	1.0 µl	2.0 µl	400 nM

Template DNA	~ 100 ng	~ 200 ng	Variable
PCR grade dH_2O	Up to 25 µl	Up to 50 µl	

Table 1. PCR reaction mixture for gene cloning.

Cycle conditions:

Cycles	Temperature	Time	Notes
1	95 °C	1 min	Initial denaturation
25-35	95 °C	15 seconds	Denaturation
	60 °C to 75 °C	15 seconds	Anneal
	72 °C	10-30 seconds/kb	Extension

Table 2. PCR cycle conditions for gene cloning.

PCRBIO Taq Mix Red was used for colony PCR.

Master Mix was prepared based on the following table:

Reagent	20 µl reaction	50 µl reaction	Final concentration
2x Taq Red Mix	10 µl	25 µl	1x
Forward Primer (10 µM)	0.75 µl	2.0 µl	400 nM
Reverse Primer (10 µM)	0.75 µl	2.0 µl	400 nM
Template DNA	~ 100 ng	~ 200 ng	Variable
PCR grade dH_2O	Up to 20 µl	Up to 50 µl	

Table 3. Master mixture for genotyping.

Cycle conditions:

Cycles	Temperature	Time	Notes
1	95 °C	1 min	Initial denaturation
25-35	95 °C	15 seconds	Denaturation
	55 °C to 65 °C	15 seconds	Anneal
	72 °C	1-120 seconds	Extension (60 sec/ kb)

Table 4. PCR cycle conditions for genotyping.

Gene amplification and colony PCR products were observed using agarose gel electrophoresis (section 2.3.2).

For gene amplification, cloning, and mutagenesis, PCR gene products were purified using AMPure XP substitute magnetic beads (see preparation below) if the gel displayed a single band of the correct size.

Two times the volume of beads was added to the PCR product and incubated at room temperature for 5 minutes. The mixture was then placed on a magnet for 3 minutes, and the supernatant was carefully removed. The beads were washed using 180 µl of 70% ethanol for three times and subsequently air-dried at room temperature for 10 minutes. 30 µl of dH_2O was added to the beads and incubated for 2 minutes. Finally, the PCR tube was placed on the magnet, and the supernatant was transferred to a new Eppendorf tube. The yield was assessed using a NanoDrop™ 1000 Spectrophotometer (Thermo Scientific).

AMPure XP substitute beads Preparation
Sera-mag SpeedBeads purchased from Thermo Fisher was resuspended. 1 ml beads were transferred to a 1.5 ml eppendorf tube and placed on magnetic stand. The supernatant was removed and replaced by 1 ml TE buffer (10 mM Tris-HCl, 1 mM EDTA = 500 µL 1 M Tris pH8.0 + 100 µL 0.5 M EDTA, fill conical to 50 mL mark with dH_20). Speedbeads was mixed with TE buffer to wash and then placed back on magnetic stand. Three more washes were repeated. A final 1 ml TE buffer was added to the Speedbeads and mixed well. In a 50 ml Falcon, 9 g PEG-8000, 10 ml 5 M NaCL (or 2.92 g), 500 µL 1 M Tris-HCL, 100 µl 0.5 M EDTA and 27.5 ul Tween 20 were added. The well-mixed Speedbeads with TE buffer were transferred to the Falcon tube. The Falcon tube was filled to 50 ml with ddH_20 and gently mixed until the solution appeared uniformly brown. The Falcon tube was wrapped in tinfoil to protect it from light and kept at 4°C.

For PCR gene products with multiple bands in the gel, the gel of the correct size were excised from the gel using a sharp scalpel, and the DNA was purified using a Gel DNA Extraction Kit (QIAGEN).

2.3.2 Agarose Gel Electrophoresis

To prepare the gel, 1g of agarose was added to 100 ml of 1 x TAE (Tris-acetate-EDTA) buffer. The mixture was microwaved at full power for approximately 2 minutes to completely dissolve the agarose. Afterward, the solution was cooled down using running water before adding 2 µl of ethidium bromide. The resulting mixture was then poured into an appropriately sized gel mould and left to set. An adequate well comb was inserted into the mould. Next, the gel was carefully placed into an electrophoresis tank filled with 1 x TAE.

Before loading the samples, 6 x loading buffer was added to the DNA samples (this step was omitted if using Taq Red Mix). Subsequently, the samples were loaded into the wells, along with 10k Hyperladder (PCRBIO). The gels were then run at 130V for 20-30 minutes. Finally, the gels were photographed using a BioRad Gel Doc 2000.

2.3.3 Gateway® Technology for Vector Construction

2.3.3.1 TOPO® Cloning

The genes of interest were amplified using PCR with gene-specific primers (5'- CACC-3' was included in the forward primers). The resulting genes were expressed optimally and fused in-frame with the TEV recognition site (specific to pENTR™/TEV/D-TOPO® from Thermo Fisher) or any desired N- or C-terminal tags, following recombination with the Gateway destination vector. Subsequently, the amplified genes were cloned into the TOPO® vector using the reaction below:

Reagent	**Chemical Transformation**
Fresh PCR Product	0.5–4 µl
Salt Solution	1 µl
Dilute Salt Solution (1::4)	—

Water TOPO® vector	to a final volume of 5 µl 1 µl
Total volume	6 µl

Table 5. TOPO reaction system.

The reactions were mixed gently and incubated at room temperature for 1-3 hours. The reaction was then subjected to *E coli*. transformation (see, 2.2.3).

2.3.3.2 LR Reaction into Destination Vectors

Correctly sequenced plasmids of entry clone were used to proceed LR reaction as follows:

Reagent	**Chemical Transformation**
Entry Clone (100-300 ng) Destination Vector (150ng/ µl) 5X LR Clonase™ Reaction Buffer TE buffer, pH 8.0	1–10 µl 1 µl 4 µl to a final volume of 16 µl
Total volume	16 µl

Table 6. LR reaction system.

The reactions were mixed gently and incubated at 37°C for 2-12 hours and proceeded to *E.coli* transformation (see, 2.2.3).

2.3.4 Greengate Technology for Vector Construction

2.3.4.1 Gene Clone and Primer Design Principle

Greengate Technology (Lampropoulos et al., 2013) is based on BsaI restriction enzyme. Therefore, the BsaI recognition and cutting sites should be added manually to the forward and reverse terminus of genes according to the function of the gene in the vector. The easy primer design principle is shown below:

		Eco31I site and filling sequence	Overhang		in frame addition
	forward				
promoter		aacaGGTCTCa	A	acct	
N-tag		aacaGGTCTCa	B	aaca	
CDS		aacaGGTCTCa	C	ggct	ca
C-tag		aacaGGTCTCa	D	tcag	gt
terminator		aacaGGTCTCa	E	ctgc	
plant resistance		aacaGGTCTCa	F	acta	
		aacaGGTCTCa	H	tagg	
	reverse				
promoter		aacaGGTCTCt	B	Tgtt	
N-tag		aacaGGTCTCt	C	agcc	
CDS		aacaGGTCTCt	D	Ctga	
C-tag		aacaGGTCTCt	E	gcag	
terminator		aacaGGTCTCt	F	tagt	
plant resistance		aacaGGTCTCt	G	atac	
		aacaGGTCTCt	H	ccta	

Table 7. Primer design principles for Greengate.

2.3.4.2. Entry Module

Genes of interest were amplified with PCR using specific primers (listed in Supplementary Table 3) and purified using PCR cleanup beads (see, 2.3.1). And then the genes were cloned into their specific entry vectors as follows:

1) BsaI-HF digestion

Reagent	Volume
BsaI-HF	1 µl
CutSmart Buffer	5 µl
entry vector (about 100 ng)	X µl
gel extract of sequence to be added (about 100 ng of each part)	X µl
water	Up to 50 µl
Total volume	50 µl

Table 8. BsaI-HF digestion mixture.

The reactions were mixed gently and incubated at 37°C for 1h and deactivated at 85°C for 10 minutes.

2) Purification of the digestion

The digestion product was purified using beads (see, 2.3.1) and eluted in 25 µl water. Left to stand for 1 minute, centrifuged for 1 minute for elution.

3) Ligation with T4 DNA Ligase

Reagent	Chemical Transformation
Purification Product	25 µl
T4 DNA Ligase Buffer	3 µl
T4 DNA Ligase	1 µl
Water	1 µl
	Up to 30 µl
Total volume	30 µl

Table 9. T4 ligation mixture.

The reaction is mixed gently and incubated at room temperature for 1-3 hours and deactivated at 70°C for 10 minutes and then proceeded to *E.coli* transformation (see 2.2.3).

2.3.4.3 Destination Vectors with Goldengate

For 6 different entry modules, 75-100 ng per entry plasmid was required. And the reaction was prepared as follow:

Reagent	Volume
Entry Clone (75-100 ng)	1 µl
Destination Vector (100ng/ µl)	1 µl
10X NEB Buffer	4 µl
NEB Assembly Mix	1 µl
Water	up to 20 µl
Total volume	20 µl

Table 10. Goldengate destination reaction mixture.

The programme for Reaction:

Cycles	Temperature	Time
50X	37 °C	5 min
	16 °C	5 min
1X	80 °C	5 min

Table 11. Goldengate reaction programme.

The transformation was performed either immediately after the assembly process, or following overnight storage in the freezer using *E.coli* transformation method (see, 2.2.3).

2.3.5 Genomic DNA Extraction from *Arabidopsis* Tissues

Arabidopsis tissue of interest was collected and placed in Eppendorf tubes on dry ice for multiple samples. The tissue was then ground in a ball mill using the Tissuelyser from QIAGEN. Subsequently, 400 µl of extraction buffer (0.14M D-Sorbitol, 0.22M TRIS-HCl pH8, 0.022M EDTA pH8, 0.8M NaCl, 0.8% CTAB (cetyltrimethylammonium bromide), 1% n-Lauroylsarcosine, ddH_2O) was added to each Eppendorf tube. The resulting mixture was lysed at 65°C for 5-30 minutes. To this, 400 µl of chloroform was added and vortexed. All tubes were then centrifuged at 13,000 rpm for 15 minutes. The supernatant was carefully transferred into new Eppendorf tubes, and 200 µl isopropanol was added, followed by vortexing. DNAs were precipitated via

centrifugation at 13,000 rpm for 15 minutes. The resulting pellet was washed with 70% ethanol and centrifuged again at 13,000 rpm for 15 minutes. Finally, the pellet was dried, resuspended using 50 µl of sterile water, and stored at -20°C.

2.3.6 mRNA Extraction from *Arabidopsis* Tissues and Reverse Transcription

RNA Extraction Prep:

Arabidopsis tissue we desired was collected into Eppendorf tubes with 3-4 Zirconia Silica beads added (in liquid Nitrogen) and then ground for 1 minute using Tissuelyser (QIAGEN). Afterward, 200 µl of lysis binding buffer (composed of 100 mM Tris-HCl, 1M LiCl, 10mM EDTA, 1% SDS, 5 mM DTT, Antifoam A, RNase-free H_2O to the desired volume) was added, and the samples were ground for an additional minute. The resulting mixture was then centrifuged at maximum speed for 10 minutes. The supernatant was collected and divided into two portions. Half of the supernatant was stored at -80°C as a backup.

mRNA Capture:

The sample lysate was heated to 65°C for 4 minutes and then promptly placed on ice. Simultaneously, SeraMag Oligo (dT) Coated Magnetic particles were vortexed, and 40 µl per prep were evenly distributed. The particles were then placed on a magnet for 2-3 minutes, allowing for the supernatant to be removed. Next, 100 µl of lysis binding buffer (LBB) was added per prep for beads washing up. Tubes were positioned on magnetic racks, and once again, the supernatant was removed.

Following this, 200 µl of the sample lysate was introduced to the beads and immediately resuspended. The tubes were placed on an agitator for 10 minutes at room temperature, followed by positioning on a magnetic rack until the solution was clear. The supernatant was then carefully removed. The beads underwent a wash with 200 µl of washing buffer A (WBA, composed of 10 mM Tris-HCl pH 8.0, 150 mM NaCl, 1 mM EDTA, 0.1% SDS, with RNase-free H_2O to the required volume) twice. This involved removing the samples from the magnetic rack, thorough mixing by pipetting, placing them back onto the magnet, and removing the supernatant. Subsequently, the

beads were washed twice with 200 µl of washing buffer B (WBB, comprising 10mM Tris-HCl, 150mM LiCl, 1mM EDTA, and RNase-Free H_2O). The same procedures were then followed for washing with LSB (consisting of 20 mM Tris-HCl, 150 mM NaCl, 1 mM EDTA, with RNase-Free H_2O to the needed volume).

Pellet with beads were then resuspended in cDNA reaction mix and incubate at 42 °C for 60 minutes and 70 °C for 15 minutes.

	1x
10 mM dNTP	1 µl
5 X RT buffer	4 µl
RNase Inhibitor (optional)	0.5 µl
Reverse transcriptase.	1 µl
RNase free water	13.5 µl

Following the reaction, 80 µl of water was added per preparation. Subsequently, the samples were heated at 80°C for 2 minutes and then promptly placed on the magnetic rack. The resulting supernatants containing the cDNA were carefully transferred to new Eppendorf tubes for future use.

2.3.7 Real Time Quantitative PCR

At least three biological replicates and three technical replicates were used per sample for qPCR analysis. The qPCR reaction mix is detailed below:

Reagent	**20 µl reaction**	**Final Concentration**
2x PCRBIO SyGreen Mix	10 µl	1 X
Forward Primer (10 µM)	0.8 µl	400 nM
Reverse Primer (10 µM)	0.8 µl	400 nM
Template DNA	< 100 ng cDNA	Variable
PCR grade dH_2O	Up to 20 µl	

Table 12. RT-qPCR reaction system.

Cycling conditions are listed below:

Cycles	Temperature	Time	Notes
1	95 °C	2 min	Polymerase activation
40	95 °C 60 °C to 65 °C	5 seconds 20-30 seconds	Denaturation Anneal/ Extension

Table 13. RT-qPCR cycle conditions.

The *ACTIN2* (AT3G18780) gene was selected as the reference gene for qPCR analysis, a widely adopted plant reference gene in prior studies. Gene expression levels were determined using the average of three biological replicates. The expression of the Gene of Interest (GOI) was calculated relative to the expression levels of the reference gene using the critical threshold (Ct) values for both the gene of interest and the reference gene in the following equation:

Relative Expression (GOI) = 2^ (Ct [Reference Gene] – Ct [GOI])

2.3.8 RNA-Seq Data Analysis

RNA was extracted from 5-week-old Arabidopsis hypocotyls in biological triplicate using ReliaPrep™ RNA Miniprep and subjected to RNA-seq on the Illumina platform (Novogene). 150 base paired end reads were mapped to the Arabidopsis TAIR10 genome (Ensemble-Plants, release 58) sequence with corresponding gtf file to obtain reads per gene using STAR aligner (v2.7.11a). Read count per gene was analysed using DESeq2(v1.40.2) to get p values, adjusted p values, and log2 fold changes. Sample PCA (principal component analysis) plot was generated using the plotPCA function of DESeq2 after variance stabilization transformation. Sample correlation heatmap and gene expression heatmap were generated using pheatmap (v1.0.12). GO (gene ontology) analyses were performed using PANTHER10 and the results were plotted using ggplot2 (v3.4.4). The raw sequencing dataset is available on the NCBI Gene Expression Omnibus (GEO) server under the accession number GSE263680.

2.4 Protein

2.4.1 *Nicotiana benthamiana* Infiltration

An overnight culture of Agrobacterium strain GV3103 containing the desired recombinants was utilized for the infiltration of *Nicotiana benthamiana*. The bacterial cells were centrifuged at 3000g for 10 minutes, and the supernatants were carefully removed. The resulting pellet was washed using 1 ml of infiltration buffer (consisting of 1 M pH 5.7 MES 2.5 ml, 0.5 M D-Glucose 2.8 ml, 0.05 M Na_3PO_4 $12H_2O$ 2 ml, 200 mM Acetosyringone 25 µl, with distilled water added to make a total volume of 50 ml). Subsequently, the cells were centrifuged again at 3000g for 10 minutes. These washing steps were repeated twice more. Finally, the cells in the infiltration buffer were diluted to 10^{-1} and 10^{-2}, and the OD_{600} of the 10^{-2} dilution was measured using a spectrophotometer (Eppendorf) to ensure the final OD_{600} fell within the range of 0.01-0.1. The appropriately diluted cells were then ready for use in *Nicotiana benthamiana* infiltration.

2.4.2 Transient Expression of Arabidopsis Suspension Culture Cells

For transfected Arabidopsis suspension culture, protoplasts were isolated from root cell suspension cultures (Grones et al., 2015). The suspension was subcultured every week using 7.5ml old culture and 42.5ml fresh medium (MS powder Sigma M5524 or equivalent, 4.32g/l, Sucrose 30g/l, B5 vitamin stock 2ml/l (0.05g nicotinic acid, 0.05g pyridoxine HCl, 0.5g thiamine HCl, 5g myo-inositol, made to 50ml, store aliquots at -20°C) 125 µl/ 12mg/ml 2,4D, 15 µl/l kinetin, use KOH to make final pH 5.7). The suspension culture was then kept in a sterile 250ml flask with aluminium foil cover with constant shaking (-120 rpm). The suspension can be spread on Petri dishes containing culture medium plus 0.8% phytoagar as a backup in case of possible contamination.

2.4.2.1 Protoplasting procedure

25ml 2-3d old suspension cells were transferred into a 50ml Falcon tube and centrifuged at 15000rpm for 5mins (room temperature). Supernatant and any residual

media were carefully removed. Cells were resuspended in 50ml enzyme solution: 1% cellulase, 0.2% macerozyme in about 45ml GM buffer (MS powder 4.4 g/L; 0.17M glucose: 30.5 g/L; 0.17M mannitol:30.5 g/L; pH 5.5 with KOH, Filter sterilize (0.22μm) and store at 4°C) stirred slowly for 30min RT. The enzyme solution was filtered before adding to the cells. Cells were then transferred to a large Petri dish and incubated at room temperature with gentle shaking (40-50 rpm) for 3-4h in the dark. Cell wall digestion was checked using microscopy by placing a drop of suspension on a slide. As cell walls are digested, the cell shape becomes more and more spherical.

Following the protoplasting, cells were transfected with 10 μg plasmid DNA of the appropriate vectors and overnight dark incubated at room temperature in glucose-mannitol (GM) medium). Once the majority of cells were completely round, the suspension was carefully transferred to a 50 ml Falcon tube. Cells in the Falcon tubes were centrifuged at 1200 rpm for 5 mins and the supernatant was removed. 5ml GM buffer was added and the tube was gently rotated to resuspend the cells. The final volume was adjusted to 25 ml with GM buffer and mixed with gentle rotation. 25ml cells were centrifuged again at 1000 rpm for 5 min. Supernatant was removed and the pellet was resuspended in 5ml Sucrose (S) buffer (MS powder 4.4 g/L; 0.28M sucrose: 96 g/L; pH 5.5 with KOH, filter sterilized (0.22μm) and stored at 4°C) by first adding 1ml to the side of the tube. Cells and S buffer were mixed carefully by gently rotating the tube. The remainder of S buffer was gently added in 2ml lots. Subsequently, cells were transferred to a 15ml Falcon tube and centrifuged at 800rpm for 5mins. The cells floated to the surface and a clear gradient with approximately 1-2ml of cells floating at the top, then clear solution and a small pellet on the bottom formed. If the majority of cells were not floating, the centrifugation time was increased. The upper protoplast layer was carefully removed with a Pasteur pipette and transferred to a 2ml Eppendorf tube. The protoplasts were counted and checked the quality.

2.4.2.2 Protoplast density estimating

20μl protoplasts was diluted 1:50 in GM buffer using cut pipette tips. The Buerker chamber was then assembled and added few ul suspension to each side by pipetting

next to the cover slide until the field was fully occupied. The numbers of protoplast were counted each of six Buerker cells (1 Buerker cell is composed of 16 smaller cells) and averaged (Count cells touching the inner line on top and left were included, cells touching the line on bottom and right were not). Protoplast density was calculated as the average protoplast number in the Buerker cells x 10 x dilution factor (50).

The volume of protoplast suspension required per transfection (recommended cell number: $5x10^5$ for each transfection) was calculated and then made up to 50µl with GM buffer.

2.4.4.3 Protoplast Transfection

10µg plasmid DNA was pipetted to a 2ml Eppendorf tube in 15µl distilled water. 5 x 10^5 cells were added into 50 µl per tube and mixed by tapping against the tube. 150 µl Polyethylene glycol (PEG) solution was immediately added and mixed by tapping against the tube. PEG was added quickly when cells are in contact with the DNA. Mixing continued until the suspension appeared homogenous. The mixture was then incubated 15-30min in the dark. Two washes with 0.5ml 0.275M $Ca(NO_3)_2$ each were then performed to wash PEG away, with mixing between each step by gently flicking the tube. The culture was centrifuged at 500rpm for 7 min and the supernatant was removed with a vacuum pump. 0.5ml GM buffer was added to the cells which were mixed with pipetting. The protoplasts were transferred from each tube to individual wells of a sterile 24-well microtiter plate and sealed with parafilm. The cells were then incubated in the dark for overnight, transferred into Eppendorf tubes the next day and centrifuged at 1200 rpm for 7-8 min. Moreover, the supernatant was removed with a vacuum pump and proteins from the cells were extracted using extraction buffer according to the specific needs (See 2.4.5; 2.4.6). Protein from this amount of cells is enough for ~2 lanes on protein gels for western blots.

2.4.3 SDS-PAGE

Acrylamide gel electrophoresis was employed to separate and visualize proteins based on their molecular weights. Here, the tertiary structure of the proteins loaded onto the gel was denatured, and they were coated with a negative charge through

sodium dodecyl sulfate (SDS), allowing for separation primarily by size. When an electric field was applied to the gel, the proteins separated into distinct bands, which were visualized using Coomassie staining or they were transferred to a PVDF membrane for Western blotting (refer to section 2.4.2). The gel consisted of both a stacking and a running gel, with the acrylamide percentage in the running gel varying based on the protein weights.

	10% Loading Gel (15 ml)	4% Stacking Gel (10 ml)
Distilled Water	5.9 ml	6 ml
Acrylamide (30%)	5.0 ml	1.33 ml
1.5 M Tris-HCl pH 8.8	3.75 ml	2.5 ml
10% SDS	150 µl	100 µl
10% APS (fresh)	150 µl	100 µl
TEMED	15 µl	10 µl

Table 14. The protein SDS-page running gel recipe.

In some experiments, commercial gels with gradient acrylamide percentage (NuPAGE Bis-Tris and Bolt Bis-Tris Plus Gels, Invitrogen, Thermo Fisher) were used as well.

2.4.4 Protein Extraction for Western Blot

Plant tissues were rapidly frozen in liquid nitrogen and finely ground using pre-cooled mortar and pestles. The resulting fine powder was then transferred to 1.5 ml or 2 ml Eppendorf tubes and combined with 150 µl of protein extraction buffer. The extraction buffer composition was as follows: 50 mM Tris HCl pH 7.5, 50 mM NaCl, 10% glycerol, 2 mM ethylenediaminetetraacetic acid (EDTA), 2 mM DL-Dithiothreitol (DTT), 1% protease inhibitor cocktail (SIGMA), 1% phenylmethylsulfonyl fluoride (PMSF), 1% phosphatase inhibitor cocktails 2 and 3 (SIGMA), and 1% IGEPAL. The Eppendorf tubes containing sample and buffer were vortexed for 20 seconds and then centrifuged at 4 °C for 15 minutes at maximum speed. Subsequently, 150 µl of the supernatants were carefully transferred to new tubes placed on ice.

Protein extractions were quantified using a Bradford assay. 200 µl Bio-rad protein assay (Coomassie blue), 800 µl water and 2 µl sample were added to cuvettes to

check the concentrations. For standard curve, 0, 1, 2.5, 5, 10, 15 µl of 10X bovine serum albumin (BSA) protein stock were added in cuvettes respectively instead of sample.

Following determination of protein concentration, an equal volume of loading dye was added to samples. Afterwards, samples were denatured at 94 °C for at least 5 mins and then kept on ice until use or at -20 °C for longer storage.

2.4.5 Western Blot

2.4.5.1 MES-SDS Gel Running

A volume of 5 µl of ladder and 20-30 µl of samples were loaded sequentially into a MES (2-(N-morpholino) ethanesulfonic acid)-SDS PAGE gel (Thermo Fisher Invitrogen Nupage 4%-12%). The gel was then run using a Surelock Mini-Cell Tank (Invitrogen, Thermo Fisher) with MES-SDS running buffer (1x MES-SDS running buffer: 50mM Tris-HCl, 0.1% SDS, 50mM MES, 1mM EDTA, pH 7.3) added until the ladder reached the expected protein size at the center of the gel (Voltage: 150V). Concurrently, transfer buffer was prepared along with ten 10 cm x 10 cm filter papers and a 7 cm x 8 cm membrane.

2.4.5.2 Semi-Dry Transfer

All the filter papers, membrane, and trimmed protein gel were moistened with transfer buffer (prepared freshly with 1.96 g Tris-HCl, 0.73 g glycine, 200 ml dH_2O, 300 µl 20% SDS, and 50 ml methanol, then stored at 4°C). The transfer machine surface was also moistened with transfer buffer. Five filter papers were sequentially placed, starting from the middle and moving towards both sides. A serological pipette was used to remove any bubbles after placing each filter paper.

Subsequently, the membrane was carefully positioned on the center of the filter papers, extending from the middle to the edges, ensuring a little transfer buffer was used before and after placement. Following this, the protein gel was gently laid on top of the membrane in the same manner (the serological pipette needs to be gentle as the gel

is vulnerable). The remaining five filter papers were arranged as previously described. The transfer machine was then closed and run at 20 V for 1 hour.

During this time, Tris-Buffered Saline-Tween (TBS-T) milk (5% w/v milk in TBS-T) was prepared (1x TBS-T: 100ml 10x TBS, 0.5ml Tween 20, distilled water to 1L; 10x TBS: 1M pH 8.0 Tris-HCl 100ml, 1.5M NaCl 87.66g, distilled water to 1L).

After the transfer, the membrane was rinsed with distilled water and subsequently stained with Ponceau S solution (0.5% w/v Ponceau S, 1% v/v glacial acetic acid) for 10 minutes. Once staining was complete, the Ponceau S solution was poured off, and the membrane was washed with distilled water and TBS-T to remove any excess staining.

2.4.5.3 Blotting

TBS-T milk was gently poured into a container containing the membrane. The container was securely covered and placed on a gentle shaker at room temperature for 1 hour.

2.4.5.4 Primary Antibody Incubation

The membrane was placed in a petri dish containing TBS-T milk and the primary antibody, with a ratio of antibody to TBS-T milk set at 1:2000. The petri dish was positioned on a gentle shaker in a cold room at 4 °C overnight. The primary antibody solution in TBS-T milk can be stored in a -20 °C freezer and reused for two additional rounds. Following incubation, the membrane was thoroughly washed three times, each wash lasting 10 minutes, using TBS-T.

2.4.5.5 Secondary Antibody Incubation

Subsequently, the membrane was incubated in a petri dish with TBS-T milk and the secondary antibody, maintaining a ratio of 1::5000 for the antibody to TBS-T milk (a suitable dilution ratio to minimize background interference). The petri dish was then

gently placed on a shaker at room temperature for 1 hour. Following this, the membrane underwent three washes in TBS-T, each lasting 10 minutes.

Next, ECL substrate (Thermo Scientific Pierce™ ECL Western Blotting Substrate, 32109) was applied to the membrane's surface and left to incubate for 1 minute. The protein bands on the membrane were visualized using Invitrogen@ iBright 1500 by Thermo Fisher Scientific.

2.4.6 Co-Immunoprecipitation

Co-Immunoprecipitation was performed on either *Nicotiana Benthamiana* leaves infiltrated with *Agrobacterium* harbouring plant expression vectors, or transfected Arabidopsis protoplasts as described above.

Plant tissue samples we re finely ground into a powder using mortar and pestles. Lysis binding buffer (composed of 50mM Tris-HCl, pH 7.6, 150mM NaCl, 1% NP-40, 0.1% SDS, 1mM PMSF, and Protease Inhibitor Cocktail - EDTA-Free) was added to the samples. The ratio of sample weight to lysis binding buffer was maintained at 1:1.5 to 1:2 (w/v). The resulting sample lysates were incubated on a shaker at 4 °C for 1 hour. Subsequently, the sample lysates were centrifuged for 20 minutes at maximum speed at 4 °C.

Meanwhile, 30-40 µl of magnetic beads binding to specific tag of the constructs were added to 1.5 ml/2.0 ml low DNA/protein binding tubes (normal Eppendorf tubes not recommended) and placed on a magnetic rack for 1 minute. The supernatants were then carefully removed. Washing buffer (consisting of 50mM Tris-HCl, pH 7.6, 150mM NaCl, 1% NP-40, 0.1% SDS, and 1mM PMSF) was added to the tubes. The beads to washing buffer ratio was maintained at 1:10 (v/v). The beads were resuspended in the washing buffer and then placed back on the magnetic rack to remove the supernatant. This washing step was repeated for two additional times.

300-400 µl of sample lysate was introduced to the beads and this mixture was incubated with gentle shaking at 4 °C in a cold room for 1-2 hours. Following incubation, the beads were washed 3-4 times using washing buffer (as described earlier). The

beads, along with the sample lysate, were spined down using centrifuge at 4000 rpm. Subsequently, the supernatants were carefully removed to the extent possible.

Additionally, 50-60 µl of SDS-loading buffer was carefully added to the beads (directly on the bead side). The beads were then spun down to ensure all beads had settled at the bottom of the tubes. The beads and SDS-loading buffer were boiled at 94 °C for 5 minutes and then placed on a magnetic rack for 1 minute. The resulting supernatants were transferred to new tubes for use in western blotting or stored in a -20 °C freezer for later use.

2.4.7 FRET (Fluorescence Energy Transfer)

4-week-old infiltrated *Nicotiana benthamiana* plants were utilized for Förster Resonance Energy Transfer (FRET) experiments. The infiltration process remained consistent with the one outlined in section 2.4.1. However, cells from various constructs and P19 protein which aids in improved Agrobacterium-mediated plant infection (Jay et al., 2023) were combined in a ratio of 1:1:1 (v/v/v). Overexpression constructs of PXf and ERf with CFP and YFP fluorescence tags respectively were used because CFP and YFP is one of the best pair fluorescence tags for FRET according to their overlapping excitation wavelength. The infiltrated *Nicotiana benthamiana* plants were subsequently placed in a growth cabinet for a period exceeding 48 hours, after which they were ready for microscopy observations to conduct FRET experiments.

A 0.5cm x 0.5cm tobacco leaf was trimmed and placed on a microscopy slide with water and covered with coverslip. Edges of coverslips were fixed using sellotape. The slides were then ready for observation.

FRET imaging and quantification was carried out on a Zeiss LSM880 confocal microscope. FRET images were acquired in normal channel imaging mode using two GaAsP detectors and a Zeiss Objective Plan-Apochromat 63x/1.4 Oil DIC M27 (420782-9900-799) objective lens. A 458nm laser was used to excite the CFP/FRET detection and a 514 nm laser was used to excite the YFP. Detector 1 (Ch1) had an

emission window set to 433-501 nm for CFP. Detector 2 (Ch2) had an emission window set to 500-566 nm for imaging the FRET/YFP. Calculation of FRET efficiencies used Lambda mode with the spectral detector set to a range of 409 to 607 nm and the 458 nm laser used as excitation source and a W Plan-Apochromat 40x/1.0 DIC M27 (421462- 9900-799) objective lens. Scans were taking of CFP-YFP pairs and CFP only (that gives values of Donor contribution to the FRET channel). After acquiring a spectral scan in Zen software, regions of interest (ROIs, at the location of the plasma membrane of a transformed cell) were selected within the Spectral Unmixing tool. Values corresponding to the peaks of emission for CFP and YFP were used for subsequent FRET calculations. FRET efficiency was calculated using the formula: FRET Efficiency = Fa[minus the CFP contribution] / (Fd+Fa[minus the CFP contribution]).

2.5 Histology

2.5.1 GUS staining

2.5.1.1 Staining

Plant tissues were initially collected in 50 mM phosphate buffer (100mM $NaPO_4$ Buffer pH 7.2: 28 ml 0.2M NaH_2PO_4, 72 ml 0.2M Na_2HPO_4, 100 ml ddH_2O) and subsequently treated with cold 90% acetone on ice for 5 minutes. Following this, the samples were rinsed in 50 mM phosphate buffer for an additional 5 minutes. Staining buffer (10 ml GUS Staining Buffer: 5 ml 0.1M PO_4 Buffer, 0.2 ml 10% Triton X-100, 0.1 ml 100mM Ferro, 0.1 ml 100mM Ferri, 4.6 ml ddH_2O) was added, and all samples were incubated in vacuum for 10 minutes (keeping the Eppendorf lids open). Subsequently, the staining buffer was removed, and fresh staining buffer with X-Gluc (5-bromo-4-chloro-3-indolyl-beta-D-glucuronic acid, cyclohexylammonium salt, final concentration: 2mM; 0.2 ml 100mM X-Gluc to 10 ml of Staining) was added. The samples were then incubated in a 37 °C incubator overnight.

2.5.1.2 Infiltration

The staining buffer was carefully removed, and the samples were immersed in FAA (50% ethanol, 3.7% formaldehyde, 5% acetic acid, water to volume, freshly prepared each time) for 30 minutes at room temperature with gentle shaking to fix the tissue. Following this fixation step, FAA was removed, and the tissues were sequentially incubated at room temperature for 30 minutes in 70%, 85%, and then 95% ethanol with gentle shaking for dehydration.

Commented [HQ1]: This is formaldehyde and acetic acid.

The ethanol was subsequently removed from the samples and replaced with a pre-infiltration solution (a mixture of ethanol and Technovit 7100 (Kuler Technik) base liquid in equal parts), allowing incubation for 90 minutes at room temperature with gentle shaking. The pre-infiltration solution was then carefully removed from the samples and substituted with an infiltration solution (comprising 1g hardener from the Technovit 7100 kit per 100 ml of base liquid). The samples were left to incubate overnight at room temperature for optimal infiltration.

2.5.1.3 Polymerization

The embedding cavities were initially filled halfway with the polymerization solution (comprising 15 ml of unused infiltration medium and 1 ml of Technovit® 7100 hardener 2). Subsequently, the prepared samples were carefully positioned within the cavities and the remaining space was filled adequately. The moulds containing tissues embedded in them were polymerized for 2 hours at room temperature, followed by an additional overnight polymerization at 37 °C.

After polymerization, any slightly sticky surface (inhibition layer) was removed using a lint-free disposable cloth. The embedded tissues were then ready for microtome sectioning.

2.5.1.4 Ruthenium Red staining

Sections on slides are stained by 0.05% (w/v) Ruthenium Red (dissolved in distilled water) for 5 seconds and then ready for GUS observation.

2.5.2 Clearsee

For microscopy analysis, 21-day-old seedlings were fixed in a 4% paraformaldehyde solution in PBS buffer and placed in a vacuum of 25-30 mmHg/Torr for 15-30 minutes (ensuring Eppendorf lids remained on). Subsequently, the seedlings were washed three times in PBS for 5 minutes each.

The washed seedlings were then immersed in Clearsee solution, composed of xylitol powder (10% w/v), sodium deoxycholate (15% w/v), and urea (25% w/v), for a period ranging from 4 days to 4 weeks or more, depending on the tissue type. The minimum incubation times for clearing were 4 days for leaves, roots, and moss, 7 days for seedlings, 2 weeks for pistils, and 4 weeks for mature stems. Samples treated with ClearSee could be stored at room temperature for at least 5 months.

For post-staining, cleared tissues were subjected to staining with Calcofluor White (Sigma, final concentration of 100 µg/ml) in Clearsee solution for 1 hour. After staining, the tissues were washed in Clearsee for an additional hour. In the case of transverse sections, the samples were encapsulated in 4% (w/v) agarose blocks, cut into 100 µm sections using a Campden Instruments 7000smz-2 Vibratome, and mounted with water.

For microscopy observation, the sectioned samples were mounted with Clearsee on slides, sealed with nail polish, and examined using a LSM 800 microscope (Zeiss).

2.5.3 FM4-64 staining

Infiltrated *Nicotiana benthamiana* plants were utilized for FM4-64 staining experiments. The infiltration process remained consistent with the one outlined in section 2.4.1. However, cells from various constructs and P19 (which aids in improved Agrobacterium-mediated plant infection) were combined in a ratio of 1:1:1 (v/v/v). Overexpression constructs of PXf and ERf with CFP and YFP fluorescence tags respectively. The infiltrated *Nicotiana benthamiana* plants were subsequently placed in a growth cabinet for a period exceeding 48 hours, after which they were ready for microscopy observations to conduct FM4-64 experiments.

A 0.5cm x 0.5cm tobacco leaf was trimmed and treated with 4µM FM4-64 (0.4µl 10mM FM4-64 in 1ml ½ MS liquid medium) in an Eppendorf tube. After 5 min treatment, samples were placed on a microscopy slide with water and covered with coverslip. Edges of coverslips were fixed using sellotape. The slides were then ready for observation.

FM4-64 Stock 10mM, diluted in DMSO, final concentration 4µM.

2.5.4 Phloroglucinol staining

Lignin was stained with Wiesner reagents (Adler et al., 1948). Phloroglucinol in acidic conditions gives a red-pink product with mainly the cinnamaldehyde groups present in lignins. Fresh sections embedded in 4% Agarose using Vibratome were incubated in phloroglucinol solution for 30-60 mins prior to immediate visualisation. Lignified cell walls stain red.

Phloroglucinol Solution:

EtOH 95%	100ml
HCl (conc)	16ml
Phloroglucinol	0.1g

Table 15. Phloroglucinol Solution.

2.5.5 Thin tissue Sections

For histology, tissues were embedded in silicon moulds using the JB-4 embedding kit (Sigma-Aldrich, 00226) prior to cutting by microtome. Tissue was fixed in FAA, dehydrated through an ethanol series, and infiltrated with JB4 monomer and catalyst. The resin is then hardened by addition of the accelerant from the kit. Measurement of the catalyst is critical because it controls the rate of polymerization of the plastic.

2.5.5.1 Fixation

Tissues (stem, hypocotyl) were cut into 1 cm pieces (for the inflorescence stem the 0.5 cm closest to the rosette leaves was discarded as secondary growth has often

initiated below that position and there can be a lot of variability) and fixed in FAA (for 100 ml:: 50 ml ethanol, 5 ml glacial acetic acid, 10 ml formaldehyde (37%), 35 ml distilled H_2O) for between 2h and several months.

2.5.5.2 Dehydration and JB4 Infiltration

The FAA was first removed from the tissue and subsequently replaced with 50% ethanol, 75% ethanol, then 95% ethanol in sequence on a rocking table, with each solution being used for 1 hour. Afterward, the ethanol was drained, and a mixture of 75% ethanol and 25% JB4 infiltration solution (prepared by dissolving 1.25 g of catalyst in 100.0 ml of JB4 Solution A) was introduced for 1 hour. Following this step, the solution was again replaced, this time with 50% ethanol and 50% JB4 infiltration solution for 1 hour, followed by 25% ethanol and 75% JB4 infiltration solution for 1 hour. Subsequently, the tissue was immersed in 100% JB4 infiltration solution for 1 hour, and this process was repeated overnight.

2.5.5.3 Embedding

Petri dish lid, paper towels, and an embedding mould were placed on the bench in order (bottom to top). Embedding solution (25.0 ml of infiltration solution and 1.0 ml of JB4 Solution B, thoroughly mixed) was prepared just prior to embedding.

The mould was filled with the embedding solution, and tissues were gently placed in the flooded moulds, ideally at one end to facilitate block trimming later. To prevent the formation of bubbles, parafilm was used to cover the mould. A petri dish base was positioned on top of the parafilm, with weight applied to it.

The blocks were allowed to harden overnight and then carefully removed from the mould. These blocks exhibited a colour spectrum ranging from light yellow to dark yellow or amber and were ready for sectioning after 2-5 days of complete hardening. 4 µM sections were taken on a rotary microtome fitted with a glass knife, which were mounted on glass slides, stained with 0.025% aqueous toluidine blue and mounted with histomount (Agar Scientific).

2.6 Microscopy

2.6.1 Compound Light Microscopy

Stem and hypocotyl sections were observed using a Zeiss Axioskop compound light microscopy (Carl Zeiss, Cambridge, UK), equipped with a QImaging Retiga-2000r camera (Photometrics, Marlow,UK) using x10 and x20 objectives.

2.6.2 Confocal Microscopy

Samples for localization observation were encased in 4% (w/v) agarose blocks and cut into 100 µm sections using a Campden Instruments 7000smz-2 Vibratome and mounted with clearsee and sealed with nail polish and then LSM 800 was used for observation using x10, x20 and x63 oil lenses. Excitation of fluorophores was performed as follows: GFP 488 nm using the Argon laser, calcofluor white 548 nm.

2.7 Materials

2.7.1 Chemicals

Acetosyringone (3′,5′-Dimethoxy-4′-hydroxyacetophenone) (Sigma, D134406)
Acetic acid (Sigma, A6283)
Agarose (Bioline, BIO-41025)
Antifoam A Concentrate (Sigma, A5633)
β -Mercaptoethanol (Sigma, M3148)
β -Estradiol (Sigma, E2758)
Bovine Serum Albumin (Sigma, A3294)
Calcofluor white stain (Sigma, 18909)
cOmplete™, Mini, EDTA-free Protease Inhibitor Cocktail (Sigma: 00000000-4693159001)
Chloroform (Thermo Scientific, 158210010)
D-Glucose (Melford, G32040)
Dimethyl sulfoxide (DMSO) (Sigma, D2650)
DTT (Sigma, 10197777001)

Ethylenediaminetetraacetic acid (Sigma, 03609)
Ethanol (Lab stock)
Ethidium bromide (Fisher: 10132863)
Formaldehyde (Lab stock)
FM4-64 (Merck, SCT127)
Glycerol (Melford, G22020)
Glycine (Melford, G36050)
Hexadecyltrimethylammonium bromide (CTAB) (Sigma, H6269)
Isopropanol (Proton Scientific, UN1219)
Lithium chloride (Sigma, L9650)
Liquid herbicide BASTA (Lab stock)
Methanol (Sigma, G8790)
MES [2-(N-Morpholino) ethanesulfonic acid] (Melford, M22040)
NP-40 Alternative (Sigma, 492016)
PEG (Polyethylene glycol) (Sigma, 528877)
Potassium chloride (Sigma, P3911)
Paraformaldehyde (Sigma, P6148)
Potassium Ferrocyanide (Sigma, 60279)
Potassium Ferricyanide (Sigma, 702587)
Phenylmethylsulfonyl fluoride (PMSF) (Melford, P20270)
Protein assay dye reagent concentrate (Bio-rad, 5000006)
Protease inhibitor cocktail (Abcam, ab271306)
Phloroglucinol (Sigma, 79330)
Ruthenium Red (Sigma, BCCC2445)
Sodium chloride (Melford, S0520)
Sodium dodecyl sulphate (SDS) (Sigma, 71725)
Sodium deoxycholate (Sigma, D6750)
Sodium phosphate tribasic dodecahydrate (Sigma, S7778)
Sodium phosphate (Melford, S23185)
Sodium phosphate dibasic (Melford, S2002)
Silwet-L77® surfactant
Tris(hydroxymethyl) methylamine (Mannheim, 10708976001)
TEMED (Fisher: 10549960)
Triton X- 100 (Sigma, X100)

Tween (Sigma, 85114)
Urea (Sigma, U5378)
Xylitol (Sigma, X3375)
X-β-Glucoside (Melford, B40020-1.0)

2.7.2 Enzymes

Taq Red Mix (PCRBIO: PB10.11)
Q5® Hot Start High-Fidelity DNA Polymerase (New ENGLAND Biolabs: MD493L)
Life Technologies pENTR/D-TOPO (Fisher: 10780335)
Life Technologies Gateway Cassette LR Clonase II (Fisher: 11791020)
Invitrogen SuperScript® II Reverse Transcriptase (Fisher: 18064014)
NEBuilder® HiFi DNA Assembly Master Mix (NEW ENGLAND Biolabs, E2621)
VeriFi™ Polymerase (PCRBIO, PB10.42)
Phusion® High-Fidelity DNA Polymerase (NEW ENGLAND Biolabs, M0530)
BsaI-HF®v2 Restriction Enzyme (NEW ENGLAND Biolabs, R3733S)
T4 DNA Ligase (NEW ENGLAND Biolabs, M0202S)
NEBridge® Golden Gate Assembly Kit (NEW ENGLAND Biolabs, E1601S)
qPCRBIO SyGreen Mix (PCRBIO, PB20.11)

2.7.3 Antibiotics

Kanamycin monosulphate (Melford: K0126) - 50mg/ml in H_2O
Spectinomycin (Melford S0188) - 50mg/ml in H_2O
Ampicilin (Melford A40040) - 50mg/ml in H_2O
Gentamicin sulphate (Melford: G0124) - 50mg/ml in 70% EtOH
Hygromycin B (Formedium, HYG5000) - 50mg/ml in H_2O
SulfR: Sulfadiazine sodium salt (Sigma, S6387) – 7.5mg/ml in H_2O

2.7.4 Kits

Monarch® PCR & DNA Cleanup Kit (NEW ENGLAND Biolabs, T1030S)
QIAquick Gel Extraction Kit (QIAGEN, 28704)
Monarch® Plasmid Miniprep Kit (NEW ENGLAND Biolabs, T1010L)
ReliaPrep™ RNA Miniprep Systems (Promega, Z6111)

2.7.5 Vectors

Life Technologies pENTR/D-TOPO (Fisher: K240020)
pGWB502 (Nakagawa et al., 2007)
pGWB501 (Nakagawa et al., 2007)
pMDC7 (Curtis and Grossniklaus, 2003)
pMDC43 (Curtis and Grossniklaus, 2003)
pB7FWG2 (Karimi et al., 2002)
pB7m34GW (Karimi et al., 2002)
pGGC000 (Lampropoulos et al., 2013)
pGGA000 (Lampropoulos et al., 2013)
pGGZ001 (Lampropoulos et al., 2013)
pGGZ003 (Lampropoulos et al., 2013)
JM284 (Torii et al., 1996)

2.7.6 Ladders

PCRBIO Ladder IV 1K Plus (PCRBIO, PB40.14)
PCRBIO Ladder II 10k (PCRBIO, PB40.12)
Precision Plus Protein Dual Color Standards (Bio-rad, 1016374)

2.7.7 Bacteria strain

DH5α: NEB® 5-alpha Competent *E. coli*, C2987H)
TOP10: One Shot™ TOP10 Chemically Competent *E. coli*, C404006)
GV3101: Agrobacterium tumefaciens (Rif/Gent)

2.7.8 Antibodies

HA tag Polyclonal antibody (Rabbit / IgG), working concentration 1::1000 (Proteintech, 51064-2-AP)
GFP tag Polyclonal antibody (Rabbit/ IgG), working concentration 1::1000 (Proteintech, 50430-2-AP)
DYKDDDDK Polyclonal antibody (Rabbit/ IgG), working concentration 1::1000 (Proteintech, 20543-1-AP)
Goat Anti-Rabbit IgG H&L (HRP), working concentration 1::2500, (Abcam, ab205718)

2.7.9 Beads

SpeedBead Magnetic Carboxylate (Cytiva, 45152105050250)
Oligo d(T)25 Magnetic Beads (Biolabs, S1419S)
Pierce™ Anti-DYKDDDDK Magnetic Agrose (Thermo Fisher, A36797)
Pierce™ Anti-HA Magnetic Beads (Thermo Fisher, 88836)

Chapter 3. Interactions between Receptor Kinases define Radial Pattern in *Arabidopsis*

3.1 Focused Introduction

3.1.1 ERECTA receptors regulate vascular proliferation and different development processes

ERECTA (ER) encodes a receptor-like kinase (RLK*)* involved in mediating several plant growth and developmental processes (Figure 3.1). *ER*, which was cloned more than a quarter century ago, has two paralogues, *ERL1 (ERECTA-LIKE1)* and *ERL2 (ERECTA-LIKE2),* collectively referred to as ER family (ERfs) (Torii et al., 1996).

The ligands for ERf receptors reside within the family of EPIDERMAL PATTERNING FACTOR (EPF)/EPFL-LIKE (EPFL) peptides. These peptides, which range from 45-75 amino acids in length, are encoded by eleven genes in *Arabidopsis* (Kondo et al., 2010; Sugano et al., 2010; Takata et al., 2013). And some of these peptides feature as regulators in stomatal development. EPF1 and EPF2 have been illustrated to control stomatal cell density and positioning on leaf surface. EPFL9 positively regulates stomata density and clustering (Hara et al., 2009; Hunt et al., 2010). EPFL4 and EPFL6 have been suggested to regulate vascular development (Uchida et al., 2012), although *epfl4 epfl5 epfl6* mutants demonstrate no secondary growth defects (DALBY, 2021).? However, the other functions of EPF/EPFLs are still unknown.

So far, ER has been implicated in a surprisingly diverse array of processes. Consistently with its ligand, the ERECTA family plays critical roles in stomatal development as well. ERfs, collectively regulate stomatal patterning, with ERL1 and ERL2 regulating the specification of stomatal stem cell fate and the differentiation of guard cells. *erfs* cause stomatal clustering. Interestingly, another LRR receptor-like protein TMM (TOO MANY MOUTHS) negatively regulates ER-family and conditionally required for the stomata formation in *er*. Therefore, it is possible TMM works in combinations with ERfs to control stomatal cell formation and differentiation (Shpak et al., 2005).

Moreover, these genes regulate longitudinal plant growth, with ER promoting organ elongation over a substantially large fraction of the growth period without altering the total growth duration (Chen et al., 2013). Additionally, while the *erl1* and *erl2* mutations themselves do not significantly affect plant morphogenesis, they do enhance the elongation defects observed in the presence of *er* mutation (Bundy et al., 2012; Shpak et al., 2004). *ER* also exerts control over inflorescence architecture by mediating the chromatin-mediated activation of PRE1 (PACLOBUTRAZOL RESISTANCE1), a basic helix-loop-helix (bHLH) transcription factor, which is required for pedicel cell proliferation and pedicel elongation, thereby promoting cell proliferation (Cai et al., 2017). ER influences the size of the shoot apical meristem and initiation of leaf primordia (Uchida et al., 2013). Notably, ER plays a crucial role in plant immunity as well, through chromatin-mediated promotion of the WRKY33 transcription factor, achieved via an interaction with the *BEK1* receptor-like kinase (Cai et al., 2021; Jorda et al., 2016). In the ER signaling, YDA (YODA), an Arabidopsis MAP3K (mitogen-activated protein kinase kinase kinase) has been found to function downstream of ER RLK controlling above developmental processes including stomatal and embryo patterning, inflorescence architecture, lateral organ shape and plant immunity (Bergmann et al., 2004; Lukowitz et al., 2004; Shpak, 2013; Sopena-Torres et al., 2018; Xu and Zhang, 2015).

Besides, ER is also involved in modulation to biotic and abiotic stresses (Sanchez-Rodriguez et al., 2009; van Zanten et al., 2010). In terms of biotic stresses, ER was illustrated to be a major contributor to regulation of plant transpiration efficiency and therefore contribute to water use efficiency and drought tolerance (Masle et al., 2005). Moreover, ERECTA is required for reducing plant sensitivity to heat stress to protect plants from heat stress in the ASYMMETRIC LEAVES1 (AS1) and ASYMMETRIC LEAVES2 (AS2) pathway to regulate adaxial-abaxial leaf polarity in *Arabidopsis* (Qi et al., 2004). ER has been implicated in enhancing the plant's resistance to various pathogens as well. For instance, ER is required for resistance in *Arabidopsis* to the soilborne bacterium *Ralstonia solanacearum*, the necrotrophic fungus *Plectosphaerella cucumerina*, and the damping-off oomycete *Phythium irregulare*, as *er* mutant are more susceptible to these pathogens than wild-type (Adie et al., 2007; Godiard et al., 2003;

Llorente et al., 2005). And ER has specific function in regulating cell wall-mediated resistance to pathogen in *Arabidopsis* (Sanchez-Rodriguez et al., 2009).

There are also studies that have illustrated the functions of ERECTA in secondary development of plants. Among these, ER receptors can regulate cell division and xylem fibre formation during secondary growth and repress the xylem expansion in hypocotyls (Ikematsu et al., 2017; Milhinhos et al., 2019; Ragni et al., 2011; Uchida et al., 2012). The phytohormone gibberellic acid (GA) and its signaling pathway are both necessary and sufficient to directly trigger enhanced expansion of xylem and control the shift in xylem development, but ERECTA acts locally to restrict xylem expansion downstream of the GA pathway (Fischer and Teichmann, 2017; Ragni et al., 2011). Furthermore, ER and ERL1 redundantly suppress excessive radial growth of the hypocotyl vasculature during secondary growth and prevent premature initiation of the fiber differentiation process mediated by the NAC SECONDARY WALL THICKENING PROMOTING FACTORs in the hypocotyl xylem. Besides, SOBIR1 (SUPPRESSOR OF BIR-1)/EVR (LRR-RLK EVERSHED), a gene which was identified using GWAS (genome-wide association studies)-guided reverse genetics, is a regulator of secondary growth. It physically interacts with ER and defects caused in *sobir1/evr* mutants are enhanced by ER mutations, indicating that SOBIR1/EVR and ERECTA act together in the control of the precocious formation of xylem fiber development (Milhinhos et al., 2019). Therefore, ERECTA-family receptor kinase genes redundantly prevent premature progression of secondary growth in the Arabidopsis hypocotyl (Fischer and Teichmann, 2017).

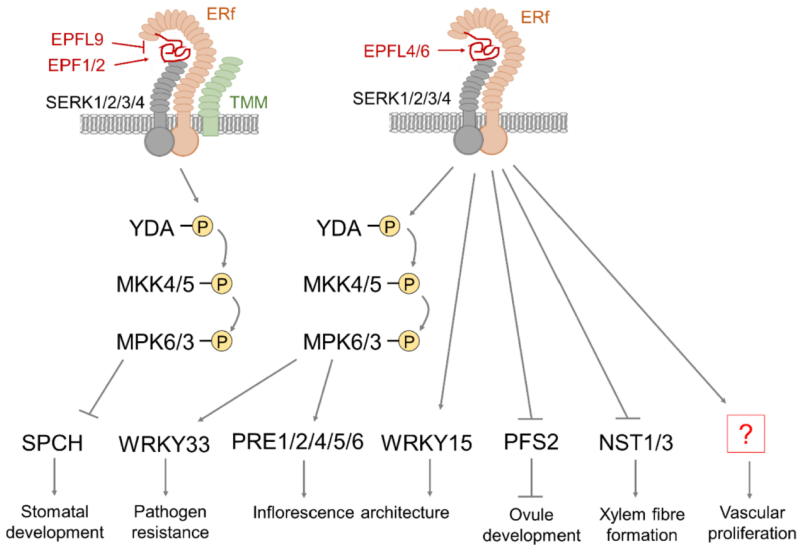

Figure 3.1 ERf signaling in diverse plant processes.

Arrows indicate positive interactions. Blunt lines indicate inhibition. '?' denotes unknown targets. The dependence of EPFL4/6-ERf-mediated regulation of WRKY15, PFS2, NST1/3 and vascular proliferation on MAPK cascades remains to be tested. See text for references and 'Abbreviations' for full protein names.

3.1.2 The PXY and ER families genetically interact

The crosstalk between RLK-mediated signalling pathways is essential in plant growth and development processes besides of the individual characteristisation. The EPFL4/6-ERf genetically interact with TDIF-PXf to control cell proliferation, cell size and organisation within plant vasculature (Etchells et al., 2013; Uchida et al., 2013; Wang et al., 2019b). In a *pxy* mutant background, as *pxf er* lines (*pxf* being *pxy pxl1 pxl2*) demonstrated fewer cells in stem vascular bundles than either *pxy er* or *pxf* lines, showing that *pxl1* and *pxl2* genetically interact with *er* (Wang et al., 2019b). *pxf erf* lines (*erf* being *er erl1 erl2*) have dramatic vascular defects including stems and hypocotyls (Figure 3.2). In hypocotyls, the sextuple mutant failed to make the transition to secondary growth, meanwhile either *pxf* or *erf* triple mutants demonstrated a delay to the onset of cambium formation, but they nevertheless still made the transition to secondary growth, although the resulting cambium is somewhat disorganized (Figure 3.2D). This analysis demonstrated that PXf and ERf genetically interact to coordinate

tissue integrity at the levels of both cell size and cell division and controls cambium stem cell initiation (Wang et al., 2019b).

The genetic interactions between PXf and ERf may be influenced by various molecular-level factors including transcriptional level, shared downstream targets regulation and protein complexes (Mani et al., 2008). Firstly, it was found that *PX*f and *ER*f signalling could regulate the expression of components of each other, potentially resulting in compensatory expression upon removal of receptors belonging to either family. Supporting this, the upregulation of ERL1 and ERL2 was observed in *pxf er* hypocotyls, implying a potential interaction where PXf and ER may collaboratively suppress ERL gene expression (Wang et al., 2019). Intriguingly, contrasting evidence indicates that PXf and ER collectively enhance the expression of EPFL6, EPFL4, ERL1, and ERL2 in inflorescence stems, underscoring the organ-specific aspect of their interaction (Wang et al., 2019).

Secondly, PXf and ERf may share downstream genes and targets in their signalling pathways. In this hypothesis, the regulation of these potential targets by PXf or ERf persists even when one receptor family is absent and the removal of both receptor families eliminates this regulation and leads to an increased negative phenotype. SERKs (SOMATIC EMBRYOGENESIS RECEPTOR KINASEs) including BRI1 associated Kinase 1 (BAK1)/SERK3 were identified as co-receptors with PXY for the TDIF peptide which induces an interaction between PXY and SERKs and SERKs are signalling components of the TDIF-PXY pathway (Zhang et al., 2016b). Xylem differentiation suppression output of TDIF-PXY signaling pathway was mediated by GSK3 (Glycogen Synthase Kinase) proteins and VND6 (VASCULAR-RELATED NAC-DOMAIN6) which is a master regulator of metaxylem formation in Arabidopsis is identified as a target of GSK3s (Han et al., 2018; Kondo et al., 2014). XVP, a NAC transcription factor was found to interact with BAK1 and form a protein complex. VND6 is downstream of XVP during xylem differentiation (Kucukoglu, 2020). However, except these, the molecular signalling components responsible for transmitting PXY signalling outputs to the nucleus are not well-understood. Similarly, components acting downstream of ER to regulate vascular proliferation are unknown. Therefore, it is possible there are co regulators of PXY and ER signalling pathways.

Commented [QH2]: The name is just XVP.

Thirdly, as we know, PXf and ERf are both located on plasma membrane, therefore it is possible for them to form protein complex to function in cambium initiation or even vascular development.

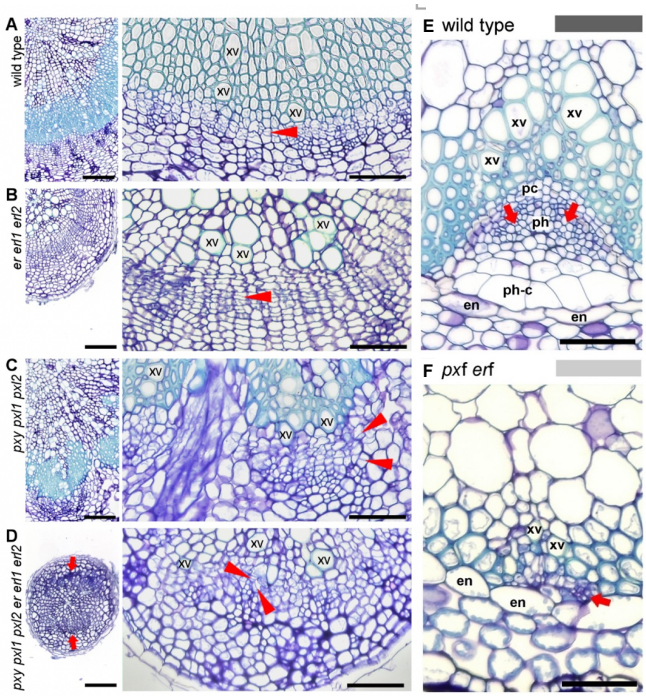

Figure 3.2 Hypocotyls and stems with differing *pxf* and *erf* mutations.

A. wild type hypocotyl

B. *erf* hypocotyl

C. *pxf* hypocotyl

D. *pxf erf* hypocotyl sections

E. wild-type stem

F. *pxf erf* stem. Phloems in *pxf erf* are marked with red arrows.

Arrowheads align with cell divisions. Scales = 100 μm (left); 50 μm (right). xv, xylem vessel.

3.1.3 PXY and ER from a structural perspective

Protein-protein and protein-ligand interactions are ubiquitous in a biological cell. virtually all biological processes are dependent on protein-protein and/or protein-ligand interactions. From a structural perspective, protein surface regions directly

contacting other proteins are known as protein-protein interfaces, whereas binding-sites for small molecule ligands are referred to as ligand-binding pockets (Gao and Skolnick, 2012). Nature may take advantage of the ligand-binding pockets by selecting and further optimizing for biological function.

Plants have developed several types of cell receptors for perception of extracellular signals, of which the extracellular leucine-rich repeat (eLRR)-containing receptors form the major class. Although the function of many plant eLRR receptors remains unclear, an increasing number of these receptors are shown to play roles in plant immunity and a wide variety of growth and developmental processes (Zhang and Thomma, 2013). Leucine-rich repeat receptor-like kinases (LRR-RKs) perceive ligands, including peptides and small molecules, to regulate various physiological processes. And leucine-rich repeat receptor-like kinases (LRR-RKs) typically contain an eLRR domain shielded by N-terminal and C-terminal flanking regions, a single-pass transmembrane domain and a cytoplasmic kinase domain. PXY and ER belong to this group.

Previous studies have revealed a conserved TDIF-recognition mechanism of PXY among plant species like *Arabidopsis thaliana*, *Zinnia elegans*, *Populus trichocarpa* and *Medicago truncatula* (Morita et al., 2016). The extracellular domain of PXY forms a twisted right-handed superhelix composed of 22 LRRs and N-terminal (residues 34–81) and C-terminal (residues 609–637) capping domains (Figure 3.3A, B). The N-terminal capping domain is assembled from a helix, a β-strand and a disordered loop (residues 61–64) that is stabilized by a disulfide bond (Cys69–Cys76; Figure 3.3A, B). The C-terminal capping domain is assembled similarly and stabilized by a disulfide bond between Cys620–Cys629 (Figure 3.3A). The crystal structure of the extracellular domain of PXY in complex with the TDIF peptide shows that the interaction occurs on the inner concave surface of PXY. A comparison of the PXY–TDIF complex structure with those of known plant LRR-RKs and their ligand complexes revealed the conserved structural features among the plant LRR-RK family members (Morita et al., 2016).

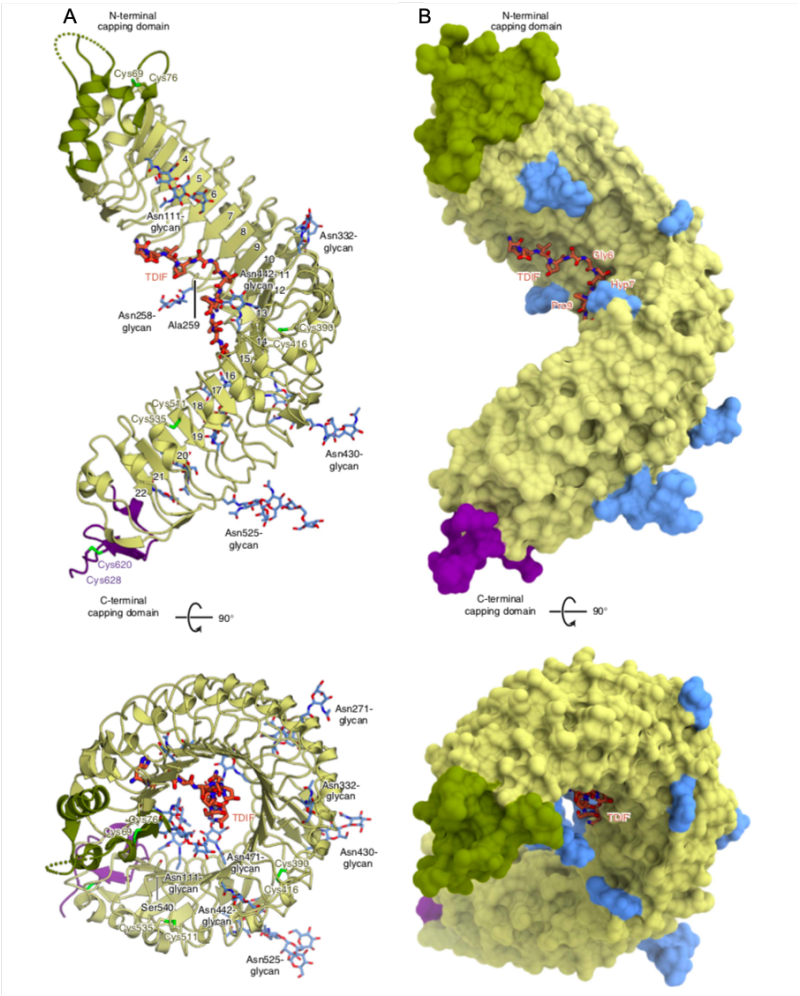

Figure 3.3 Overall structure of the TDR–TDIF complex.

A, B. Ribbon representation (A) and surface representation (B) of the crystal structure of the extracellular LRR domain of PXY in complex with TDIF. TDIF, N-linked glycans and Cys residues that form disulfide bonds are shown as orange, blue and yellow-green sticks, respectively. Two residues mutated from cysteines (Ala259 and Ser540) are also shown as sticks. The N-terminal capping domain is colored dark green. The positions of the LRRs are indicated.

3.1.4 Testing PXY-ER protein-protein interactions

Genetic interactions between PXf and ERf has been identified in previous studies. *pxy er* double mutants displayed significant changes in vascular bundle shape, with notable increase in the width: length (tangential: radial) ratio and clear intercalation of xylem and phloem. The reduced vascular cell divisions in *pxy er* compared to *pxy* or *er* single mutant suggested the genetic interactions between PXY and ER in secondary growth (Etchells et al., 2013). Additionally, *pxl1 pxl2* enhanced *pxy er* stem phenotypes, showing dramatic defects in vascular bundle shape and redistribution of vascular cell types in *pxy pxl1 pxl2 er* stem. This indicated that PXL1 and PXL2 play a crucial role in regulating radial pattern in the stem, especially in the absence of ER and PXY, supporting the notion that ER and PXf are involved in organising vascular cell layers (Wang et al., 2019b).

Furthermore, in *pxf (pxy pxl1 pxl2) erf (er erl1 erl2)* sextuple mutants, characteristic xylem and phloem cell types were present, but only very small xylem vessels were observed. Tissue layer organisation defects were apparent, with a lack of clearly defined organisation between endodermal and adjacent phloem cap cells, which seems to extend into the cortex or be absent altogether. In hypocotyls, cambium division was dramatically decreased in *pxfs erfs* mutants and they failed to undergo the transition to secondary growth while *pxf* or *erf* triple mutants nevertheless still make the transition to secondary growth, although the resulting cambium is somewhat disorganised (Figure 3.2) (Wang et al., 2019b). These results demonstrated strong interactions between PXf and ERf in vascular development. Nevertheless it is unlikely that these observations entirely explain the *pxf erf* sextuple mutant phenotype (Figure 3.2).

The overarching objective here is thus to define how PXf and ERf control cambium initiation. We have different hypothesise. Firstly, it is possible that genetic interactions between PXf and ERf are underpinned by physical interactions between the receptor proteins. If such an interaction exists it may dictate how signalling occurs. On the other hand, PXY signaling pathway involved in vascular development may share common downstream regulators with ERECTA family like co-transcription factors. Here, we sought to determine the first possibility that if PXY and ER family member form complexes.

3.2 Results

3.2.1 Physical interactions between PXf and ERf

A recent *in vitro* global analysis of receptor kinase interactions did not include direct interactions between ERf and PXf family members because putative interactions did not pass cut-offs for inclusion in the high confidence bidirectional dataset (Smakowska-Luzan et al., 2018). Nevertheless, such interactions may well occur, as they were observed between the extracellular domains of PXf and ERf family proteins in an Extracellular Interactome Assay (ECIA), which has been reported to have a relatively low false positive rate (Özkan et al., 2013). Basically, Extracellular domains of cell surface receptors and ligands mediate cell-cell communication, adhesion, and initiation of signaling events. ECIA is a a high-throughput oligomerization-based methodology for detecting extracellular interactions between individually expressed recombinant extracellular domains (ECDs) which are expressed in bait and prey formats. And these protein-protein interactions can be visualized in vivo by using oligomerized fusion proteins to stain live-dissected embryos. Strong *in vitro* interactions were found between ER and PXY, and ER and PXL1 proteins in one orientation, while PXL2 and ERL2 showed interactions in both bait-prey and prey-bait directions (Mott et al., 2019; Smakowska-Luzan et al., 2018). Therefore, the hypothesis that the genetic interactions between PXf and ERf are underpinned by physical interactions were tested at least *in vitro*.

3.2.2 Members of the PXY and ER family are expressed in overlapping domains

A prerequisite for physical interactions is their presence in the same cell types. To investigate the expression pattern of PXfs and ERfs. *pPXY::GUS*; *pER::GUS*; *pER::NLS-3xVenus*; *pERL1::GUS*; *pERL2::GUS*) transgenic Arabidopsis were obtained from previous authors and *pPXL1::GUS*; *pPXL2::GUS* transcriptional reporters were generated and then transformed into *Arabidopsis*. Homozygous transgenic lines were cultivated on ½ MS plates with sucrose for 10 days before being transferred into soil. 5-week old plants were then subjected to GUS staining (*pPXY::GUS*; *pPXL1::GUS*; *pPXL2::GUS*; *pER::GUS pERL1::GUS*; *pERL2::GUS*).

For GUS staining treated seedlings, fixation and embedding in Technovit 7100 preceded microtone sectioning. A previous study indicated that PXY expression was predominantly confined to procambial cells (Figure 3.4A) (Hirakawa et al., 2008). And GUS staining result indicated *pPXL1::GUS* and *pPXL2::GUS* expressed in the majority of hypocotyl cells with peaks within xylem and cambium (Figure 3.4B, C). ERL1 and ERL2 exhibit similar patterns with ER expression pattern which has been described previously: primarily observed in various hypocotyl cell types with two distinct peaks; the first in the cambium and xylem initials, and the second in the periderm (Figure 3.4D, E, F) (Wang et al., 2019b).

Consequently, in the case of hypocotyls, it became evident that the receptor kinases under investigation exhibited distinct expression domains. Notably, PXf and ERf shared overlapping expression in vascular tissues especially cambium, providing a plausible basis for their physical interactions.

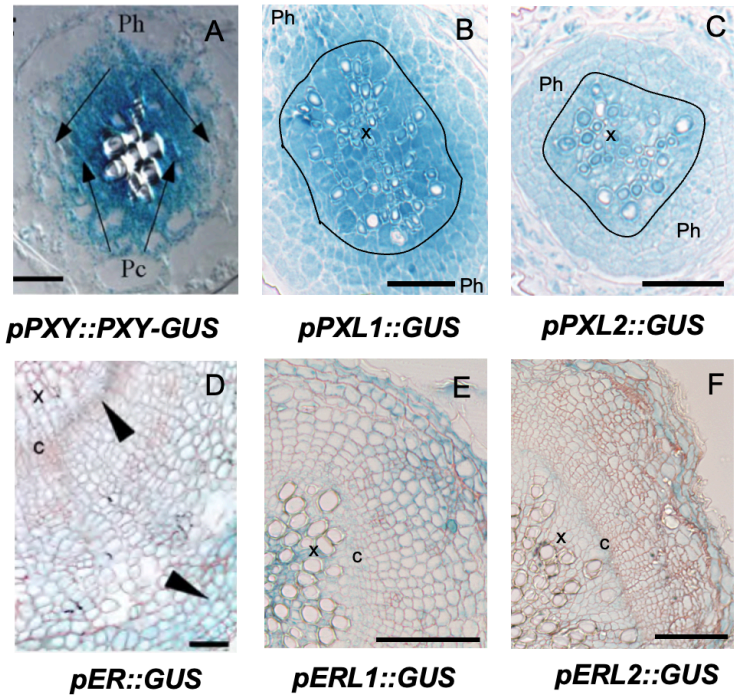

Figure 3.4 The expression patterns of *PX*f and *ER*f.

A. Vascular cell-specific localization of *PXY* in root, Ph, phloem; Pc, procambium. Scale bar: 20 μm (Hirakawa et al., 2008).
B, C. Vascular cell-specific localization of *PXL1* and *PXL2* in hypocotyls. Ph, Phloem; Xy, xylem. Scale bar: 50 μm. 7-day-old *Arabidopsis* were used.
D. *ER* expression profile in hypocotyl. x, xylem. c, cambium. Scale bar: 50 μm (Wang et al., 2019b).
E, F. *ERL1* and *ERL2* expression patterns in hypocotyls. x, xylem; c, cambium. Scale bar: 50 μm. Four-week-old plants were used.

3.2.3 Members of the *PXY* and *ER* families are co-localised at the plasma membrane

FM4-64, a red fluorescent dye, can specifically bind to cell membrane and inner membrane organelles and be used investigate endocytosis and vesicle trafficking in living eukaryotic cells. To explore whether *PX*f and *ER*f proteins co-localize at the membrane, overexpressed, and tagged constructs of *PX*f and *ER*f were cloned using gateway vector construction system. Subsequently, wild-type *N. benthamiana* plants were co-infiltrated with agrobacterium carrying *35S::PXY-CFP*, *35S::PXL1-CFP*, or

35S::PXL2-CFP and *35S::ER-YFP*, *35S::ERL1-YFP*, or *35S::ERL2-YFP*) constructs to achieve simultaneous transient expression of both a PXf and ERf protein. Following 48h-72h post- infiltration, the tobacco leaves were incubated with 4 μM FM4-64 in ½ MS for 0, 5, 10, and 15 minutes, respectively. Optical sectioning and LSM880 confocal microscopy was employed to observe co-localization events.

At approximately 10 mins after FM4-64 incubation, all transiently expressed tobacco leaves (*35S::PXf-CFP* with *35S::ERf-YFP*) exhibited presence of PXf-CFP, ERf-YFP and FM4-64 signal at the plasma membrane (Table 16). Here is an example between *35S::PXY-CFP* and *35S::ERL2-YFP*. Interestingly, they showed signals not only at the plasma membrane but also within the same vesicle (Figure 3.5A-D) while no FM4-64 signal was observed either at the membrane or in vesicles 0-min post staining (Figure 3.5E-H). And after 15-min staining, the FM4-64 signal was distributed throughout the entire cells. Transiently expressed tobacco leaves subjected to 0-minute FM4-64 staining served as control to illustrate the dynamic trafficking of FM4-64.

To analyse the images further, FIJI software was utilized to generate plot profiles. The plot profile confirmed the strong signals of CFP, YFP and FM4-64 within the same vesicle, which is consistent with the images (Figure 3.5I, J). This suggests that physical interactions between PXfs and ERfs proteins are possible at the plasma membrane and within vesicles, as family members are expressed in overlapping cell types and co-localise within cells.

	PXY+ ER	PXY+E RL1	PXY+E RL2	PXL1 +ER	PXL1+ ERL1	PXL1+ ERL2	PXL2 +ER	PXL2+ ERL1	PXL2+ ERL2
membr ane	√	√	√	√	√	√	√	√	√
vesicle s			√						

Table 16. Co-localisation between PXfs and ERfs.

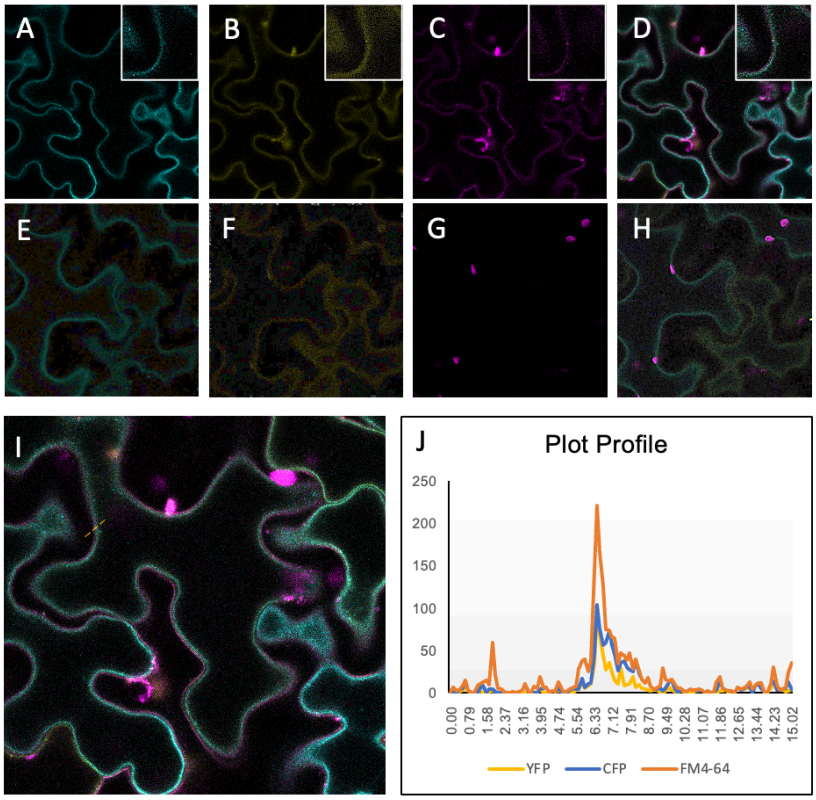

Figure 3.5 The co-localisation of PXY and ERL2.

A. Transient expression pattern of *35S::PXY-CFP* in *35S::PXY-CFP* and *35S::ERL2-YFP* co-infiltrated *N. benthamiana* after 10 min FM4-64 staining;

B. Transient expression pattern of *35S::ERL2-YFP* in *35S::PXY-CFP* and *35S::ERL2-YFP* co-infiltrated *N. benthamiana* after 10 min FM4-64 staining;

C. FM4-64 staining pattern of *35S::PXY-CFP* and *35S::ERL2-YFP* co-infiltrated *N. benthamiana* after 10 min FM4-64 staining;

D. Merged expression patterns of *35S::PXY-CFP*, *35S::ERL2-YFP* and FM4-64 of *35S::PXY-CFP* and *35S::ERL2-YFP* co-infiltrated *N. benthamiana* after 10 min FM4-64 staining;

E. Transient expression pattern of *35S::PXY-CFP* in *35S::PXY-CFP* and *35S::ERL2-YFP* co-infiltrated *N. benthamiana* 0 min post FM4-64 staining;

F. Transient expression pattern of *35S::ERL2-YFP* in *35S::PXY-CFP* and *35S::ERL2-YFP* co-infiltrated *N. benthamiana* 0 min post FM4-64 staining;

G. FM4-64 staining pattern of *35S::PXY-CFP* and *35S::ERL2-YFP* co-infiltrated *N. benthamiana* 0 min post FM4-64 staining;
H. Merged expression patterns of *35S::PXY-CFP*, *35S::ERL2-YFP* and FM4-64 of *35S::PXY-CFP* and *35S::ERL2-YFP* co-infiltrated *N. benthamiana* 0 min post FM4-64 staining.
I. Merged image of *35S::PXY-CFP* and *35S::ERL2-YFP* co-infiltrated *N. benthamiana* after 10 min FM4-64 staining was used to conduct plot profile analysis.
J. Plot profile analysis using FIJI showed strongest signal of CFP, YFP and FM4-64 at the same plot. 5-week-old *N. benthamiana* was used.

3.2.4 FRET suggests that members of the *PXY* and *ER* families are in close enough proximity to physically interact

Since interactions were observed between the extracellular domains of *PX*f and *ER*f family proteins in an Extracellular Interactome Assay (ECIA), which is reported to have a relatively low false positive rate (Ozkan et al., 2013). And given the overlapping expression and colocalization of *PX*fs and *ER*fs on the membrane, we sought to investigate if there are physical interactions between them.

To perform this analysis, we employed Förster resonance energy transfer (FRET), a nonradiative energy transfer process that occurs between an excited donor fluorophore and a nearby acceptor fluorophore. FRET allows the detection and localization of physical interactions between tagged proteins in vivo. *PX*fs and *ER*fs were fused with ECFP and EYFP protein tags, respectively, and the transiently expressed *N. benthamiana* model system was used with confocal microscopy for observation.

FRET was observed on the membrane in several combinations: 35S::PXY-CFP and 35S::ER-YFP (Figure 3.6); 35S::PXY-CFP and 35S::ERL2-YFP; 35S::PXL1-CFP and 35S::ERL2-YFP; 35S::PXL2-CFP and 35S::ERL2-YFP (Figure S3.1). The FRET result shown in the figure 3.6 was an example between PXY and ERL2.

In order to know the FRET efficiencies between PXfs and ERfs, fluorescence strength at different emission wavelengths was obtained using Confocal Microscopy LSM880 lambda mode, and FRET efficiencies were calculated and organized based on the emission wavelengths of different channels. The results indicated that the FRET

efficiency of PXY-CFP and ERL1-YFP is around 0, consistent with FRET images (Figure 3.7), suggesting no significant interaction between these two proteins. However, PXY-CFP and ER-YFP; PXY-CFP and ERL2-YFP; PXL1-CFP and ERL2-YFP; PXL2-CFP and ERL2-YFP exhibited relatively high efficiencies: 21.38%, 28.1%, 20.80% and 30.00% respectively. These efficiencies represented a significant difference from the PXY-ERL1 pair, indicating strong physical interactions between the remaining pairs tested (Figure 3.8).

Combining the results, multiple PXfs and ERfs could physically interact with each other or at least they are close enough to have physical interactions which may explain the genetic interactions between PXfs and ERfs in cambium initiation.

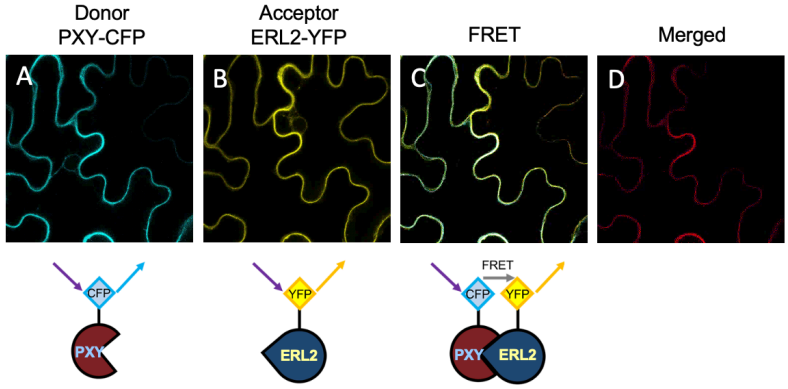

Figure 3.6 FRET example between PXY and ERL2.

A. The expression pattern of 35S::PXY-CFP in 35S::PXY-CFP and 35S::ERL2-YFP co-infiltrated *Nicotiana benthamiana*;

B. The expression pattern of 35S::ERL2-YFP in 35S::PXY-CFP and 35S::ERL2-YFP co-infiltrated *Nicotiana benthamiana*;

C. FRET between 35S::PXY-CFP and 35S::ERL2-YFP in 35S::PXY-CFP and 35S::ERL2-YFP co-infiltrated *Nicotiana benthamiana*;

D. Merged result of 35S::PXY-CFP and 35S::ERL2-YFP co-infiltrated *Nicotiana benthamiana*.

Combining the FRET images and efficiencies, the physical interactions between PXfs and ERfs on the membrane were confirmed preliminary in vivo.

Figure 3.7 FRET between PXf and ERf.

A-D. No FRET observed between 35S::PXY-CFP and 35S::ER-YFP.

E-H. FRET signal between 35S::PXY-CFP and 35S::ERL2-YFP.

I-L. FRET signal between 35S::PXL1-CFP and 35S::ERL2-YFP.

M-P. FRET signal between 35S::PXL2-CFP and 35S::ERL2-YFP.

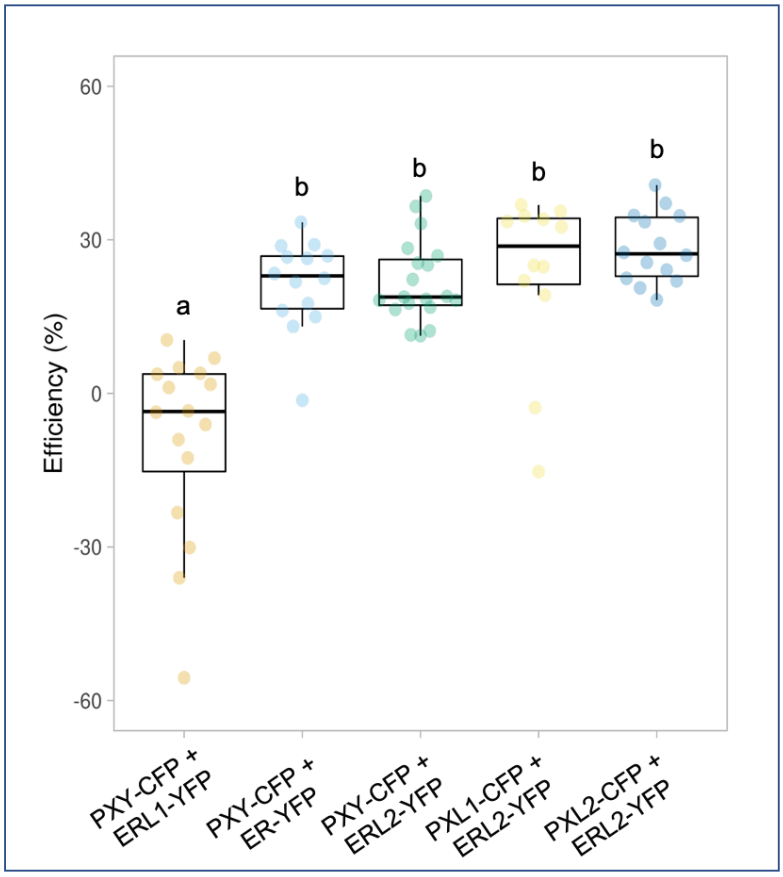

Figure 3.8. The FRET efficiencies between PXfs and ERfs.

PXY-CFP+ERL1-YFP was used as negative control, Letter above boxes mark significance groups (ANOVA and an LSD post-hoc test).

3.2.5 Members of the PXY and ER families physically interact

The FRET analysis provided insights into potential physical interactions between PXfs and ERfs. Subsequently, co-immunoprecipitation was employed to corroborate these findings. In order to explore the interactions, overexpression constructs of PXfs and ERfs with various epitope tags (*35S::PXY-FLAG*; *35S::ER-HA*; *35S::ERL2-HA*) were

prepared using gateway construct system and subsequently transformed into Agrobacterium strain GV3101 for transient expression.

Infiltration of *N. benthamiana* was performed. To confirm the successful expression of recombinant 35S::PXY-FLAG; 35S::ER-HA; 35S::ERL2-HA transient expression in *Nicotiana*, expression was validated via western blotting using anti -HA monoclonal antibodies (Proteintech) and DYKDDDDK tag monoclonal antibodies (Proteintech) respectively. In the input lanes, bands corresponding to 35S::ER-HA, 35S::ERL2-HA and a slightly larger band of 35S::PXY-FLAG (~160kDa) were observed. The slight size difference of 35S::PXY-FLAG compared to prediction may be attributed to post-translational modifications and decorations.

To determine the direct physical interactions between PXfs and ERfs, Co-IP was conducted with *N. benthamiana* infiltrated with 35S::PXY-FLAG and 35S::ER-HA or 35S::ERL2-HA. As a control to account for non-specific binding, 35S::PXY-FLAG single transiently expressed recombinant was used. P19 recombinant was co-infiltrated with PXY and ER or ERL2 to enhance the agro-injection efficiency (Jay et al., 2023). Samples were harvested 48-72 hours post injection, and total proteins were extracted. Co-IP was performed using anti HA and anti DYKDDDDK (FLAG) magnetic beads respectively, followed by western blotting to reveal the co-immunoprecipitation results. In the input samples, specific bands of PXY-FLAG; ER-HA and ERL2-HA were observed using FLAG or HA antibody respectively. As expected, specific bands for PXY-FLAG were detected following pull-downs with anti-HA beads and detected with FLAG antibodies when both PXY-FLAG and ER-HA, or PXY-FLAG and ERL2-HA were co-infiltrated. Furthermore, ER-HA or ERL2-HA were observed in samples exposed to beads and anti-HA antibodies. Thus PXY and ER/ERL2 receptor kinases formed complexes in *Nicotiana* leaves. These findings confirmed the interactions observed earlier using FRET. A specific band appeared in 35S::PXY-FLAG transiently-expressed samples when using anti-FLAG magnetic beads and flag monoclonal antibodies, and no bands were observed using anti-HA magnetic beads and anti-FLAG antibodies. This ensures that no unspecific binding of the anti-FLAG and anti-DYKDDDDK magnetic beads, further strengthening the robustness of these observations (Figure 3.9A-B).

The results from *Nicotiana bethamiana* demonstrated that PXY and ER/ERL2 interacted in plant cells, however, *Arabidopsis* suspension cultures were used to confirm the interactions within *Arabidopsis* cells. *35S::PXY-FLAG*, *35S::ER-HA*, and *35S::ERL2-HA* constructs were generated and cells carrying either *35S::PXY-FLAG* and *35S::ER-HA*, or, *35S::PXY-FLAG* and *35S::ERL2-HA* were tested for interactions. ER-HA or ERL2-HA were detected in the presence of PXY-FLAG when protein extracts were co-incubated with anti-FLAG beads. Furthermore, PXY-FLAG was detected in the presence of ER-HA or ERL2-HA, when pulled down using anti-HA beads (Figure 3.9C-D).

In summary, the combination of FRET and co-immunoprecipitation; results from both Infiltrated *Nicotiana bethamiana* leaves and *Arabidopsis* suspension culture provided robust evidence that PXfs and ERfs physically interact, potentially forming a protein complex involved in cambium initiation and vascular development.

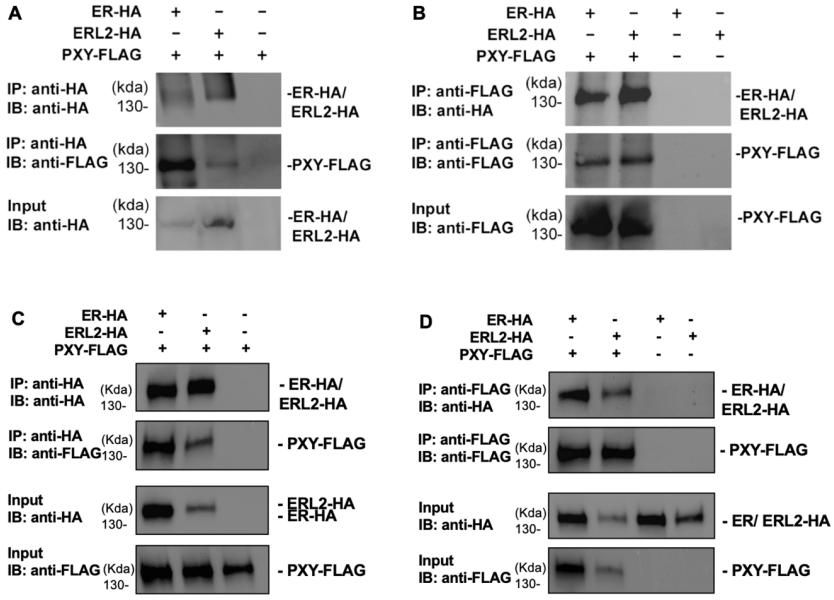

Figure 3.9 PXY and ER/ERL2 heterodimerize in *Nicotiana* epidermis and *Arabidopsis* suspension culture

A-B. Co-immunoprecipitation of PXY-FLAG with ER-HA or ERL2-HA and vice versa in *Nicotiana* epidermis.
C-D. Co-immunoprecipitation of PXY-FLAG with ER-HA or ERL2-HA and vice versa in *Arabidopsis* suspension culture.

3.2.6 *erf* mutations suppressed *IRX3::CLE41* Phenotypes

To further understand the function of *ER*/*ERL2* in PXY signalling pathway and the interactions of PXY-ER/ERL2 in vascular development, genetic analysis was performed.

TDIF, the PXY ligand, is the cleavage product of two genes, *CLE41* and *CLE44*. *CLE41* is specifically expressed in phloem. Previous studies showed that localised *CLE41* expression is important for determining cell division orientation in the vascular tissue (Etchells and Turner, 2010). Both 35S overexpression and xylem-specific promoter were used to disrupt the highly localised pattern of CLE41 (Gardiner et al., 2003; Mitsuda et al., 2007). Vascular bundles in *35S::CLE41* exhibited a notably higher cell count compared to wild-type bundles, in line with earlier findings that demonstrated how CLE41 overexpression leads to increased vascular tissue within the root (Hirakawa et al., 2008). In contrast to the highly polarized periclinal divisions observed in the wild-type procambium, *35S::CLE41* and *IRX3::CLE41* exhibited cell divisions in various orientations. The disorganized cell divisions resulted in the phloem expanding towards the centre of the stem and developing in regions where xylem is typically formed. These phenotypes are thus associated with a significant increase in signaling through *PXY* receptors (Figure 3.10). To assess whether *ER* and *ERL2* contribute to these phenotypes, *er IRX3::CLE41* and *erl2 IRX3::CLE41* lines were generated through crossing. *IRX3::CLE41* was used because of its significant xylem specific phenotypes. Homozygotes of *er* plants were identified by their phenotype, which included a compact rosette, short petioles, blunt siliques, and bright green stems and siliques due to abnormal wax layer formation (Redei, 1965). *erl2* was an insertion mutation (Shpak et al., 2004) so homozygotes were genotyped using specific primers. As for *IRX3::CLE41*, being a transgenic line, homozygotes were screened based on survival ratio derived from the plant resistance of the vector used for construct building. T_2 lines with a survival rate of 75% were selected as single insertions and used for

subsequent screening. T_3 lines with a 100% survival rate were homozygotes of *IRX3::CLE41* that were required for our study.

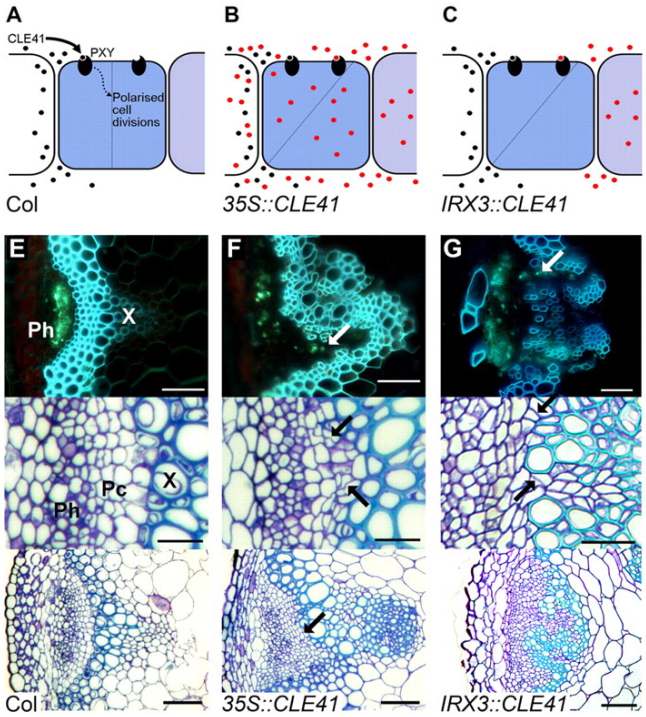

Figure 3.10 Ectopic CLE41 expression results in disrupted vascular bundles.

A-C. Diagrammatic representation of vascular cell divisions specified by *CLE41* and *PXY* in wild-type and transgenic lines. Native CLE41 is represented by black dots, CLE41 from overexpression in red.

A. In wild type, CLE41 is expressed in the phloem and signals to PXY in the procambium, thus providing positional information to the dividing cell, which sets the appropriate division plane (dotted line).

B. In *35S::CLE41* lines, the polar nature of the CLE41 signal is disrupted, resulting in loss of oriented cell division.

C. In *IRX3::CLE41* lines, the polar nature of the CLE41 signal is disrupted, resulting in loss of oriented cell division, same as the phenotype in *35S::CLE41*.

Figure adapted from (Etchells and Turner, 2010).

As shown in Figure 3.11, cambium cell divisions in wild type were restricted to a narrow ring of tissue and showed organized and oriented directions whereas ectopic disorganised cambium was apparent across the radial axis of the hypocotyl in *IRX3::CLE41* lines (Figure 3.11A, D). By contrast, aligned cell divisions in a cambial zone in a position comparable to that present in wild type plants was restored in *er IRX3::CLE41* and *erl2 IRX3::CLE41* plants (Figure 3.11E, F).

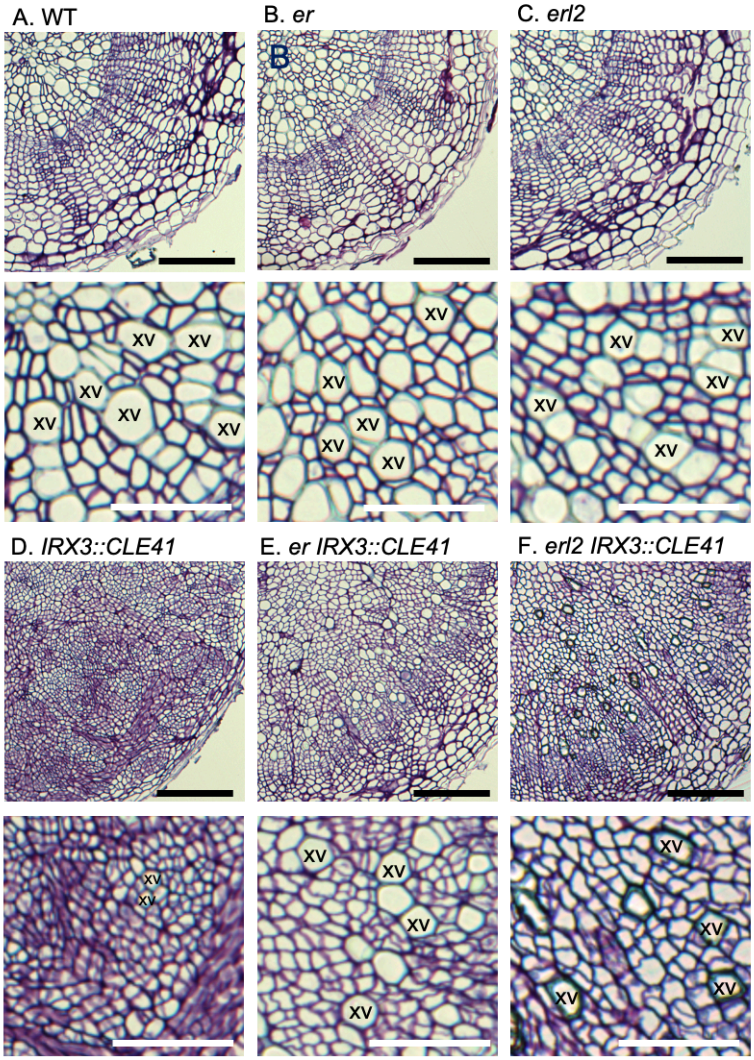

Figure 3.11 ERfs rescue *IRX3::CLE41.*

A-F Cross section of WT, *er*, *erl2*, *IRX3::CLE41*, *er IRX3::CLE41* and *erl2 IRX3::CLE41*. 5-week-old plants. JB4 embedding. 4µm sections. xv, xylem vessel. Scale bar: 100 µm (black); 50 µm (white).

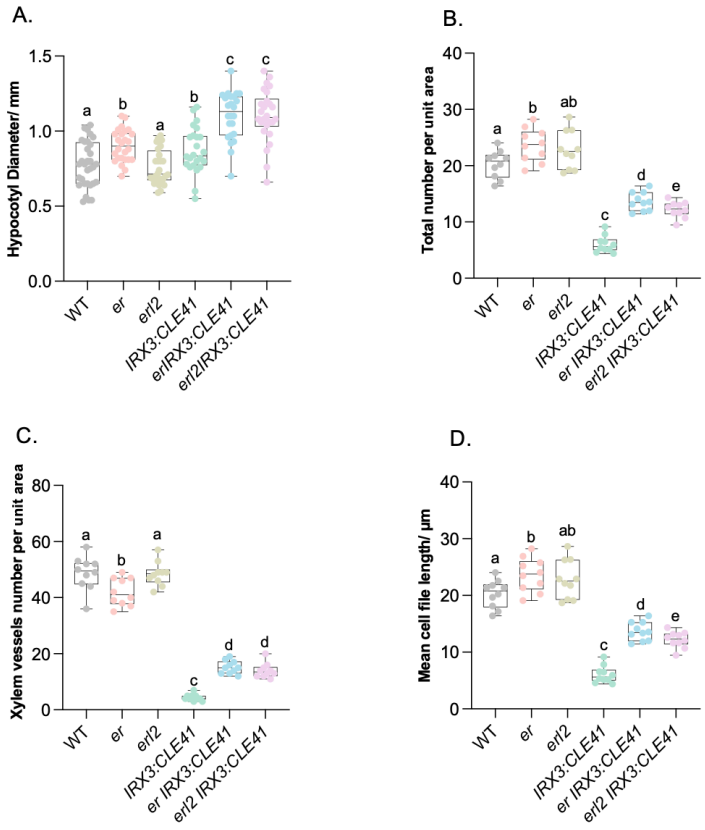

Figure 3.12 *er* and *erl2* rescue the decreased xylem vessels number and mean cell file length in *IRX3::CLE41*.

A. Boxplot showing hypocotyl diameter.
B. Boxplot showing total cells per unit area (14400 µM^2) in hypocotyl transverse sections.
C. Boxplot showing xylem vessels per unit area (14400 µM^2) in hypocotyl transverse sections.
D. Boxplot showing length of cell files running parallel to the radial axis of the stem. Letter above boxes mark significance groups (ANOVA + Tukey). Scales are 50 µM.

There also appeared to be more xylem vessels in *er IRX3::CLE41* and *erl2 IRX3::CLE41* relative to *IRX3::CLE41* (Figure 3.11). The quantitative result showed consistent result with the phenotype (3.12C).

In wild type, the centre of the hypocotyl is occupied by the xylem tissue, which is constituted of vessels, characterised by the presence of a secondary cell wall, and parenchyma which lack a secondary wall. Parenchyma are smaller than vessels but larger than dividing cambium cells. Remarkably few xylem vessels were present in *IRX3::CLE41* lines, rather the tissue was occupied predominantly with small dividing cells. By contrast, cells in the centre of the hypocotyl of *er IRX3::CLE41* and *erl2 IRX3::CLE41* lines were larger than those observed in *IRX3::CLE41* lines (figure 3.12C) suggesting that they were less mitotically active.

There also appeared to be more xylem vessels in *er IRX3::CLE41* and *erl2 IRX3::CLE41* relative to *IRX3::CLE41* (figure 3.11). Lignin is predominant in xylem secondary cell walls such as those of xylem vessels. To investigate xylem differentiation further, transverse sections of fresh tissue were taken and treated with phloroglucinol which stains lignin subunits. Here, dramatic differences were observed between *IRX3::CLE41*, *er IRX3::CLE41*, and *erl2 IRX3::CLE41*. Few lignified xylem vessels were present in *IRX3::CLE41*, but when either ER or ERL2 was mutated, many were apparent. When thin sections were analysed the proportion of xylem vessels in er *IRX3::CLE41*, and *erl2 IRX3::CLE41* had dramatically increased relative to *IRX3::CLE41*(Figure 3.13; Figure 3.12C).

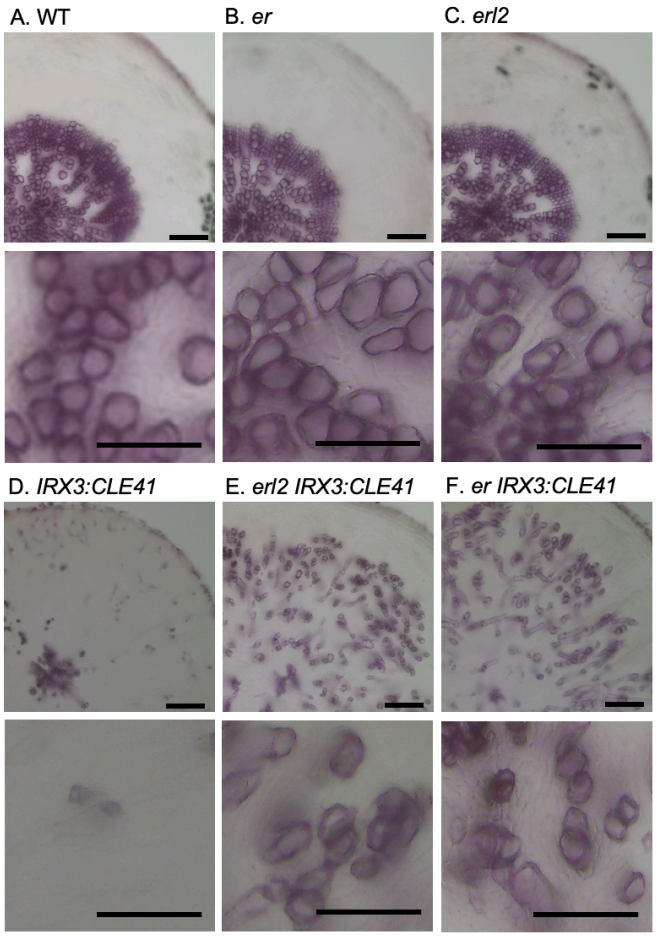

Figure 3.13 Lignin phloroglucinol Staining.

Transverse sections of fresh samples of 5-week-old WT, *er*, *erl2*, *er IRX3::CLE41*, *erl2 IRX3::CLE41* using vibratome. Thickness: 100µm; scale bar: 100µm

3.2.7 Transcriptomic results of *IRX3::CLE41* and *er IRX3::CLE41*

To better understand the processes governed by TDIF-PXY signalling to which the ER family contributes, transcriptomes *of IRX3::CLE41* and *er IRX3::CLE41* were obtained alongside hypocotyls of wild type and *er* controls (Supplemental dataset 1A).

Principal Component Analysis (PCA) and Cluster Analysis (CA) were utilized to evaluate the similarity among the four genotypes tested. On the first principal component, which explained 76% of the transcriptomic variance, *er IRX3::CLE41* exhibited greater similarity to the wild type and *er* genotypes than to *IRX3::CLE41* (Figure 3. 14A).

A corresponding outcome was observed via Spearman correlation (Figure 3.14B), where once again, *er IRX3::CLE41* clustered more closely with the wild type and *er* genotypes than *IRX3::CLE41*, validating previous phenotypic findings indicating that *er* suppressed *IRX3::CLE41*.

Consequently, differential gene expression was further investigated, with specific attention to expression alterations in *IRX3::CLE41* and *er IRX3::CLE41* to elucidate the PXY-ER interaction (Supplemental dataset 1B). Gene Ontology (GO) analysis of biological functions (Figure 3.15; Supplemental dataset 1C) supported earlier observations, indicating attenuated cell division in *er IRX3::CLE41* compared to *IRX3::CLE41* (Figure 3.13A-B, F).

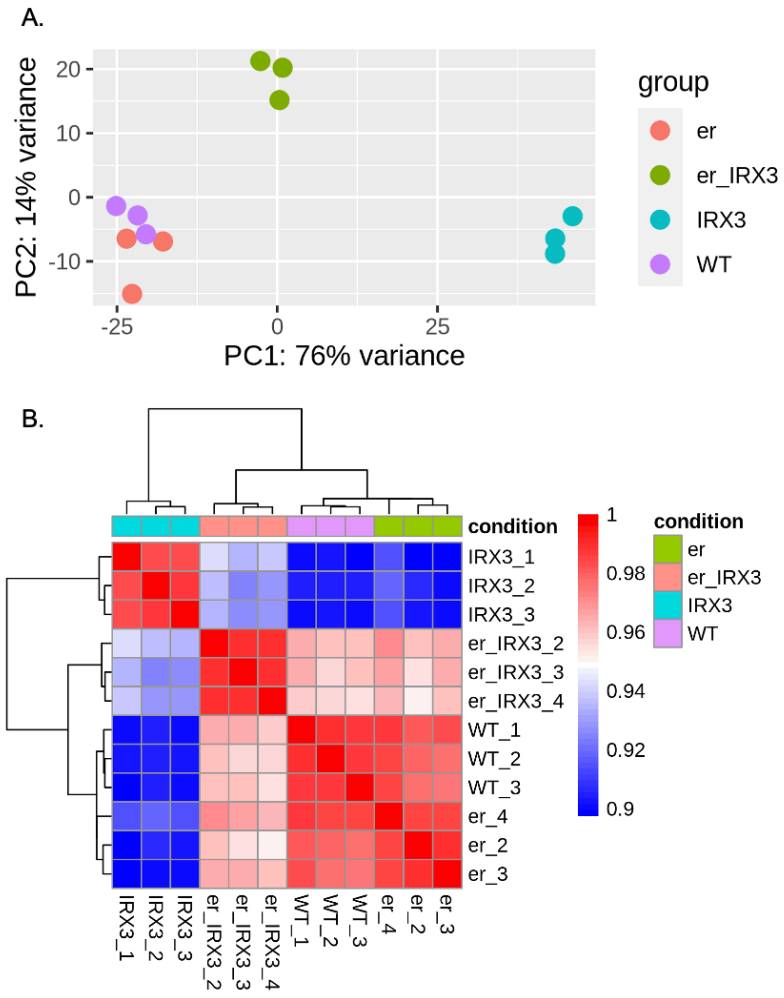

Figure 3.14. Principal Component Analysis (PCA) and Cluster analysis of *er IRX3::CLE41* transcriptome.

A. Principal Component Analysis (PCA) showed *er IRX3::CLE41* is more similar to that of wild type and *er* than *er IRX3::CLE41*.

B. Cluster analysis of wild type, *er*, *IRX3::CLE41* and *er IRX3::CLE41* transcriptomes demonstrates that of *er IRX3::CLE41* is more similar to that of wild type and *er* than *er IRX3::CLE41*.

In pairwise comparisons between these genotypes, enriched GO categories in *IRX3::CLE41* included several associated with cell division (Figure 3.15A). PXY signaling has been demonstrated to act as a positive regulator of transcriptional targets promoting cell division in the cambium. These targets comprise four cambium-expressed AINTEGUMENTA-like (AIL) transcription factors (*CAIL*s; *ANT*, *AIL5/PLT5*, *AIL6*/*PLT3*, and *AIL7*/*PLT7*), two WUSCHEL RELATED HOMEOBOX transcription factors (*WOX4* and *WOX14*). *WOX14* transcriptional targets encompass TARGET OF MONOPTEROS 6 (*TMO6*) and LATERAL ORGAN BOUNDARIES DOMAIN 4 (*LBD4*). Expression levels of all four *CAILS*, *WOX4*, *WOX14*, *TMO6*, and *LBD4* were lower in *er IRX3::CLE41* compared to *IRX3::CLE41* (Figure 3.15B).

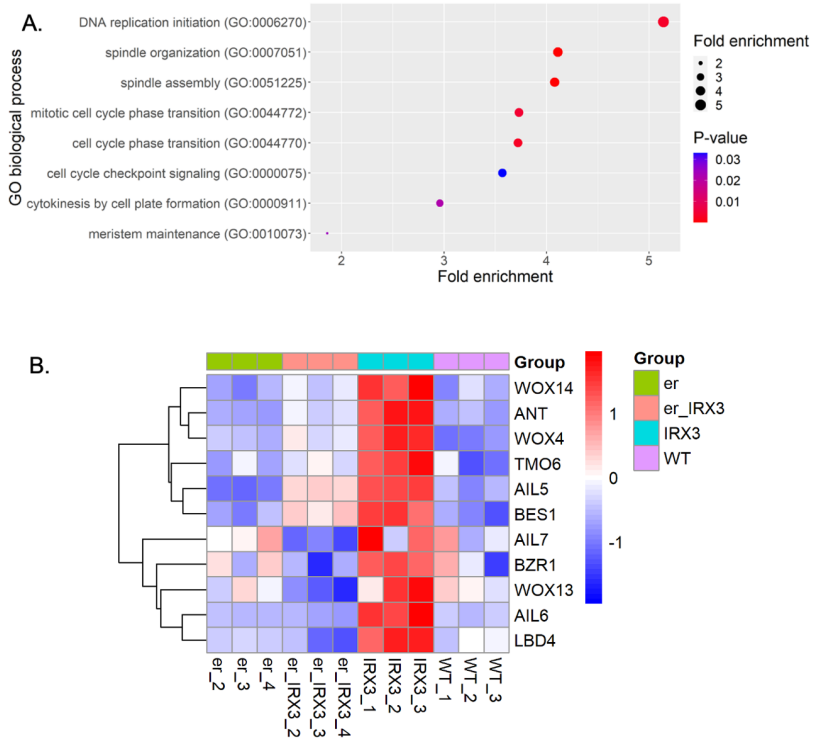

Figure 3.15 Analysis of *er IRX3::CLE41* transcriptome.

A. Biological function ontogenies associated with cell division enriched in er IRX3:CLE41 transcriptomes relative to IRX3:CLE41.
B. Heatmap showing expression of transcriptional targets of TDIF-PXY signalling in er IRX3::CLE41 relative to IRX3::CLE41.

Furthermore, GO categories enriched in *er IRX3:CLE41* relative to *IRX3:CLE41* included those associated with regulation and deposition of secondary cell walls (Supplemental dataset 1D). 23% of genes that demonstrated a higher expression in xylem cells relative to all other cell types in a high-resolution *Arabidopsis* root single cell transcriptome were up-regulated in *er IRX3:CLE41* relative to *IRX3:CLE41* representing a significant enrichment ($p = 0.0031$; Supplemental dataset 1E). Among the genes expressed at a higher level in *er IRX3:CLE41* relative to *IRX3:CLE41* were regulatory genes *KNAT7*, *MYB46*, *NAC007*, and *VRLK1*; *CAGE1*, a cytoskeleton component that directs secondary cell wall deposition; enzymes that synthesise sugar polymers that constitute the cell wall, *IRX1*, *IRX3*, *IRX9*, *IRX14*, *FRA8*, *FLA11*, *FLA12*, *CORD1*; and *XCP* which promotes programmed cell death in xylem (Figure 3.16B). The gene expression date here thus places the PXY-ER complex repressing xylem differentiation and promoting pluripotency.

To conclude, The co-immunoprecipitation and FRET data shown here demonstrated that members of the PXY and ER families of receptor kinases form complexes at the plasma membrane (Figure 3.6-9). In genetic analysis, where PXY ligand was manipulated in the presence or absence of er or erl2, we have shown that PXY-ER heterodimers influence cell division (Figure 3.11-12) and repression of xylem differentiation (Figure 3.11-13), two key components required for cambium homeostasis. We propose that the interaction between PXY and ER defines ER outputs in the cambium. It remains an interesting question for future research as to the consequences of complex formation to signal transduction. ER has previously been shown to form complexes with receptor kinase SOBIR1 to control the rate of differentiation in xylem cells (Milhinhos et al., 2019), and with receptor-like protein TOO MANY MOUTHS to define epidermal patterning (Hara et al., 2007; Lee et al., 2012), thus ER receptor heterodimerization with different tissue specific partners defines specific ER outputs within those tissues. In vascular tissue, there is abutment of tissues containing PXY-ER (cambium; Figure 3.6-7) and SOBIR1-ER (xylem) heterodimers (Milhinhos et al., 2019) likely collectively contribute to vascular tissue patterning and formation. Previously, we described loss of secondary growth in *pxy pxl1 pxl2 er erl2* lines (Wang et al., 2019b), demonstrating a genetic interaction between members of the PXY and ER receptor families. Here we have shown that this

genetic interaction underpins exclusion of xylem identity from the cambium via formation of PXY-ER receptor complexes.

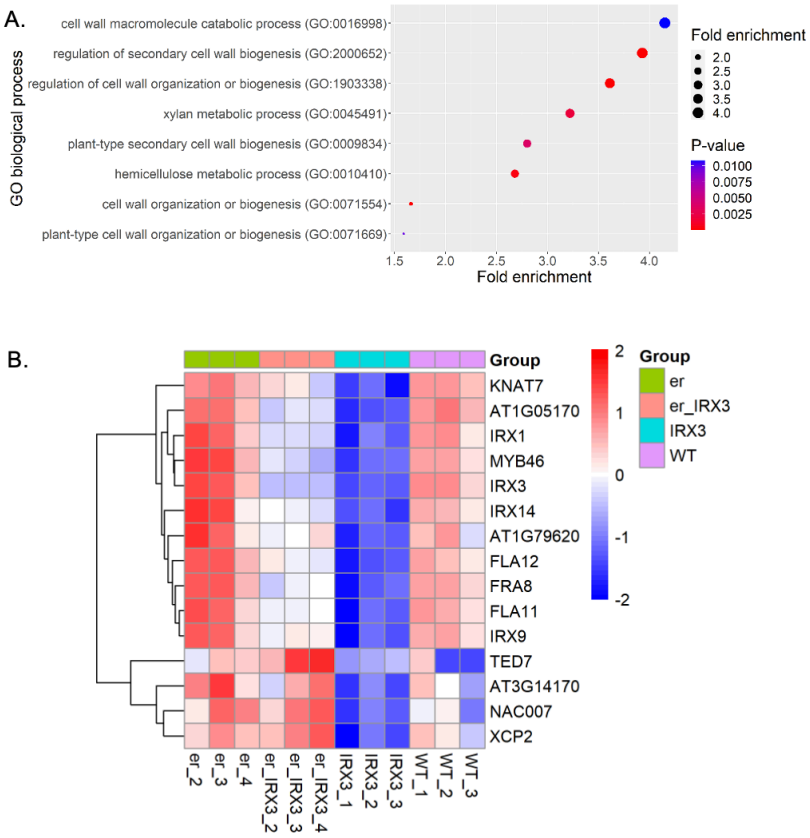

Figure 3.16 *er IRX3::CLE41* transcriptome

A. Biological function ontogenies enriched in *er IRX3:CLE41* transcriptomes relative to *IRX3:CLE41.*

B. Heatmap showing expression of select xylem-enriched genes with differential expression in er IRX3:CLE41 relative to IRX3:CLE41.

3.3 Discussion

Cellular signalling events mediated by TDIF-PXf and EPFL-ERf are crucial for proper vascular development in plants. While the genetic interaction between these two families is understood to promote cambial proliferation and maintain organisation of vascular tissues (Uchida et al., 2013; Wang et al., 2019b). The mechanism(s) underlying the genetic interaction are presently unclear. This work has highlighted a likely mechanism that the genetic interactions maybe underpinned by PXY-ER complex formation, and this was further validated using genetic aspect.

3.3.1 ER may heterodimerizes with PXY at the plasma membrane

It has been well established that TDIF-PXY signaling plays a crucial role in vascular development, and the initiation and maintenance of cambium are disrupted in its absence. This disruption is evidenced by reduced cambial cell division in triple mutants lacking PXY, PXL1, and PXL2 (PXf). These phenotypes are notably exacerbated by mutations in members of the ER family. However, in stems, due to significant disruptions in vascular morphology near the endodermis, it is plausible that these alterations are a consequence of disturbances in the organization of xylem, phloem, and procambium (Wang et al., 2019b).

A comprehensive Extracellular Interactome Assay (EICA) dataset, which identified potential extracellular interactions among Arabidopsis receptor kinases, revealed interactions involving the LRR domains of ER and PXY, ER and PXL1, and PXL2 and ERL2, albeit with low confidence levels (Smakowska-Luzan et al., 2018). GUS staining and FM4-64 imaging demonstrated overlapping expression patterns and co-localisation within cells between PXfs and ERfs (Figure 3.4-5), suggesting the potential for physical interaction.

Using Förster Resonance Energy Transfer (FRET), YFP signals were observed upon excitation of CFP (Figure 3.6-8), indicating PXY-ER and PXY-ERL2 heterodimerization. In contrast, no evidence was found for interactions between PXY and ERL1 (Figure 3.7-8). The application of FRET provided evidence suggesting close proximity and potential physical interactions between PXfs and ERfs. Interestingly, *px*f

er erl2 quintuple mutants are more severe than *px*f *er erl1* lines (Wang et al., 2019) providing genetic support for a greater role for *erl2*. Furthermore, co-immunoprecipitation (Co-IP) solidified the observed heterodimerization between PXY and ER, and PXY and ERL2, both in the *Nicotiana* system and *Arabidopsis* suspension culture. ER-HA or ERL2-HA were detected in the presence of PXY-FLAG when protein extracts were co-incubated with anti-FLAG beads. Furthermore, PXY-FLAG was detected in the presence of ER-HA or ERL2-HA, when pulled down using anti-HA beads (Figure 3.9). The EICA, FRET, and Co-IP in *Nicotiana* and *Arabidopsis* experiments all supported the hypothesised heterodimerisation between PXY and ER or ERL2 (Figure 3.6-9).

3.3.2 Novel mechanism(s) of the physical interactions

In plants, leucine-rich repeat receptor-like kinases (LRR-RKs) perceive peptides and small molecules, to regulate various physiological processes (Morita et al., 2016). They primarily engage with the extracellular domains of membrane-associated leucine-rich receptor kinases (LRR-RKs), initiating intracellular signaling cascades as a result. (Hirakawa et al., 2008; Oelkers et al., 2008). Recently, several crystal structures of receptor kinases have been revealed. The crystal structures of BRI1 and PSKR, bound with brassinolide and phytosulfokine, respectively, indicated the mechanism by which LRR-RKs recognize phytohormones (Hothorn et al., 2011; Wang et al., 2015). The crystal structures of FLS and PEPR1, interacting with the bacterial flagella-derived peptide flg22 and the self-derived danger signal Pep1, respectively, elucidated the epitope recognition mechanism employed by LRR-RKs in plant immune systems (Sun et al., 2013; Tang et al., 2015). Moreover, the plant Pattern Recognition Receptor (PRR) FLS2, a leucine-rich repeat-receptor kinase, identifies bacterial flagellin and triggers immune signaling through its interaction with another leucine-rich repeat-receptor-like kinase, BAK1 (Wang et al., 2019a).

PXY is categorized within the LRR-RK class XI subfamily, comprising an extracellular LRR domain coupled with a cytoplasmic kinase domain (Fisher and Turner, 2007). The previous study demonstrated that the crystal structure of the extracellular domain of PXY in complex with its ligand, TDIF (Zhang et al., 2016a). Furthermore, PXY forms a heterodimer reliant on TDIF with the extracellular LRR domain of SERK1, a homolog

of BAK1 (also recognized as SERK3), thereby suggesting that SERK1 functions as a co-receptor alongside PXY (Zhang and Thomma, 2013). Therefore, expanding upon the statement, one might anticipate that through the elucidation of the crystal structure, we can gain insight into the precise mechanism by which PXY forms a heterodimeric complex with ER. This structural information could provide valuable details regarding the interaction interfaces, conformational changes, and molecular determinants involved in the formation and stabilization of the PXY-ER heterodimer.

Besides, the physical interaction between PXY and ER may be post-translational modifications-mediated interactions: Receptor kinases can undergo post-translational modifications such as phosphorylation, ubiquitination, or SUMOylation, and furthermore create binding sites for interacting proteins or regulate their interaction dynamics. For instance, phosphorylation, the addition of a phosphate group to specific amino acid residues, is one of the most common and well-studied PTMs in signaling pathways. Receptor kinases can undergo phosphorylation either at their activation loop or other regulatory sites upon ligand binding or other stimuli. This phosphorylation can create binding sites for proteins containing phospho-specific interaction domains, such as SH2 or PTB domains, thereby facilitating protein-protein interactions and modulating downstream signaling cascades (Hubbard and Till, 2000).

Thus, the exploration of the details of the heterodimerization would be the next step to further understand the mechanism(s) of the interactions between PXY and ER.

3.3.3 Loss of ER attenuates PXY signalling

As one of the most extensively studied LRR-RLKs, the function of ER in vascular development is not very well understood. And it remains unclear as to how the TDIF-PXY outputs interact with ER modules in a complex network to specify vascular development.

Previous study demonstrated that, in the inflorescence stem, endodermis derived EPFL ligands signal to ER in the phloem to regulate cell division in the adjacent procambium (Uchida et al., 2012; Uchida et al., 2013). Moreover, the higher PXL expression in the stem of *er* mutants suggested that ER may attenuate PXf-related

vascular development (Wang et al., 2019b). And it was confirmed in my previous work that PXY heterodimerizes with ER/ERL2. Furthermore, in our observation, cambium cell divisions were restricted to a narrow ring of tissue in wild type whereas ectopic disorganised cambium was apparent across the radial axis of the hypocotyl in *IRX3::CLE41* lines. By contrast, aligned cell divisions in a cambial zone in a position comparable to that present in wild type plants was restored in *er IRX3::CLE41* and *erl2 IRX3::CLE41* plants (Figure 3.11-12). Other aspects of the *IRX3::CLE41* phenotype were partially suppressed. More xylem vessels were observed in *er IRX3::CLE41* and *erl2 IRX3::CLE41* relative to *IRX3::CLE41* which showed remarkably few xylem vessels. And transverse sections treated with phloroglucinol which stains lignin subunits demonstrated few lignified xylem vessels in *IRX3::CLE41*, but many more in *er IRX3::CLE41* and *erl2 IRX3::CLE41* (Figure 3.13). The reduction of cell division, restoration of the cambium ring, and increase in xylem differentiation in *er IRX3::CLE41*, and *erl2 IRX3::CLE41* plants relative to *IRX3::CLE41* controls collectively demonstrate that the PXY signalling pathway is attenuated in the absence of ER and ERL2.

It was reported that CLE/PXY signaling is multifunctional in repressing xylem development, regulating the number and orientation of cell divisions (Etchells and Turner, 2010). Our data revealed the role of ER in CLE/PXY signaling pathway in vascular development. And regulation of a receptor by another receptor is a quite common mechanism. For instance, ERECTA and BAK1 Receptor Like Kinases interact to regulate stomata patterning and immune responses in *Arabidopsis* and they function in the same protein complex (Jorda et al., 2016). But the function of the PXY-ER complex is likely to be different than that of ER-SERK, because in the ER-SERK case, the heterodimer forms the ligand binding pocket for EPF1 and EPF2 (Jorda et al., 2016). Here we suggest that ER and PXY independently bind their respective ligands and that the function of the interaction here may be that signalling is potentially coordinated in the phospho-relay.

3.3.4 ER is required for TDIF-PXY mediated repression of xylem differentiation.

Transcriptome of *IRX3::CLE41* and *er IRX3::CLE41* were obtained alongside wild type and *er* controls to further understand the contributions of ER family to TDIF-PXY associated vascular development.

The separation of *er IRX3::CLE41* and *IRX3:CLE41* on the first principal component (accounting for 76% transcriptomic variance) within the PCA, and Spearmans correlation indicated the greater similarity of *er IRX3::CLE41* to the wild type and *er* genotypes than to *IRX3::CLE41* (Figure 3.14), confirming the earlier phenotypic analysis that *er* suppressed *IRX3::CLE41* (Figure 3.11-12). Gene Ontology (GO) analysis of biological functions was used to conduct differential gene expression, highlighting that *er IRX3:CLE41* plants exhibited reduced expression of genes associated with cell division and meristem maintenance compared to *IRX3:CLE41*: *CAILS*, *WOX4*, *WOX14*, *TMO6* and *LBD4*.

Stem cell pools are generally maintained by controlled cell division, but also by exclusion of differentiation-promoting factors. Given that PXY promotes maintenance of the cambium stem cell pool, in part by excluding xylem differentiation from those cells, it follows that the reduction in expression of genes associated with cell division and meristem maintenance in *er IRX3:CLE41* relative to *IRX3:CLE41* may be concomitant with increases in those involved in xylem formation. A hallmark of xylem vessel formation is deposition of a large secondary cell wall which is a composite of cellulose, hemicellulose and lignin, followed by programmed cell death. Conversely, Figure 3.16C showed genes related to secondary cell wall regulation and deposition were upregulated in *er IRX3:CLE41*, indicating a shift towards xylem differentiation. This is further supported by the observation of increased expression of genes specific to xylem cells.

Collectively these results demonstrate that PXY signalling pathway is attenuated in the absence of ER and ERL2. PXY-ER heterodimers promote cambium cell division and exclude in xylem differentiation in cambium, and as such these developmental outputs are attenuated in *er IRX3:CLE41*, and *erl2 IRX3:CLE41* plants presumably as PXY-ER or PXY-ERL2 heterodimers would be unable to form.

3.3.5 PXY and ER may have common downstream regulators

Cellular signalling events mediated by TDIF-PXf and EPFL-ERf are crucial for proper vascular development in plants. While a synergistic genetic interaction and physical interaction between these two families is understood in cell division and xylem repression etc (Uchida et al., 2012; Wang et al., 2019b). The specific molecular mechanisms through ERf influence PXY signaling still need to be investigated. A possibility of the interaction mechanism is that they share the same downstream regulators or transcription factors. NST1 and NST3, the master regulators of xylem differentiation, were upregulated in *er erl1* plants (Ikematsu et al., 2017). Analysis of expression patterns in *nst1 nst3* mutants indicated that these transcription factors play a positive regulatory role in the expression of enzymes essential for secondary cell wall biosynthesis, notably including cellulose synthases such as IRX3 and IRX5 (Mitsuda et al., 2007). Consequently, it is possible that ER and ERL1 act to suppress premature xylem fiber formation by downregulating NST genes (Ikematsu et al., 2017; Mitsuda et al., 2007). NST1 and NST3 are critical regulators of xylem differentiation. PXY, a principal signaling pathway of vascular development may repress their expression, excluding them from the meristem. It would be straight forward to confirm the expression levels and transcriptomic relations between them. And it is possible NST1/3 to be the co downstream transcription factor of both receptor kinases.

In conclusion, the findings presented in this work indicated the physical interactions between receptor kinases in secondary development. It raises questions about the exact mechanism(s) involving the complex network of intercellular signalling events and downstream target genes underlying plant radial growth. Further investigations could delve into elucidating the specific molecular mechanisms through which ER and ERL2 influence PXY signaling. Additionally, exploring the broader regulatory networks involving other common downstream regulators or transcription factors and signaling pathways associated with cambium activity and xylem differentiation could provide a more comprehensive understanding of plant vascular development.

Chapter 4. PXY SUMOylation involved in Cambium Initiation

4.1 Focused Introduction

4.1.1 The Small Ubiquitin Modifier (SUMO)-Conjugation Pathway

Post-translational protein modification (PTM) is a dynamic process in which functional groups of varying complexity are covalently attached to proteins (Mann and Jensen, 2003). PTMs have been identified playing crucial roles in protein folding, stability, affinity, conformation and thus regulating their structure, localisation and function in response to a variety of signals (Marín-García et al., 2014; Saraswathy et al., 2011). Of all the post-translational modifications, many PTMs result from the attachment of small chemical groups such as phosphate, methyl and acetyl groups. Phosphorylation is the major player in many protein functions. Most proteins undergo some modification before undertaking any function assigned to them. Methylation is the addition of the methyl group to the lysine side chain and is, for example, responsible for chromatin transcription activity state (Saraswathy et al., 2011). Besides small chemical group addition, there are large biomolecule conjugation involved in PTMs too such as ubiquitination which is another major post-translational modification that plays important roles in protein degradation. Small ubiquitin-related modifiers are responsible for SUMO conjugation. SUMO conjugation (SUMOylation) is reversible and is involved in many developmental processes including signal transduction, protein subcellular localization, protein aggregation and the epigenetic control of transcription. SUMO family proteins are found in essentially all eukaryotes. And the roles of SUMO in plants are growing. For instance, misregulation of SUMOylation is associated with various developmental defects, such as an inability to form normal seeds in plants, embryonic patterning defects and biotic and abiotic stress defence among others (Augustine and Vierstra, 2018; Nie et al., 2009).

Small ubiquitin-related modifier (SUMO) is a highly conserved ~90 amino acid ubiquitin-like protein (Bayer et al., 1998; Mahajan et al., 1997; Matunis et al., 1996). The attachment of SUMO to lysine residues of target proteins is a multi-step process

which occurs via an enzymatic cascade involving a Ubl activating enzyme (E1), a Ubl conjugating enzyme (E2), and typically a Ubl protein ligase (E3) (Hay, 2005). The SUMO precursor is processed by a SUMO specific protease to reveal the C-terminal diglycine that is activated by the E1 enzyme (SAE1/SAE2 in humans and Aos1p/Uba2p in yeast; (Desterro et al., 1999; Gong et al., 1999; Johnson et al., 1997; Okuma et al., 1999). After transesterification onto the E2 SUMO conjugating enzyme (Ubc9), the protein target is selected (Lin et al., 2002; Tatham et al., 2003), and with the help of an E3 ligase, the SUMO is ligated to the substrate (Hay, 2005; Johnson and Gupta, 2001). SUMO can be deconjugated from the target protein by the action of SUMO specific proteases (Figure 4.1).

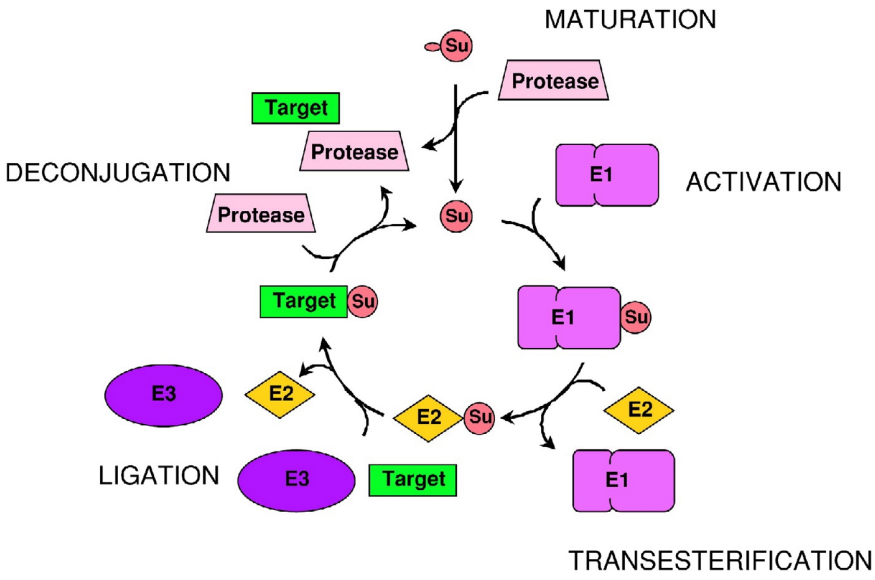

Figure 4.1 The SUMO Cycle (Hay, 2005).

4.1.2 Biological Role of SUMOylation

Although research on SUMOylation in plants remains limited, it has been demonstrated to be essential in various physiological and developmental processes. Plants with deficient SUMOylation, whether due to disruption of SUMO conjugation or

de-conjugation, exhibit defects in organ growth, reproduction, and decreased tolerance to biotic or abiotic stresses (Elrouby and Coupland, 2010).

Mutants of components of the SUMO conjugation cascade or deconjugation enzymes show dramatic phenotypes and have been instrumental in understanding the role of SUMOylation in plants. The knockouts of components of SUMO E1 and E2 enzymes are embryonic lethal, demonstrating that SUMO conjugation is essential for plant viability (Saracco et al., 2007). The SUMO E3s, SIZ1 (SAP AND MIZ1 DOMAIN-CONTAINING LIGASE1) and MMS21 (METHYL METHANE SULFONATE SENSITIVITY), SUMO protein ligases, play a predominant role. The single mutant of SIZ1 or MMS21 showed strong phenotype and could not be complemented by overexpression of the other and the double mutant *siz1 mms21* is embryonic lethal, therefore they are essential for viability and have diverse roles in plants physiology (Saracco et al., 2007). *siz1* mutant showed a dwarf-like shoot phenotype with accumulation of salicylic acid (SA), and the expression of nahG, a bacterial salicylate hydroxylase that catabolizes SA, in *siz1* reduced the SA level and suppressed dwarfism. Moreover, *SIZ1* gene regulates cell division and elongation through regulating the SA level (Miura et al., 2010).

SUMO proteases absence also shows strong phenotypes with higher expression levels of SUMOylated proteins compared to wild type plants. The SUMO protease mutant *esd4* (*early in short days4)* shows a dwarf phenotype with various developmental abnormalities (Reeves et al., 2002), while double mutant of proteases, *ots1(overly tolerant to salt1) ots2 (overly tolerant to salt2)* show sensitivity to salt stress. Consistent with the phenotype of double mutant *ost1 ost2*, overexpression of *OTS1* in wild type plants showed increased resistance to salt stress (Conti et al., 2008).

Besides, SUMO is implicated in stress responses. Previous studies showed that SUMOylation can be induced by drought, salt, high temperature etc (Conti et al., 2008; Kurepa et al., 2003; Yoo et al., 2006). The E3 MMS21 negatively regulates drought resistance. The expression level of MMS21 decreased by drought treatment. *mms21* mutants showed higher drought tolerance than wild type plants while overexpression of MMS21 was less tolerant. MMS21 acts by repressing the expression of stress genes through abscisic acid signalling (Zhang et al., 2023). Proteomic analyses of

SUMOylation during heat shock treatment has indicated that the heat stress induced increased SUMOylation of the same SUMOylated proteins under normal conditions rather than SUMOylation of new targets. And the increased SUMOylation results in differential gene expression: the highest increase in SUMOylation were RNA, chromatin related genes and the heat shock protein transcription factor HSF2A (Miller et al., 2010).

The E3 ligase has been confirmed to function in nutrient assimilation processes. Phosphate starvation leads to induction of lateral roots to increase phosphate uptake. SIZ1 can negatively regulate this process through auxin patterning. During phosphate starvation, SIZ1 protein expression level decreased and furthermore led to expression changes of various genes associated with root development (Miura et al., 2011) as well as genes involved in phosphate uptake, transport and assimilation (Miura et al., 2005).

SUMOylation is involved in plant hormone regulation pathways including SA, ABA and GA. While SIZ1 is essential for correct SA signalling (Miura et al., 2010), the SUMOylation of the transcription factors MYB30 and ABI5, which interact in ABA signalling, inhibits their activity (Finkelstein and Lynch, 2000), but SUMOylation also protects ABI5 from proteasome degradation (Miura et al., 2009). Apart from SA and ABA, SUMOylation plays a crucial role in gibberellins signalling pathway. GA binding to its receptor GID1 enables association of GID1 with DELLAs and result in the ubiquitin-mediated proteasomal degradation of DELLAs, leading to growth promotion. DELLA-dependent growth control can be regulated independently of GA. These DELLA genes undergo rapid SUMOylation under stress. Moreover, a SUMO-interacting motif in GID1 binds to SUMO-conjugated DELLA in a GA-independent manner. The consequent sequestration of GID1 by SUMO-conjugated DELLAs leads to an accumulation of non-SUMOylated DELLAs, resulting in beneficial growth restraint during stress (Conti et al., 2014).

4.1.3 RLKs are SUMOylated in Plants

SUMOylation is emerging as a key PTM in plants. Previous research has revealed that many receptor-like kinases (RLKs) were SUMOylated and the SUMOylation of

these RLKs plays important roles in different developmental processes of plants. Receptor-like kinases (RLKs) constitute a substantial gene family within the RLK/Pelle family in plants, featuring a cytosolic domain with Ser/Thr kinase activity (Osakabe et al., 2013). Arabidopsis alone possesses over 600 members of this gene family (Shiu et al., 2004). RLKs are recognized as pivotal regulators of plant architecture and growth patterns, and they also play crucial roles in defence mechanisms and stress responses (Marshall et al., 2012). And Receptor-like kinases (RLKs) fulfil significant functions in sensing extracellular signals and initiating downstream pathways by phosphorylating their intracellular serine/threonine kinase domains.

Brassinosteroids (BRs) are a class of steroid molecules perceived at the cell surface that act as plant hormones. The activity of BR receptor BRASSINOSTEROID INSENSITIVE1 (BRI1) is found to be targeted and regulated by SUMOylation. BRI1 is SUMOylated *in planta* on two lysine residues and BRI1 deSUMOylation acts as a mechanism necessary to keep temperature responses in check and as such represents a means of molecular crosstalk mechanism between temperature and BR signalling (Naranjo-Arcos et al., 2023) (Figure 4.2A-C). Another receptor-like kinase, FLAGELLIN-SENSITIVE 2 (FLS2) receptor, perceives bacterial flagellin which in turn activates BAK1 and the cytoplasmic-kinase BIK1 to form an active co-receptor complex to initiate antibacterial immunity in *Arabidopsis*. Flagellin induces the conjugation of SUMO protein to FLS2 to trigger release of BIK1. Disruption of FLS2 SUMOylation can abolish immune responses and then result in susceptibility to bacterial pathogens in Arabidopsis and flagellin can also enhance FLS2 SUMOylation to promote BIK1 dissociation and trigger intracellular immune signalling (Orosa et al., 2018) (Figure 4.2D). Therefore, RLKs may serve as the archetypal plant receptor protein in the study of post-translational modifications (PTMs) and their interplay and their role in signalling/signal integration.

Based on previous study, PXY-mediated TDIF sequestration generates a robust patterning mechanism. And the localization of the cambial stem cells as well as cambium size were determined by the auxin and TDIF gradients. The patterning mechanism or the sequestration flexibly enables adjustment of both phloem to xylem ratio and overall growth. CAILs were shown to be activated by TDIF-PXY mechanism

(Eswaran et al., 2023). Therefosre, the sequestration

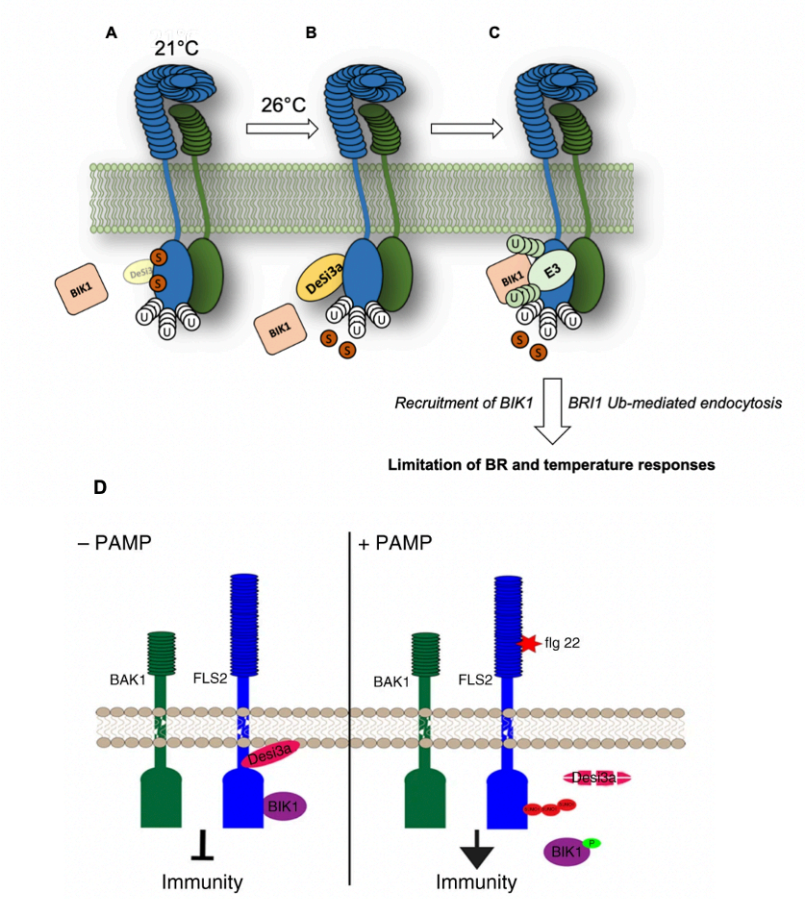

Figure 4.2 RLKs are SUMOylated in Plants.

A-C. Model for Desi3a function in the control of BR signaling at 21°C and 26°C. A. At standard growth temperature (21°C), Desi3a SUMO protease levels are low and BRI1 is SUMOylated at residues K1066 and K1118. B. At warmer growth temperature (26°C), Desi3a accumulates leading to the deSUMOylation of BRI1. C. DeSUMOylated BRI1 shows increased interaction with the negative regulator of the brassinosteroid signaling pathway BIK1 and promotes BRI1 internalization from the plasma membrane. These two parallel mechanisms downregulate BRI1,

thus preventing plants from over-growing in response to temperature elevation. We postulate that the increased internalization and degradation of BRI1 observed at 26°C results from the ubiquitination of BRI1 at residues K1066 and K1118 (Orosa et al., 2018).
D. A schematic of flg22-mediated SUMO conjugation of the FLS2 receptor during PAMP signalling. In the presence of flg22 (+PAMP) FLS2 SUMOylation facilitates the release of BIK1 from the FLS2-BAK1 immune complex. This is concomitant with the flg22-dependant degradation of Desi type SUMO protease, Desi3a (Sun et al., 2013).

Therefore, we hypothesize that PXY is SUMOylated and is likely to be significant on affecting TDIF-PXY signaling pathway through or even the vascular development. Both PXY-ER interactions, and PXY turnover will dictate how signaling occurs. Having determined whether and how these events occur, we will determine how they fit together in a single system. What is the relative importance of these phenomena?

4.2 Results

4.2.1 Loss of PXY SUMOylation retards PXY signalling

While research on the SUMOylation of receptor-like kinases (RLKs) is still in its early stages, several studies have highlighted the role of RLKs' SUMOylation in plant growth and development. For instance, the SUMOylation of the BR (Brassinosteroids) receptor BRASSINOSTEROID INSENSITIVE1 (BRI1) has emerged as a novel modification that targets BRI1, regulating its activity. The control of BRI1 SUMO conjugation is exerted by the Desi3a SUMO protease. Consequently, the deSUMOylation of BRI1 acts as a molecular interface linking temperature cues with BR signalling, enabling plants to convert environmental stimuli into growth responses (Naranjo-Arcos et al., 2023).

Furthermore, the activation of the SMALL UBIQUITIN-LIKE MODIFIER (SUMO) protein conjugation to FLS2 (FLAGELLIN-SENSITIVE 2) is initiated by flagellin, leading to the release of BIK1. Disruption of FLS2 SUMOylation can abolish immune responses, rendering Arabidopsis susceptible to bacterial pathogens. Notably, the involvement of Desi3a in plant immunity has also been established (Orosa et al., 2018). These findings collectively underscore the significance of this post-translational modification in both plant growth and development as well as in plant immunity.

Previous investigations to determine whether PXY undergoes SUMOylation demonstrated that and its role in vascular development. Immunoprecipitation (IP) was performed using anti-HA beads, followed by Western blot analysis using α-HA/α-SUMO1/2 antibodies with proteins from two different *pPXY::PXY-HA* transgenic Arabidopsis lines: pPXY::PXY-HA-573 and pPXY::PXY-HA-874 (Beatriz Orosa & Ari Sadanandom, personal communication). The results revealed the presence of PXY-SUMO in pull-down assays using anti-HA beads and α-HA antibody, as well as anti-HA beads and α-SUMO1 antibody, providing evidence that the receptor-like kinase PXY undergoes SUMOylation in vivo (Figure 4.3).

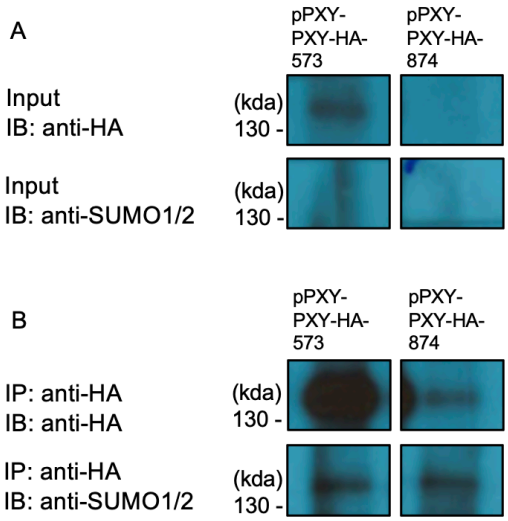

Figure 4.3 PXY is SUMOylated.

A. Western blot using total protein extracted from *pPXY::PXY-HA* transgenic Arabidopsis with anti-HA/ anti-SUMO1 antibody.

B. Immunoprecipitation using *pPXY::PXY-HA* transgenic Arabidopsis using anti-HA beads and anti-HA/ SUMO1 antibody showed PXY is SUMOylated. pPXY::PXY-HA-573 and pPXY::PXY-HA-874 are two different transgenic lines. Data obtained from Beatriz Orosa & Ari Sadanandom.

4.2.2 Publicly available datasets suggest that PXY is SUMOylated

To further investigate the hypothesis that PXY is SUMOylated, and to putatively identify SUMOylated lysines, the protein sequence of PXY was scanned potential SUMO binding sites using the bioinformatics software, HyperSUMO (Nelis, 2014) as shown in Table 17. Potential SUMO binding sites (K130, K216, K252, K645, K720 and K735) were identified in PXY.

Protein	Position	Type	Confidence	Sequence
AtPXY	K735	I	99	VYKAEM

AtPXY	K130	II	87	LTKLTT
AtPXY	K216	II	86	GGKLPP
AtPXY	K252	II	87	NLKYFD
AtPXY	K645	II	89	HHKEER
AtPXY	K720	II	91	LSKTDN

Table 17. SUMO sites prediction for PXY.

4.2.3 Generation of lines with putative SUMO sites deleted

Although the prediction of SUMO sites in PXY identified 6 potential sites, only three of them are located within the kinase domain: K645, K720, and K735. As the remaining sites were located on the extracellular domain of PXY, there would be no mechanism for their modification. Using this information, we generated 8 constructs in which the three lysine residues were substituted with arginines: *pPXY::PXY(Lys645►Arg)-HA*; *pPXY::PXY(Lys720►Arg)-HA*; *pPXY::PXY(Lys735►Arg)-HA*; *pPXY::PXY (Lys646►Arg; Lys720►Arg; Lys735►Arg)-HA*; *35S::PXY(Lys645►Arg)-HA*; *35S::PXY(Lys720►Arg)-HA*; *35S::PXY(Lys735►Arg)-HA*; *35S::PXY (Lys646►Arg; Lys720►Arg; Lys735►Arg)-HA*. These constructs were generated using NEB VeriFi Mix from cDNA derived from 7-day-old Col-0 seedlings (see Methods 2.3.1). Overlapping primers encompassing the mutation sites, along with a forward primer containing -CACC and a reverse primer incorporating an HA tag, were designed. NEBuilder was employed to ligate the overlapped segments of the gene. The resulting PCR products were purified using beads (see Methods 2.3.1) and subsequently cloned into the entry vector pENTR/D-TOPO (see Methods 2.3.3.1). The constructs were then transformed into E. coli DH5α (see Methods 2.2.3), and clones were screened by PCR using M13F/R primers (see Method 2.3.1). Two colonies for each construct were selected for plasmid purification, followed by in-house sequencing via DBS Genomics. Constructs containing the accurate gene sequence were subsequently cloned into Gateway® destination vectors pGWB501 or pGWB502 using LR clonase (see Methods 2.3.3.2). Confirmed PXY SUMO-mutated clones in pGWB501/pGWB502, identified via colony PCR with AttB primers, were then

transformed into the Agrobacterium strain GV3101 for transient expression (see Methods 2.2.4).

To confirm PXY SUMOylation in vivo, wild type (WT), *pPXY::PXY-HA*, *pPXY::PXY (Lys645►Arg)-HA*, *pPXY::PXY(Lys720►Arg)-HA*, *pPXY::PXY(Lys735►Arg)-HA*, and *pPXY::PXY (Lys646►Arg; Lys720►Arg; Lys735►Arg)-HA* transiently expressing tobacco were used for Immunoprecipitation. Anti-HA beads and α-SUMO1 primary antibody were utilized. The WT served as the negative control, showing no PXY-SUMO band, while *pPXY::PXY-HA* served as the positive control with the strongest PXY-SUMO signal. All transgenic tobacco lines with PXY SUMO site mutations displayed a diminished PXY-SUMO signal, with the triple PXY SUMO mutation line exhibiting barely any band in Figure 4.4. The IP results confirmed the PXY SUMOylation and the constructs mutating PXY SUMOylation sites are working properly.

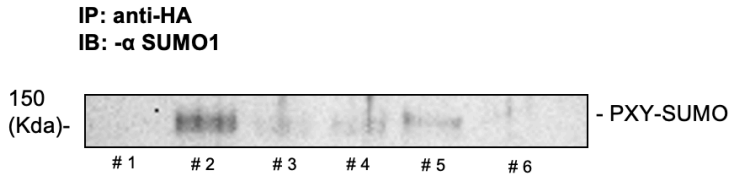

Figure 4.4 Level of PXY SUMOylation decreased when PXY SUMO sites were mutated.

#1. wild type; #2. *pPXY::PXY-HA*; #3. *pPXY::PXY (Lys645►Arg)-HA*; #4. *pPXY::PXY (Lys720►Arg) -HA*; #5. *pPXY::PXY(Lys735►Arg)-HA*; #6. *pPXY::PXY (Lys646►Arg; Lys720►Arg; Lys735►Arg)-HA* transient expressed tobacco. Three technical replicates were conducted.

4.2.4 Loss of PXY SUMOylation affect vascular development

In order to investigate the function of PXY SUMOylation in vascular development, eight constructs: *pPXY::PXY(Lys645►Arg)-HA*; *pPXY::PXY(Lys720►Arg)-HA*; pPXY::PXY(Lys735►Arg)-HA; *pPXY::PXY (Lys646►Arg; Lys720►Arg;*

Lys735►Arg)-HA; *35S::PXY(Lys645►Arg)-HA*; *35S::PXY(Lys720►Arg)-HA*; *35S::PXY(Lys735►Arg)-HA*; *35S::PXY (Lys646►Arg; Lys720►Arg; Lys735►Arg)-HA* were transformed to WT and *pxy* Arabidopsis using floral dipping method (see Method 2.1.5). Due to time constraints, only the *pxy pPXY::PXY (Lys646►Arg; Lys720►Arg; Lys735►Arg)-HA* were analysed with the aim of testing whether *pPXY::PXY (Lys646►Arg; Lys720►Arg; Lys735►Arg)-HA* could complement the *pxy* mutant phenotype. 5-week-old Homozygous transgenic T_3 plants were used for phenotyping, both for gross morphology, and thin sections to visualise vascular tissues.

As shown in Figure 4.5, WT and *pxy* had limited morphological differences, while *pPXY::PXY (Lys646►Arg; Lys720►Arg; Lys735►Arg)-HA* transgenic *pxy* demonstrated decreased height (Figure 4.5A, C, E). Such height reductions have previously been observed in plants over-expressing *CLE41* (Smit et al., 2020). Moreover, in thin sections taken from the hypocotyl, in wild type, cambial cell divisions were present in a narrow ring of tissue between xylem and phloem. Furthermore, xylem, cambium and phloem were well organized, while *pxy* mutants were characterised by fewer vascular cells and reduced vascular organisation (Figure 4.5B, D). Interestingly, there were vasculature defects observed in *pxy pPXY::PXY (Lys646►Arg; Lys720►Arg; Lys735►Arg)-HA*. But they differed from those observed in *pxy* mutants. Indeed, the transgenic plants had phenotypes consistent with dramatically increased cell division and formation of ectopic cambium. The xylem differentiation appeared further inhibited. *pPXY::PXY (Lys646►Arg; Lys720►Arg; Lys735►Arg)-HA* did not complement *pxy*, rather, it had phenotypes consistent with constitutive PXY activity. Consequently, it is therefore possible that PXY SUMOylation functions as a negative regulator in PXY involved vascular signaling pathway thus playing a crucial role in vascular development.

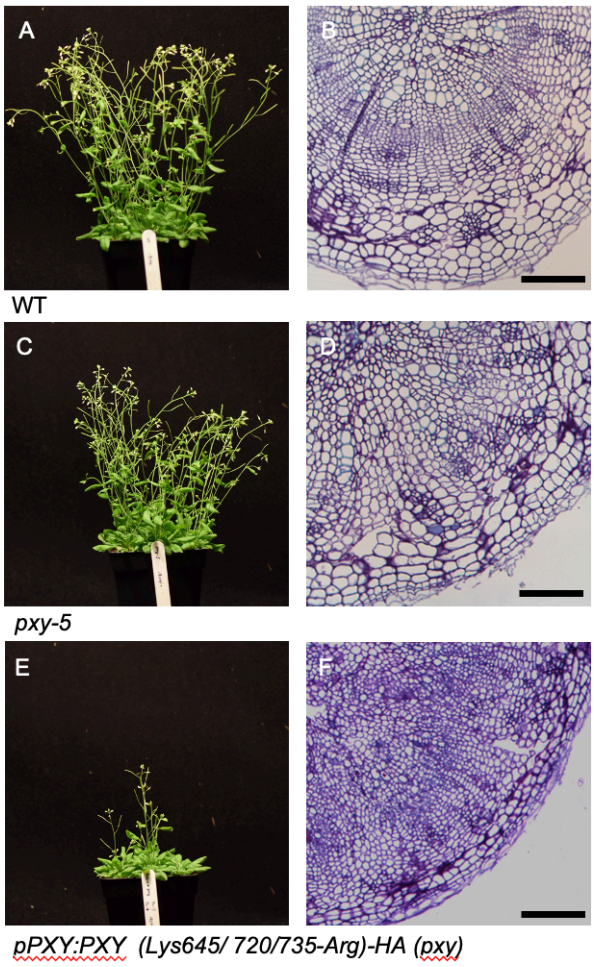

Figure 4.5 SUMOylation may function negatively in PXY signaling pathway.

A. Morphology of 5-week-old wild type.

B. Sectioning of wild type (5 weeks old, JB4 embedding and sectioned using Microtome with 4μm thickness, scale bar 50μm).

C. Morphology of 5-week-old *pxy*.

D. Sectioning of *pxy* (5 weeks old, JB4 embedding and sectioned using Microtome with 4μm thickness, scale bar 50μm).

E. Morphological phenotype of 5-week-old *pPXY::PXY (Lys646►Arg; Lys720►Arg; Lys735►Arg)-HA* transgenic *pxy*.

F. Sectioning of *pPXY::PXY (Lys646►Arg; Lys720►Arg; Lys735►Arg)-HA* transgenic *pxy* (5 weeks old, JB4 embedding and sectioned using Microtome with 4μm thickness, scale bar 50μm).

4.3 Discussion

SUMOylation is a reversible post-translational modification that can either repress or promote ubiquitination. It achieves this by competing for target lysine residues of substrates or by recruiting SUMO-targeted ubiquitin ligases (STUbLs) to poly-SUMOylated substrates (Elrouby et al., 2013; Geoffroy and Hay, 2009). Additionally, SUMOylation impacts the subcellular localization, enzymatic activity, and protein-protein interactions (Augustine and Vierstra, 2018). SUMOs are covalently attached to lysine residues of substrates through SUMO-activating E1 enzymes, SUMO-conjugating E2 enzymes, and SUMO E3 ligases (Augustine and Vierstra, 2018). The reversal of SUMOylation is conducted by SUMO proteases, which are believed to determine substrate specificity and fine-tune SUMOylation levels (Yates et al., 2016).

SUMOylation plays crucial roles in regulating various aspects of plant development and responses to hormonal and environmental signals. These include root development (Zhang et al., 2017), flowering time (Jin et al., 2008; Kong et al., 2017), plant immunity (Hammoudi et al., 2018; Niu et al., 2019; Orosa et al., 2018), auxin signaling (Orosa-Puente et al., 2018), abscisic acid (ABA) signaling (Miura et al., 2009), cold stress (Miura et al., 2007), heat stress (Rytz et al., 2018). However, the function of SUMOylation in plant vasculature development is lack of exploration.

The programme HyperSUMO revealed the predicted presence of several SUMO sites of PXY (Figure 4.2.2) supporting research that indicated that PXY is indeed SUMOylated (Figure 4.3). Based on the predicted SUMO sites which locate within kinase domain, constructs were generated to mutate different PXY SUMO sites and transformed into Arabidopsis to be used for function analysis. *pPXY::PXY (Lys646►Arg; Lys720►Arg; Lys735►Arg)-HA* transgenic *pxy* showed dramatic defects and was phenotypically distinct from either wild type or a *pxy* mutant with increased cell division, ectopic cambium formation, and inhibited xylem differentiation. PXY SUMOylation thus likely functions to negatively regulate PXY signaling in vascular development.

However, our research is still in its initial stages. Predictions have identified three potential SUMO sites in PXY: K645, K720, and K735. PXY function may be altered by

a single SUMO site or mono-SUMOylation at multiple sites. It's possible that one or two of these sites serve as key regulators, influencing PXY signaling and vasculature. Further studies involving single PXY SUMO-mutated transgenic plants are necessary to conduct phenotypical analyses, confirming the function of PXY SUMOylation both individually and collectively. Thus, the specific effects of PXY SUMOylation on different vascular tissues and developmental stages remain unclear. PXY SUMOylation may contribute more to cambium initiation, cell division, or xylem differentiation, and it may also regulate cell polarity or tissue organization.

Interstingly, in Figure 4.5, the morphological phenotype of pPXY::PXY (Lys646►Arg; Lys720►Arg; Lys735►Arg)-HA transgenic pxy showed later flowering/inflorescence architecture phenotype. It is possibly affected by PXY SUMOylation or due to the vascular defects. Flowering/inflorescence architecture phenotype inducible version of PXY SUMO mutated plants and RNA-Seq can potentially be used to answer the question.

Additionally, the regulation of SUMOylation on PXY within the vasculature is not understood. Previous studies have identified SUMO-interacting proteins in Arabidopsis (Elrouby et al., 2013). These proteins may promote PXY SUMOylation or accelerate the degradation of non-SUMOylated PXY, thereby affecting PXY function and will be an avenue for further study.

Chapter 5. General Discussion

The conjugation of small ubiquitin-related modifier (SUMO) to intracellular proteins offers a dynamic regulatory mechanism that allows plants to quickly respond to environmental challenges. SUMOylation, primarily affecting nuclear proteins, is one of the most rapid stress responses observed in plants. However, the exact role of this post-translational modification is still not fully understood.

Previous studies indicated the SUMO system and its expanding target catalog (Over 1000 mostly nuclear proteins are targets of SUMOylation) in *Arabidopsis.* Stress-induced SUMO addition is important for abiotic and biotic stress defense. Reproductive development and success is linked to SUMOylation. Moreover, SUMO has emerging roles in transcriptional gene silencing and epigenetic regulation.

Interestingly, SUMOylation has been found to influence protein-protein interactions, creating binding sites for proteins containing SUMO-interacting motifs (SIMs), thereby modulating protein-protein interactions and downstream signaling pathways (Yang and Sharrocks, 2004).. For example, SUMOylation of TPR1 enhances its interaction with SNC1 (Niu et al., 2019).

In chapter 4, PXY was predicted and confirmed to be SUMOylated and the PXY SUMOylation probably function negatively in TDIF-PXY signaling pathway which indicated the potential important role of SUMOylation in other aspects like plant secondary growth. Considering our previous findings that PXY can heterodimerize with ER, it is possible that SUMOylation of PXY not only directly impacts vascular development but also traps PXY in a complex with ER. Therefore, examining the physical interactions between PXY SUMO-mutated proteins and ER can help confirm the influence of PXY SUMOylation on the heterodimerization between PXY and ER and further function of SUMOylation in protein-protein interactions.

Furthermore, it also arises another relevant question that do other members of PXY or ER family contain SUMO sites? I can try to predict the potential SUMO sites using the prediction program. Future endeavours that expand the SUMOylome will certainly

enrich our understanding of this post-translational decoration in different plant growth and developmental processes.

References

Adie, B.A., Perez-Perez, J., Perez-Perez, M.M., Godoy, M., Sanchez-Serrano, J.J., Schmelz, E.A., Solano, R., 2007. ABA is an essential signal for plant resistance to pathogens affecting JA biosynthesis and the activation of defenses in Arabidopsis. Plant Cell 19, 1665-1681.
Adler, E., Bjorkqvist, K.J., Haggroth, S., 1948. Uber Die Ursache Der Farbreaktionen Des Holzes. Acta Chem Scand 2, 93-94.
Alonso, J.M., Stepanova, A.N., Leisse, T.J., Kim, C.J., Chen, H., Shinn, P., Stevenson, D.K., Zimmerman, J., Barajas, P., Cheuk, R., Gadrinab, C., Heller, C., Jeske, A., Koesema, E., Meyers, C.C., Parker, H., Prednis, L., Ansari, Y., Choy, N., Deen, H., Geralt, M., Hazari, N., Hom, E., Karnes, M., Mulholland, C., Ndubaku, R., Schmidt, I., Guzman, P., Aguilar-Henonin, L., Schmid, M., Weigel, D., Carter, D.E., Marchand, T., Risseeuw, E., Brogden, D., Zeko, A., Crosby, W.L., Berry, C.C., Ecker, J.R., 2003. Genome-wide insertional mutagenesis of Arabidopsis thaliana. Science 301, 653-657.
Anne, P., Azzopardi, M., Gissot, L., Beaubiat, S., Hematy, K., Palauqui, J.C., 2015. OCTOPUS Negatively Regulates BIN2 to Control Phloem Differentiation in Arabidopsis thaliana. Curr Biol 25, 2584-2590.
Augustine, R.C., Vierstra, R.D., 2018. SUMOylation: re-wiring the plant nucleus during stress and development. Curr Opin Plant Biol 45, 143-154.
Bar-On, Y.M., Phillips, R., Milo, R., 2018. The biomass distribution on Earth. Proc Natl Acad Sci U S A 115, 6506-6511.
Bastin, J.F., Finegold, Y., Garcia, C., Mollicone, D., Rezende, M., Routh, D., Zohner, C.M., Crowther, T.W., 2019. Response to Comment on "The global tree restoration potential". Science 366.
Bayer, P., Arndt, A., Metzger, S., Mahajan, R., Melchior, F., Jaenicke, R., Becker, J., 1998. Structure determination of the small ubiquitin-related modifier SUMO-1. J Mol Biol 280, 275-286.
Bergmann, D.C., Lukowitz, W., Somerville, C.R., 2004. Stomatal development and pattern controlled by a MAPKK kinase. Science 304, 1494-1497.
Bundy, M.G., Thompson, O.A., Sieger, M.T., Shpak, E.D., 2012. Patterns of cell division, cell differentiation and cell elongation in epidermis and cortex of Arabidopsis pedicels in the wild type and in erecta. PLoS One 7, e46262.
Busch, W., Miotk, A., Ariel, F.D., Zhao, Z., Forner, J., Daum, G., Suzaki, T., Schuster, C., Schultheiss, S.J., Leibfried, A., Haubeiss, S., Ha, N., Chan, R.L., Lohmann, J.U., 2010. Transcriptional control of a plant stem cell niche. Dev Cell 18, 849-861.
Cai, H., Huang, Y., Chen, F., Liu, L., Chai, M., Zhang, M., Yan, M., Aslam, M., He, Q., Qin, Y., 2021. ERECTA signaling regulates plant immune responses via chromatin-mediated promotion of WRKY33 binding to target genes. New Phytol.
Cai, H., Zhao, L., Wang, L., Zhang, M., Su, Z., Cheng, Y., Zhao, H., Qin, Y., 2017. ERECTA signaling controls Arabidopsis inflorescence architecture through chromatin-mediated activation of PRE1 expression. New Phytol 214, 1579-1596.
Campilho, A., Nieminen, K., Ragni, L., 2020. The development of the periderm: the final frontier between a plant and its environment. Curr Opin Plant Biol 53, 10-14.
Chaffey, N., Cholewa, E., Regan, S., Sundberg, B., 2002. Secondary xylem development in Arabidopsis: a model for wood formation. Physiol Plant 114, 594-600.

Chandrasekara, A., Josheph Kumar, T., 2016. Roots and Tuber Crops as Functional Foods: A Review on Phytochemical Constituents and Their Potential Health Benefits. Int J Food Sci 2016, 3631647.
Chen, M.K., Wilson, R.L., Palme, K., Ditengou, F.A., Shpak, E.D., 2013. ERECTA family genes regulate auxin transport in the shoot apical meristem and forming leaf primordia. Plant Physiol 162, 1978-1991.
Clark, S.E., Williams, R.W., Meyerowitz, E.M., 1997. The CLAVATA1 gene encodes a putative receptor kinase that controls shoot and floral meristem size in Arabidopsis. Cell 89, 575-585.
Clough, S.J., Bent, A.F., 1998. Floral dip: a simplified method for Agrobacterium-mediated transformation of Arabidopsis thaliana. Plant J 16, 735-743.
Conti, L., Nelis, S., Zhang, C., Woodcock, A., Swarup, R., Galbiati, M., Tonelli, C., Napier, R., Hedden, P., Bennett, M., Sadanandom, A., 2014. Small Ubiquitin-like Modifier protein SUMO enables plants to control growth independently of the phytohormone gibberellin. Dev Cell 28, 102-110.
Conti, L., Price, G., O'Donnell, E., Schwessinger, B., Dominy, P., Sadanandom, A., 2008. Small ubiquitin-like modifier proteases OVERLY TOLERANT TO SALT1 and -2 regulate salt stress responses in Arabidopsis. Plant Cell 20, 2894-2908.
Curtis, M.D., Grossniklaus, U., 2003. A gateway cloning vector set for high-throughput functional analysis of genes in planta. Plant Physiol 133, 462-469.
DALBY, P., 2021. From solving climate change to building space rockets,
ERECTA - a multifaceted Receptor-Like Kinase.
De Rybel, B., Mahonen, A.P., Helariutta, Y., Weijers, D., 2016. Plant vascular development: from early specification to differentiation. Nat Rev Mol Cell Biol 17, 30-40.
Denis, E., Kbiri, N., Mary, V., Claisse, G., Conde, E.S.N., Kreis, M., Deveaux, Y., 2017. WOX14 promotes bioactive gibberellin synthesis and vascular cell differentiation in Arabidopsis. Plant J 90, 560-572.
Desterro, J.M., Rodriguez, M.S., Kemp, G.D., Hay, R.T., 1999. Identification of the enzyme required for activation of the small ubiquitin-like protein SUMO-1. J Biol Chem 274, 10618-10624.
DeYoung, B.J., Bickle, K.L., Schrage, K.J., Muskett, P., Patel, K., Clark, S.E., 2006. The CLAVATA1-related BAM1, BAM2 and BAM3 receptor kinase-like proteins are required for meristem function in Arabidopsis. Plant J 45, 1-16.
Dinneny, J.R., Benfey, P.N., 2008. Plant stem cell niches: standing the test of time. Cell 132, 553-557.
Elrouby, N., Bonequi, M.V., Porri, A., Coupland, G., 2013. Identification of Arabidopsis SUMO-interacting proteins that regulate chromatin activity and developmental transitions. Proc Natl Acad Sci U S A 110, 19956-19961.
Elrouby, N., Coupland, G., 2010. Proteome-wide screens for small ubiquitin-like modifier (SUMO) substrates identify Arabidopsis proteins implicated in diverse biological processes. Proc Natl Acad Sci U S A 107, 17415-17420.
Esau, 1977. <ESAU'S PLANT ANATOMY.pdf>.
Etchells, J.P., Provost, C.M., Mishra, L., Turner, S.R., 2013. WOX4 and WOX14 act downstream of the PXY receptor kinase to regulate plant vascular proliferation independently of any role in vascular organisation. Development 140, 2224-2234.
Etchells, J.P., Provost, C.M., Turner, S.R., 2012. Plant vascular cell division is maintained by an interaction between PXY and ethylene signalling. PLoS Genet 8, e1002997.

Etchells, J.P., Smit, M.E., Gaudinier, A., Williams, C.J., Brady, S.M., 2016. A brief history of the TDIF-PXY signalling module: balancing meristem identity and differentiation during vascular development. New Phytol 209, 474-484.
Etchells, J.P., Turner, S.R., 2010. The PXY-CLE41 receptor ligand pair defines a multifunctional pathway that controls the rate and orientation of vascular cell division. Development 137, 767-774.
Evert, R.F., Esau, K., Esau, K., 2006. Esau's Plant anatomy : meristems, cells, and tissues of the plant body : their structure, function, and development, 3rd ed. Wiley-Interscience, Hoboken, N.J.
Fiers, M., Golemiec, E., Xu, J., van der Geest, L., Heidstra, R., Stiekema, W., Liu, C.M., 2005. The 14-amino acid CLV3, CLE19, and CLE40 peptides trigger consumption of the root meristem in Arabidopsis through a CLAVATA2-dependent pathway. Plant Cell 17, 2542-2553.
Finkelstein, R.R., Lynch, T.J., 2000. The Arabidopsis abscisic acid response gene ABI5 encodes a basic leucine zipper transcription factor. Plant Cell 12, 599-609.
Fischer, U., Kucukoglu, M., Helariutta, Y., Bhalerao, R.P., 2019. The Dynamics of Cambial Stem Cell Activity. Annu Rev Plant Biol 70, 293-319.
Fischer, U., Teichmann, T., 2017. The ERECTA and ERECTA-like genes control a developmental shift during xylem formation in Arabidopsis. New Phytol 213, 1562-1563.
Fisher, K., Turner, S., 2007. PXY, a receptor-like kinase essential for maintaining polarity during plant vascular-tissue development. Curr Biol 17, 1061-1066.
Fletcher, J.C., Brand, U., Running, M.P., Simon, R., Meyerowitz, E.M., 1999. Signaling of cell fate decisions by CLAVATA3 in Arabidopsis shoot meristems. Science 283, 1911-1914.
Gao, M., Skolnick, J., 2012. The distribution of ligand-binding pockets around protein-protein interfaces suggests a general mechanism for pocket formation. Proc Natl Acad Sci U S A 109, 3784-3789.
Gardiner, J.C., Taylor, N.G., Turner, S.R., 2003. Control of cellulose synthase complex localization in developing xylem. Plant Cell 15, 1740-1748.
Geoffroy, M.C., Hay, R.T., 2009. An additional role for SUMO in ubiquitin-mediated proteolysis. Nat Rev Mol Cell Biol 10, 564-568.
Godiard, L., Sauviac, L., Torii, K.U., Grenon, O., Mangin, B., Grimsley, N.H., Marco, Y., 2003. ERECTA, an LRR receptor-like kinase protein controlling development pleiotropically affects resistance to bacterial wilt. Plant J 36, 353-365.
Gong, L., Li, B., Millas, S., Yeh, E.T., 1999. Molecular cloning and characterization of human AOS1 and UBA2, components of the sentrin-activating enzyme complex. FEBS Lett 448, 185-189.
Grones, P., Chen, X., Simon, S., Kaufmann, W.A., De Rycke, R., Nodzynski, T., Zazimalova, E., Friml, J., 2015. Auxin-binding pocket of ABP1 is crucial for its gain-of-function cellular and developmental roles. J Exp Bot 66, 5055-5065.
Hafke, J.B., van Amerongen, J.K., Kelling, F., Furch, A.C., Gaupels, F., van Bel, A.J., 2005. Thermodynamic battle for photosynthate acquisition between sieve tubes and adjoining parenchyma in transport phloem. Plant Physiol 138, 1527-1537.
Hammoudi, V., Fokkens, L., Beerens, B., Vlachakis, G., Chatterjee, S., Arroyo-Mateos, M., Wackers, P.F.K., Jonker, M.J., van den Burg, H.A., 2018. The Arabidopsis SUMO E3 ligase SIZ1 mediates the temperature dependent trade-off between plant immunity and growth. PLoS Genet 14, e1007157.

Han, S., Cho, H., Noh, J., Qi, J., Jung, H.J., Nam, H., Lee, S., Hwang, D., Greb, T., Hwang, I., 2018. BIL1-mediated MP phosphorylation integrates PXY and cytokinin signalling in secondary growth. Nat Plants 4, 605-614.
Hara, K., Kajita, R., Torii, K.U., Bergmann, D.C., Kakimoto, T., 2007. The secretory peptide gene EPF1 enforces the stomatal one-cell-spacing rule. Genes Dev 21, 1720-1725.
Hara, K., Yokoo, T., Kajita, R., Onishi, T., Yahata, S., Peterson, K.M., Torii, K.U., Kakimoto, T., 2009. Epidermal cell density is autoregulated via a secretory peptide, EPIDERMAL PATTERNING FACTOR 2 in Arabidopsis leaves. Plant Cell Physiol 50, 1019-1031.
Hay, R.T., 2005. SUMO: a history of modification. Mol Cell 18, 1-12.
Hilleary, R., Gilroy, S., 2018. Systemic signaling in response to wounding and pathogens. Curr Opin Plant Biol 43, 57-62.
Hirakawa, Y., Kondo, Y., Fukuda, H., 2010. TDIF peptide signaling regulates vascular stem cell proliferation via the WOX4 homeobox gene in Arabidopsis. Plant Cell 22, 2618-2629.
Hirakawa, Y., Shinohara, H., Kondo, Y., Inoue, A., Nakanomyo, I., Ogawa, M., Sawa, S., Ohashi-Ito, K., Matsubayashi, Y., Fukuda, H., 2008. Non-cell-autonomous control of vascular stem cell fate by a CLE peptide/receptor system. Proc Natl Acad Sci U S A 105, 15208-15213.
Hoang, N.V., Park, C., Kamran, M., Lee, J.Y., 2020. Gene Regulatory Network Guided Investigations and Engineering of Storage Root Development in Root Crops. Front Plant Sci 11, 762.
Hothorn, M., Belkhadir, Y., Dreux, M., Dabi, T., Noel, J.P., Wilson, I.A., Chory, J., 2011. Structural basis of steroid hormone perception by the receptor kinase BRI1. Nature 474, 467-471.
Hu, J., Hu, X., Yang, Y., He, C., Hu, J., Wang, X., 2022. Strigolactone signaling regulates cambial activity through repression of WOX4 by transcription factor BES1. Plant Physiol 188, 255-267.
Hubbard, S.R., Till, J.H., 2000. Protein tyrosine kinase structure and function. Annu Rev Biochem 69, 373-398.
Hunt, L., Bailey, K.J., Gray, J.E., 2010. The signalling peptide EPFL9 is a positive regulator of stomatal development. New Phytol 186, 609-614.
Ikematsu, S., Tasaka, M., Torii, K.U., Uchida, N., 2017. ERECTA-family receptor kinase genes redundantly prevent premature progression of secondary growth in the Arabidopsis hypocotyl. New Phytol 213, 1697-1709.
Ito, Y., Nakanomyo, I., Motose, H., Iwamoto, K., Sawa, S., Dohmae, N., Fukuda, H., 2006. Dodeca-CLE peptides as suppressors of plant stem cell differentiation. Science 313, 842-845.
Jay, F., Brioudes, F., Voinnet, O., 2023. A contemporary reassessment of the enhanced transient expression system based on the tombusviral silencing suppressor protein P19. Plant J 113, 186-204.
Jin, J.B., Jin, Y.H., Lee, J., Miura, K., Yoo, C.Y., Kim, W.Y., Van Oosten, M., Hyun, Y., Somers, D.E., Lee, I., Yun, D.J., Bressan, R.A., Hasegawa, P.M., 2008. The SUMO E3 ligase, AtSIZ1, regulates flowering by controlling a salicylic acid-mediated floral promotion pathway and through affects on FLC chromatin structure. Plant J 53, 530-540.
Johns, S., Hagihara, T., Toyota, M., Gilroy, S., 2021. The fast and the furious: rapid long-range signaling in plants. Plant Physiol 185, 694-706.
Johnson, E.S., Gupta, A.A., 2001. An E3-like factor that promotes SUMO conjugation to the yeast septins. Cell 106, 735-744.

Johnson, E.S., Schwienhorst, I., Dohmen, R.J., Blobel, G., 1997. The ubiquitin-like protein Smt3p is activated for conjugation to other proteins by an Aos1p/Uba2p heterodimer. EMBO J 16, 5509-5519.
Jorda, L., Sopena-Torres, S., Escudero, V., Nunez-Corcuera, B., Delgado-Cerezo, M., Torii, K.U., Molina, A., 2016. ERECTA and BAK1 Receptor Like Kinases Interact to Regulate Immune Responses in Arabidopsis. Front Plant Sci 7, 897.
Jun, J., Fiume, E., Roeder, A.H., Meng, L., Sharma, V.K., Osmont, K.S., Baker, C., Ha, C.M., Meyerowitz, E.M., Feldman, L.J., Fletcher, J.C., 2010. Comprehensive analysis of CLE polypeptide signaling gene expression and overexpression activity in Arabidopsis. Plant Physiol 154, 1721-1736.
Karimi, M., Inze, D., Depicker, A., 2002. GATEWAY vectors for Agrobacterium-mediated plant transformation. Trends Plant Sci 7, 193-195.
Kondo, T., Kajita, R., Miyazaki, A., Hokoyama, M., Nakamura-Miura, T., Mizuno, S., Masuda, Y., Irie, K., Tanaka, Y., Takada, S., Kakimoto, T., Sakagami, Y., 2010. Stomatal density is controlled by a mesophyll-derived signaling molecule. Plant Cell Physiol 51, 1-8.
Kondo, Y., Ito, T., Nakagami, H., Hirakawa, Y., Saito, M., Tamaki, T., Shirasu, K., Fukuda, H., 2014. Plant GSK3 proteins regulate xylem cell differentiation downstream of TDIF-TDR signalling. Nat Commun 5, 3504.
Kong, X., Luo, X., Qu, G.P., Liu, P., Jin, J.B., 2017. Arabidopsis SUMO protease ASP1 positively regulates flowering time partially through regulating FLC stability. J Integr Plant Biol 59, 15-29.
Kucukoglu, M., 2020. A novel NAC domain transcription factor XVP controls the balance of xylem formation and cambial cell divisions. New Phytol 226, 5-7.
Kurepa, J., Walker, J.M., Smalle, J., Gosink, M.M., Davis, S.J., Durham, T.L., Sung, D.Y., Vierstra, R.D., 2003. The small ubiquitin-like modifier (SUMO) protein modification system in Arabidopsis. Accumulation of SUMO1 and -2 conjugates is increased by stress. J Biol Chem 278, 6862-6872.
Lampropoulos, A., Sutikovic, Z., Wenzl, C., Maegele, I., Lohmann, J.U., Forner, J., 2013. GreenGate---a novel, versatile, and efficient cloning system for plant transgenesis. PLoS One 8, e83043.
Larson, P.R., 1994. The vascular cambium : development and structure. Springer-Verlag, Berlin ; New York.
Lazar, T., 2003. Taiz, L. and Zeiger, E. Plant physiology. 3rd edn. Annals of Botany 91, 750-751.
Lee, J.S., Kuroha, T., Hnilova, M., Khatayevich, D., Kanaoka, M.M., McAbee, J.M., Sarikaya, M., Tamerler, C., Torii, K.U., 2012. Direct interaction of ligand-receptor pairs specifying stomatal patterning. Genes Dev 26, 126-136.
Lee, J.S., Torii, K.U., 2012. A tale of two systems: peptide ligand-receptor pairs in plant development. Cold Spring Harb Symp Quant Biol 77, 83-89.
Lehmann, F., Hardtke, C.S., 2016. Secondary growth of the Arabidopsis hypocotyl-vascular development in dimensions. Curr Opin Plant Biol 29, 9-15.
Lin, D., Tatham, M.H., Yu, B., Kim, S., Hay, R.T., Chen, Y., 2002. Identification of a substrate recognition site on Ubc9. J Biol Chem 277, 21740-21748.
Llorente, F., Alonso-Blanco, C., Sanchez-Rodriguez, C., Jorda, L., Molina, A., 2005. ERECTA receptor-like kinase and heterotrimeric G protein from Arabidopsis are required for resistance to the necrotrophic fungus Plectosphaerella cucumerina. Plant J 43, 165-180.

Lukowitz, W., Roeder, A., Parmenter, D., Somerville, C., 2004. A MAPKK kinase gene regulates extra-embryonic cell fate in Arabidopsis. Cell 116, 109-119.
Mahajan, R., Delphin, C., Guan, T., Gerace, L., Melchior, F., 1997. A small ubiquitin-related polypeptide involved in targeting RanGAP1 to nuclear pore complex protein RanBP2. Cell 88, 97-107.
Mani, R., St Onge, R.P., Hartman, J.L.t., Giaever, G., Roth, F.P., 2008. Defining genetic interaction. Proc Natl Acad Sci U S A 105, 3461-3466.
Mann, M., Jensen, O.N., 2003. Proteomic analysis of post-translational modifications. Nat Biotechnol 21, 255-261.
Marín-García, J., Akhmedov, A., Rybin, V., Moe, G.W., ScienceDirect, 2014. Post-genomic cardiology, 2nd ed. Academic Press, London England.
Marshall, A., Aalen, R.B., Audenaert, D., Beeckman, T., Broadley, M.R., Butenko, M.A., Cano-Delgado, A.I., de Vries, S., Dresselhaus, T., Felix, G., Graham, N.S., Foulkes, J., Granier, C., Greb, T., Grossniklaus, U., Hammond, J.P., Heidstra, R., Hodgman, C., Hothorn, M., Inze, D., Ostergaard, L., Russinova, E., Simon, R., Skirycz, A., Stahl, Y., Zipfel, C., De Smet, I., 2012. Tackling drought stress: receptor-like kinases present new approaches. Plant Cell 24, 2262-2278.
Masle, J., Gilmore, S.R., Farquhar, G.D., 2005. The ERECTA gene regulates plant transpiration efficiency in Arabidopsis. Nature 436, 866-870.
Matunis, M.J., Coutavas, E., Blobel, G., 1996. A novel ubiquitin-like modification modulates the partitioning of the Ran-GTPase-activating protein RanGAP1 between the cytosol and the nuclear pore complex. J Cell Biol 135, 1457-1470.
Meinke, D.W., Cherry, J.M., Dean, C., Rounsley, S.D., Koornneef, M., 1998. Arabidopsis thaliana: a model plant for genome analysis. Science 282, 662, 679-682.
Milhinhos, A., Vera-Sirera, F., Blanco-Tourinan, N., Mari-Carmona, C., Carrio-Segui, A., Forment, J., Champion, C., Thamm, A., Urbez, C., Prescott, H., Agusti, J., 2019. SOBIR1/EVR prevents precocious initiation of fiber differentiation during wood development through a mechanism involving BP and ERECTA. Proc Natl Acad Sci U S A 116, 18710-18716.
Miller, M.J., Barrett-Wilt, G.A., Hua, Z.H., Vierstra, R.D., 2010. Proteomic analyses identify a diverse array of nuclear processes affected by small ubiquitin-like modifier conjugation in. P Natl Acad Sci USA 107, 16512-16517.
Mitsuda, N., Iwase, A., Yamamoto, H., Yoshida, M., Seki, M., Shinozaki, K., Ohme-Takagi, M., 2007. NAC transcription factors, NST1 and NST3, are key regulators of the formation of secondary walls in woody tissues of Arabidopsis. Plant Cell 19, 270-280.
Miura, K., Jin, J.B., Lee, J., Yoo, C.Y., Stirm, V., Miura, T., Ashworth, E.N., Bressan, R.A., Yun, D.J., Hasegawa, P.M., 2007. SIZ1-mediated sumoylation of ICE1 controls CBF3/DREB1A expression and freezing tolerance in Arabidopsis. Plant Cell 19, 1403-1414.
Miura, K., Lee, J., Gong, Q., Ma, S., Jin, J.B., Yoo, C.Y., Miura, T., Sato, A., Bohnert, H.J., Hasegawa, P.M., 2011. SIZ1 regulation of phosphate starvation-induced root architecture remodeling involves the control of auxin accumulation. Plant Physiol 155, 1000-1012.
Miura, K., Lee, J., Jin, J.B., Yoo, C.Y., Miura, T., Hasegawa, P.M., 2009. Sumoylation of ABI5 by the Arabidopsis SUMO E3 ligase SIZ1 negatively regulates abscisic acid signaling. Proc Natl Acad Sci U S A 106, 5418-5423.
Miura, K., Lee, J., Miura, T., Hasegawa, P.M., 2010. SIZ1 controls cell growth and plant development in Arabidopsis through salicylic acid. Plant Cell Physiol 51, 103-113.
Miura, K., Rus, A., Sharkhuu, A., Yokoi, S., Karthikeyan, A.S., Raghothama, K.G., Baek, D., Koo, Y.D., Jin, J.B., Bressan, R.A., Yun, D.J., Hasegawa, P.M., 2005. The Arabidopsis SUMO E3

ligase SIZ1 controls phosphate deficiency responses. Proc Natl Acad Sci U S A 102, 7760-7765.
Morita, J., Kato, K., Nakane, T., Kondo, Y., Fukuda, H., Nishimasu, H., Ishitani, R., Nureki, O., 2016. Crystal structure of the plant receptor-like kinase TDR in complex with the TDIF peptide. Nat Commun 7, 12383.
Mott, G.A., Smakowska-Luzan, E., Pasha, A., Parys, K., Howton, T.C., Neuhold, J., Lehner, A., Grunwald, K., Stolt-Bergner, P., Provart, N.J., Mukhtar, M.S., Desveaux, D., Guttman, D.S., Belkhadir, Y., 2019. Map of physical interactions between extracellular domains of Arabidopsis leucine-rich repeat receptor kinases. Sci Data 6, 190025.
Nakagawa, T., Suzuki, T., Murata, S., Nakamura, S., Hino, T., Maeo, K., Tabata, R., Kawai, T., Tanaka, K., Niwa, Y., Watanabe, Y., Nakamura, K., Kimura, T., Ishiguro, S., 2007. Improved Gateway binary vectors: high-performance vectors for creation of fusion constructs in transgenic analysis of plants. Biosci Biotechnol Biochem 71, 2095-2100.
Naranjo-Arcos, M., Srivastava, M., Deligne, F., Bhagat, P.K., Mansi, M., Sadanandom, A., Vert, G., 2023. SUMO/deSUMOylation of the BRI1 brassinosteroid receptor modulates plant growth responses to temperature. Proc Natl Acad Sci U S A 120, e2217255120.
Nie, M., Xie, Y., Loo, J.A., Courey, A.J., 2009. Genetic and proteomic evidence for roles of Drosophila SUMO in cell cycle control, Ras signaling, and early pattern formation. PLoS One 4, e5905.
Nieminen, K., Blomster, T., Helariutta, Y., Mahonen, A.P., 2015. Vascular Cambium Development. Arabidopsis Book 13, e0177.
Niu, D., Lin, X.L., Kong, X., Qu, G.P., Cai, B., Lee, J., Jin, J.B., 2019. SIZ1-Mediated SUMOylation of TPR1 Suppresses Plant Immunity in Arabidopsis. Mol Plant 12, 215-228.
Oelkers, K., Goffard, N., Weiller, G.F., Gresshoff, P.M., Mathesius, U., Frickey, T., 2008. Bioinformatic analysis of the CLE signaling peptide family. BMC Plant Biol 8, 1.
Okuma, T., Honda, R., Ichikawa, G., Tsumagari, N., Yasuda, H., 1999. In vitro SUMO-1 modification requires two enzymatic steps, E1 and E2. Biochem Biophys Res Commun 254, 693-698.
Orosa, B., Yates, G., Verma, V., Srivastava, A.K., Srivastava, M., Campanaro, A., De Vega, D., Fernandes, A., Zhang, C., Lee, J., Bennett, M.J., Sadanandom, A., 2018. SUMO conjugation to the pattern recognition receptor FLS2 triggers intracellular signalling in plant innate immunity. Nat Commun 9, 5185.
Orosa-Puente, B., Leftley, N., von Wangenheim, D., Banda, J., Srivastava, A.K., Hill, K., Truskina, J., Bhosale, R., Morris, E., Srivastava, M., Kumpers, B., Goh, T., Fukaki, H., Vermeer, J.E.M., Vernoux, T., Dinneny, J.R., French, A.P., Bishopp, A., Sadanandom, A., Bennett, M.J., 2018. Root branching toward water involves posttranslational modification of transcription factor ARF7. Science 362, 1407-1410.
Osakabe, Y., Yamaguchi-Shinozaki, K., Shinozaki, K., Tran, L.S., 2013. Sensing the environment: key roles of membrane-localized kinases in plant perception and response to abiotic stress. J Exp Bot 64, 445-458.
Ozkan, E., Carrillo, R.A., Eastman, C.L., Weiszmann, R., Waghray, D., Johnson, K.G., Zinn, K., Celniker, S.E., Garcia, K.C., 2013. An extracellular interactome of immunoglobulin and LRR proteins reveals receptor-ligand networks. Cell 154, 228-239.
Qi, Y., Sun, Y., Xu, L., Xu, Y., Huang, H., 2004. ERECTA is required for protection against heat-stress in the AS1/ AS2 pathway to regulate adaxial-abaxial leaf polarity in Arabidopsis. Planta 219, 270-276.

Ragni, L., Nieminen, K., Pacheco-Villalobos, D., Sibout, R., Schwechheimer, C., Hardtke, C.S., 2011. Mobile gibberellin directly stimulates Arabidopsis hypocotyl xylem expansion. Plant Cell 23, 1322-1336.
Redei, G.P., 1965. Non-Mendelian Megagametogenesis in Arabidopsis. Genetics 51, 857-872.
Reeves, P.H., Murtas, G., Dash, S., Coupland, G., 2002. early in short days 4, a mutation in Arabidopsis that causes early flowering and reduces the mRNA abundance of the floral repressor FLC. Development 129, 5349-5361.
Rodriguez-Villalon, A., Gujas, B., Kang, Y.H., Breda, A.S., Cattaneo, P., Depuydt, S., Hardtke, C.S., 2014. Molecular genetic framework for protophloem formation. Proc Natl Acad Sci U S A 111, 11551-11556.
Rytz, T.C., Miller, M.J., McLoughlin, F., Augustine, R.C., Marshall, R.S., Juan, Y.T., Charng, Y.Y., Scalf, M., Smith, L.M., Vierstra, R.D., 2018. SUMOylome Profiling Reveals a Diverse Array of Nuclear Targets Modified by the SUMO Ligase SIZ1 during Heat Stress. Plant Cell 30, 1077-1099.
Saito, M., Kondo, Y., Fukuda, H., 2018. BES1 and BZR1 Redundantly Promote Phloem and Xylem Differentiation. Plant Cell Physiol 59, 590-600.
Sanchez-Rodriguez, C., Estevez, J.M., Llorente, F., Hernandez-Blanco, C., Jorda, L., Pagan, I., Berrocal, M., Marco, Y., Somerville, S., Molina, A., 2009. The ERECTA Receptor-Like Kinase Regulates Cell Wall-Mediated Resistance to Pathogens in Arabidopsis thaliana. Mol Plant Microbe Interact 22, 953-963.
Saracco, S.A., Miller, M.J., Kurepa, J., Vierstra, R.D., 2007. Genetic analysis of SUMOylation in Arabidopsis: conjugation of SUMO1 and SUMO2 to nuclear proteins is essential. Plant Physiol 145, 119-134.
Saraswathy, N., Ramalingam, P., Elsevier, 2011. Concepts and techniques in genomics and proteomics. Woodhead Pub, Oxford ; Philadelphia.
Schoof, H., Lenhard, M., Haecker, A., Mayer, K.F., Jurgens, G., Laux, T., 2000. The stem cell population of Arabidopsis shoot meristems in maintained by a regulatory loop between the CLAVATA and WUSCHEL genes. Cell 100, 635-644.
Shi, D., Lebovka, I., Lopez-Salmeron, V., Sanchez, P., Greb, T., 2019. Bifacial cambium stem cells generate xylem and phloem during radial plant growth. Development 146.
Shiu, S.H., Karlowski, W.M., Pan, R., Tzeng, Y.H., Mayer, K.F., Li, W.H., 2004. Comparative analysis of the receptor-like kinase family in Arabidopsis and rice. Plant Cell 16, 1220-1234.
Shpak, E.D., 2013. Diverse roles of ERECTA family genes in plant development. J Integr Plant Biol 55, 1238-1250.
Shpak, E.D., Berthiaume, C.T., Hill, E.J., Torii, K.U., 2004. Synergistic interaction of three ERECTA-family receptor-like kinases controls Arabidopsis organ growth and flower development by promoting cell proliferation. Development 131, 1491-1501.
Shpak, E.D., McAbee, J.M., Pillitteri, L.J., Torii, K.U., 2005. Stomatal patterning and differentiation by synergistic interactions of receptor kinases. Science 309, 290-293.
Smakowska-Luzan, E., Mott, G.A., Parys, K., Stegmann, M., Howton, T.C., Layeghifard, M., Neuhold, J., Lehner, A., Kong, J., Grunwald, K., Weinberger, N., Satbhai, S.B., Mayer, D., Busch, W., Madalinski, M., Stolt-Bergner, P., Provart, N.J., Mukhtar, M.S., Zipfel, C., Desveaux, D., Guttman, D.S., Belkhadir, Y., 2018. An extracellular network of Arabidopsis leucine-rich repeat receptor kinases. Nature 553, 342-346.
Smetana, O., Makila, R., Lyu, M., Amiryousefi, A., Sanchez Rodriguez, F., Wu, M.F., Sole-Gil, A., Leal Gavarron, M., Siligato, R., Miyashima, S., Roszak, P., Blomster, T., Reed, J.W.,

Broholm, S., Mahonen, A.P., 2019. High levels of auxin signalling define the stem-cell organizer of the vascular cambium. Nature 565, 485-489.
Smit, M.E., McGregor, S.R., Sun, H., Gough, C., Bagman, A.M., Soyars, C.L., Kroon, J.T., Gaudinier, A., Williams, C.J., Yang, X., Nimchuk, Z.L., Weijers, D., Turner, S.R., Brady, S.M., Etchells, J.P., 2020. A PXY-Mediated Transcriptional Network Integrates Signaling Mechanisms to Control Vascular Development in Arabidopsis. Plant Cell 32, 319-335.
Song, S.K., Hofhuis, H., Lee, M.M., Clark, S.E., 2008. Key divisions in the early Arabidopsis embryo require POL and PLL1 phosphatases to establish the root stem cell organizer and vascular axis. Dev Cell 15, 98-109.
Song, S.K., Lee, M.M., Clark, S.E., 2006. POL and PLL1 phosphatases are CLAVATA1 signaling intermediates required for Arabidopsis shoot and floral stem cells. Development 133, 4691-4698.
Sopena-Torres, S., Jorda, L., Sanchez-Rodriguez, C., Miedes, E., Escudero, V., Swami, S., Lopez, G., Pislewska-Bednarek, M., Lassowskat, I., Lee, J., Gu, Y., Haigis, S., Alexander, D., Pattathil, S., Munoz-Barrios, A., Bednarek, P., Somerville, S., Schulze-Lefert, P., Hahn, M.G., Scheel, D., Molina, A., 2018. YODA MAP3K kinase regulates plant immune responses conferring broad-spectrum disease resistance. New Phytol 218, 661-680.
Suer, S., Agusti, J., Sanchez, P., Schwarz, M., Greb, T., 2011. WOX4 imparts auxin responsiveness to cambium cells in Arabidopsis. Plant Cell 23, 3247-3259.
Sugano, S.S., Shimada, T., Imai, Y., Okawa, K., Tamai, A., Mori, M., Hara-Nishimura, I., 2010. Stomagen positively regulates stomatal density in Arabidopsis. Nature 463, 241-244.
Sun, Y., Li, L., Macho, A.P., Han, Z., Hu, Z., Zipfel, C., Zhou, J.M., Chai, J., 2013. Structural basis for flg22-induced activation of the Arabidopsis FLS2-BAK1 immune complex. Science 342, 624-628.
Taiz, L., Møller, I.M., Murphy, A.S., Zeiger, E., 2023. Plant physiology and development, Seventh edition. ed. Sinauer Associates : Oxford University Press, New York.
Takata, N., Yokota, K., Ohki, S., Mori, M., Taniguchi, T., Kurita, M., 2013. Evolutionary relationship and structural characterization of the EPF/EPFL gene family. PLoS One 8, e65183.
Tang, J., Han, Z., Sun, Y., Zhang, H., Gong, X., Chai, J., 2015. Structural basis for recognition of an endogenous peptide by the plant receptor kinase PEPR1. Cell Res 25, 110-120.
Tatham, M.H., Chen, Y., Hay, R.T., 2003. Role of two residues proximal to the active site of Ubc9 in substrate recognition by the Ubc9.SUMO-1 thiolester complex. Biochemistry 42, 3168-3179.
Torii, K.U., Mitsukawa, N., Oosumi, T., Matsuura, Y., Yokoyama, R., Whittier, R.F., Komeda, Y., 1996. The Arabidopsis ERECTA gene encodes a putative receptor protein kinase with extracellular leucine-rich repeats. Plant Cell 8, 735-746.
Trewavas, A., 2021. Awareness and integrated information theory identify plant meristems as sites of conscious activity. Protoplasma 258, 673-679.
Uchida, N., Lee, J.S., Horst, R.J., Lai, H.H., Kajita, R., Kakimoto, T., Tasaka, M., Torii, K.U., 2012. Regulation of inflorescence architecture by intertissue layer ligand-receptor communication between endodermis and phloem. Proc Natl Acad Sci U S A 109, 6337-6342.
Uchida, N., Shimada, M., Tasaka, M., 2013. ERECTA-family receptor kinases regulate stem cell homeostasis via buffering its cytokinin responsiveness in the shoot apical meristem. Plant Cell Physiol 54, 343-351.

van Zanten, M., Basten Snoek, L., van Eck-Stouten, E., Proveniers, M.C., Torii, K.U., Voesenek, L.A., Peeters, A.J., Millenaar, F.F., 2010. Ethylene-induced hyponastic growth in Arabidopsis thaliana is controlled by ERECTA. Plant J 61, 83-95.
Wang, C., Huang, X., Li, Q., Zhang, Y., Li, J.L., Mou, Z., 2019a. Extracellular pyridine nucleotides trigger plant systemic immunity through a lectin receptor kinase/BAK1 complex. Nat Commun 10, 4810.
Wang, H., 2020. Regulation of vascular cambium activity. Plant Sci 291, 110322.
Wang, J., Li, H., Han, Z., Zhang, H., Wang, T., Lin, G., Chang, J., Yang, W., Chai, J., 2015. Allosteric receptor activation by the plant peptide hormone phytosulfokine. Nature 525, 265-268.
Wang, N., Bagdassarian, K.S., Doherty, R.E., Kroon, J.T., Connor, K.A., Wang, X.Y., Wang, W., Jermyn, I.H., Turner, S.R., Etchells, J.P., 2019b. Organ-specific genetic interactions between paralogues of the PXY and ER receptor kinases enforce radial patterning in Arabidopsis vascular tissue. Development 146.
Weigel, D., Glazebrook, J., 2006. Setting up Arabidopsis crosses. CSH Protoc 2006.
Xu, J., Zhang, S., 2015. Mitogen-activated protein kinase cascades in signaling plant growth and development. Trends Plant Sci 20, 56-64.
Yang, S., Wang, S., Li, S., Du, Q., Qi, L., Wang, W., Chen, J., Wang, H., 2020. Activation of ACS7 in Arabidopsis affects vascular development and demonstrates a link between ethylene synthesis and cambial activity. J Exp Bot 71, 7160-7170.
Yang, S.H., Sharrocks, A.D., 2004. SUMO promotes HDAC-mediated transcriptional repression. Mol Cell 13, 611-617.
Yates, G., Srivastava, A.K., Sadanandom, A., 2016. SUMO proteases: uncovering the roles of deSUMOylation in plants. J Exp Bot 67, 2541-2548.
Yoo, C.Y., Miura, K., Jin, J.B., Lee, J., Park, H.C., Salt, D.E., Yun, D.J., Bressan, R.A., Hasegawa, P.M., 2006. SIZ1 small ubiquitin-like modifier E3 ligase facilitates basal thermotolerance in Arabidopsis independent of salicylic acid. Plant Physiol 142, 1548-1558.
Zhang, C., Yang, Y., Yu, Z., Wang, J., Huang, R., Zhan, Q., Li, S., Lai, J., Zhang, S., Yang, C., 2023. SUMO E3 ligase AtMMS21-dependent SUMOylation of AUXIN/INDOLE-3-ACETIC ACID 17 regulates auxin signaling. Plant Physiol 191, 1871-1883.
Zhang, H., Lin, X., Han, Z., Qu, L.J., Chai, J., 2016a. Crystal structure of PXY-TDIF complex reveals a conserved recognition mechanism among CLE peptide-receptor pairs. Cell Res 26, 543-555.
Zhang, H., Lin, X., Han, Z., Wang, J., Qu, L.J., Chai, J., 2016b. SERK Family Receptor-like Kinases Function as Co-receptors with PXY for Plant Vascular Development. Mol Plant 9, 1406-1414.
Zhang, J., Lai, J., Wang, F., Yang, S., He, Z., Jiang, J., Li, Q., Wu, Q., Liu, Y., Yu, M., Du, J., Xie, Q., Wu, K., Yang, C., 2017. A SUMO Ligase AtMMS21 Regulates the Stability of the Chromatin Remodeler BRAHMA in Root Development. Plant Physiol 173, 1574-1582.
Zhang, Z., Thomma, B.P., 2013. Structure-function aspects of extracellular leucine-rich repeat-containing cell surface receptors in plants. J Integr Plant Biol 55, 1212-1223.

Appendix

Supplementary Tables

Supplementary Table 1. Gene names and AGI.

Accession numbers central to this research. Synonyms and corresponding links to The Arabidopsis Information Resource (TAIR) are provided.

Acession Number	Name	Synonyms	External Link
PXY Family			
AT5G61480	PXY	TDR	TAIR
AT1G08590	PXL1		TAIR
AT4G28650	PXL2	MIK1	TAIR
ER Family			
AT2G26330	ER	QRP1	TAIR
AT5G62230	ERL1		TAIR
AT5G07180	ERL2		TAIR
AT3G24770	CLE41		TAIR
AT1G22710	SUC2		TAIR

Supplementary Table 2. Exploratory analysis of quantitative FRET Efficiency data (Figure 3.2.).

Test statistic and significant difference from Post Hoc Tests were given. Shaded boxes indicate significant (at the α = 0.05 level) deviations from the non-homogenous variances.

Multiple Comparisons

Dependent Variable: Tukey HSD

(I) FRETpair		Mean Difference (I-J)	Std. Error	Sig.	95% Confidence Interval	
					Lower Bound	Upper Bound
PXL1d_ERL2a	PXL2d_ERL2a	-5.0594	4.87254	0.837	-18.7032	8.5845
	PXYd_ERa	1.9563	4.87254	0.994	-11.6875	15.6002
	PXYd_ERL1a	32.5146*	4.72990	0.000	19.2701	45.7590
	PXYd_ERL2a	1.5153	4.56706	0.997	-11.2731	14.3038
PXL2d_ERL2a	PXL1d_ERL2a	5.0594	4.87254	0.837	-8.5845	18.7032

	PXYd_ERa	7.0157	4.68139	0.567	-6.0929	20.1243
	PXYd_ERL1a	37.5740*	4.53273	0.000	24.8816	50.2663
	PXYd_ERL2a	6.5747	4.36254	0.561	-5.6411	18.7905
PXYd_ERa	PXL1d_ERL2a	-1.9563	4.87254	0.994	-15.6002	11.6875
	PXL2d_ERL2a	-7.0157	4.68139	0.567	-20.1243	6.0929
	PXYd_ERL1a	30.5583*	4.53273	0.000	17.8659	43.2506
	PXYd_ERL2a	-0.4410	4.36254	1.000	-12.6568	11.7748
PXYd_ERL1a	PXL1d_ERL2a	-32.5146*	4.72990	0.000	-45.7590	-19.2701
	PXL2d_ERL2a	-37.5740*	4.53273	0.000	-50.2663	-24.8816
	PXYd_ERa	-30.5583*	4.53273	0.000	-43.2506	-17.8659
	PXYd_ERL2a	-30.9993*	4.20263	0.000	-42.7673	-19.2313
PXYd_ERL2a	PXL1d_ERL2a	-1.5153	4.56706	0.997	-14.3038	11.2731
	PXL2d_ERL2a	-6.5747	4.36254	0.561	-18.7905	5.6411
	PXYd_ERa	0.4410	4.36254	1.000	-11.7748	12.6568
	PXYd_ERL1a	30.9993*	4.20263	0.000	19.2313	42.7673

Based on observed means.
The error term is Mean Square (Error) = 153.408.
*. The mean difference is significant at the 0.05 level. d, donor; a, acceptor.

Supplementary Table 3. DNA primers.

Primers used in this research for cloning gene promoters (A) or coding sequences (B), screening of transformed E. coli (C) and sequencing of expression clones (D).

Primer Name	Sequence (5'-3')	Function
PXY-CDS-topoF	caccATGAAAAAGAAGAACATTT	A
PXY-CDS-topoR	TCACACCCCAATCCTTTGACATT	A
PXY-CDS-HA-R	gtatgggtATCTAGATCCGGTCACCCCAATCC	A
PXY-fast-F	TCAATCGCCGACGTAGATC	B

PXY-fast-R	CTGCATTTCCGGCGTTAA	B
PXL1-CDS-topoF	CACCATGGCGATCCCTCGACTT	A
PXL1-CDS-topoR	AAATCAGCCCTACCACTGGCG	A
PXL1-fast-R	AGGGAAGCTCTGAATCTGA	B
PXL2-CDS-topoF	AAATCAGCCCTACCACTGGCG	A
PXL2-CDS-topoR	CACCATGGCGATCCCTCGACTT	A
PXL2-fast-R	TGTTAAACGAGACAAGGCTAC	B
ER-CDS-topoF		A
ER-CDS-topoR		A
ER-fast-R	TCGCAGATCAATTGACAAGAG	B
ERL1-CDS-topoF	CACCATGAAGGAGAAGATGCAGCG	A
ERL1-CDS-topoR	TATGCTACTTTTGGAGATGA	A
ERL1-fast-R	ATTCCGTAGGTCTCCAATAGC	B
ERL2-CDS-topoF	caccATGAGAAGGATAGAGACCATG	A
ERL2-CDS-topoR	TAAGCTACTTTTGGAGATAT	A
ERL2-fast-R	TCAAATCTCCAAGGGCAGA	B
CFP-S-R	CGCTCATCTGAATCCGTC	B
YFP-S-R	AACTTGTGGCCGTTTACGTCGCCG	B
attB1	GGGGACAAGTTTGTACAAAAAAGCAGGCT	B,C
attB2	GGGGACCACTTTGTACAAGAAAGCTGGGT	B,C
M13-F	GTA AAA CGA CGG CCA GT	B,C
M13-R	CAGGAAACAGCTATGAC	B,C
pxy-CDS-m645-F-1	ATGAAAAAGAAGAACATTTC	A
pxy-CDS-m645-R-1	TCTATGATGACCGTCTATAT	A
pxy-CDS-m645-F-2	ATATAGACGGTCATCATAGAGAGGAACGAC CTAAGAAAAC	A
pxy-CDS-m645-R-2	tggaacatcgtatgggtATCTAGATCCGGTCACCC CAATCCTTTGACATT	A
pxy-CDS-m645-R-3	cggcgcgcccacccttcaagcgtaatctggaacatcgtatgg gtATC	A

pxy-CDS-m720-F-1	ATGAAAAAGAAGAACATTTC	A
pxy-CDS-m720-R-1	CCTTGAGAGACACTCAACCA	A
pxy-CDS-m720-F-2	TGGTTGAGTGTCTCTCAAGGACTGATAACATCCTCGGAAT	A
pxy-CDS-m720-R-2	tggaacatcgtatgggtATCTAGATCCGGTCACCCCAATCCTTTGACATT	A
pxy-CDS-m720-R-3	cggcgcgcccacccttcaagcgtaatctggaacatcgtatggtATC	A
pxy-CDS-m735-F-1	ATGAAAAAGAAGAACATTTC	A
pxy-CDS-m735-R-1	CCATTAGGCATCTCTGCTCTGTACACTGTTCCTGTTGATC	A
pxy-CDS-m735-F-2	AGAGCAGAGATGCCTAATGG	A
pxy-CDS-m735-R-2	tggaacatcgtatgggtATCTAGATCCGGTCACCCCAATCCTTTGACATT	A
pxy-CDS-m735-R-3	cggcgcgcccacccttcaagcgtaatctggaacatcgtatggtATC	A
pB7-Seq-F	TGATTTTTGCGGACTCTAGCATG	B,C
pB7-Seq-R	CGACAATCTGATCCAAGCTC	B,C
35S-Seq-F	GAAAGGCTATCGTTCAAGATGCCTC	B,C
JL202 LB	CATTTTATAATAACGCTGCGGACATCTAC	
ERL2-LP	TTCCCATGAACATTGCTGAA	
ERL2-RP	CCGGAAGTGATTGGTCTGAT	

Supplementary Datasets

Dataset	contents	Notes
1A	Complete DESeq2 dataset	
1B	Differential gene expression *IRX3:CLE41* vs *er IRX3:CLE41*	
1C	Gene Ontology Analysis for Biological function (Genes with higher expression in *IRX3:CLE41/er IRX3:CLE41*)	Cut-offs for inclusion were q<0.05 with minimum fold-change of 1.5. Go categories represented in Figure S3 are in bold text.
1D	Gene Ontology Analysis for Biological function (Genes with higher expression in *er IRX3:CLE41/IRX3:CLE41*)	Cut-offs for inclusion were q<0.05 with minimum fold-change of 1.5. Go categories represented in Figure 3 are in bold text.
1E	Genes from Supplemental dataset 1B showing differential expression compared with those with enriched expression in xylem (Wendrich et al., 2020)	